Spontaneously Broken Spacetime Symmetries and Many-Body Phenomena

by

Shashin Padmanabhan Pavaskar

Submitted in partial fulfillment of the
requirements for the degree of
Doctor of Philosophy
at
Carnegie Mellon University
Department of Physics
Pittsburgh, Pennsylvania

Advised by Professor Ira Zvi Rothstein

July 9, 2023

To Nina, who I wish was still with us.

Abstract

In this thesis, I discuss the application of Effective Field Theory (EFT) methods to a variety of problems across condensed matter and particle physics. Understanding how symmetries are realized by the system can put strong constraints on the low energy EFT which then dictates the macroscopic behavior of the system. We begin by utilizing these techniques to predict the leading order Landau parameter in the normal state of a strongly interacting cold-atomic fermi gas. We then use methods of coset construction to study magnon-phonon interactions in magnetic insulators where we are able to calculate the magnon lifetime as well predict interesting phenomena that can arise from explicit symmetry breaking effects. We also utilize the EFT in the context of dark matter detection to calculate one-magnon and multi-magnon emission rates for dark matter scattering. Finally, we study the dynamical modes of dislocations in solids and make predictions about the dispersion of these modes based on the lattice structure.

Acknowledgments

First and foremost, I would like to thank my advisor Ira Rothstein for letting me work with him on a variety of interesting topics. His continued support and patience has helped me a lot during my graduate career and I was able to appreciate physics more than ever due to his teachings. He will always serve as an inspiration to me for learning physics and beyond.

I would like to thank Riccardo Penco for answering many questions as well as for his valuable advice on a variety of things. I would also like to thank my collaborator Angelo Esposito for introducing me to the exciting area of Dark matter detection and sharing his expertise with me. His enthusiasm and modesty are highly contagious. Additionally, specific thanks to Amit Acharya, Scott Dodelson and Grisha Tarnopolskiy.

I would like to thank my parents and my brother: without their sacrifices, this would not have been possible. I would also like to thank my partner and my best friend, Olga Navros for her unconditional support throughout my graduate school. I am also extremely grateful to her for introducing me to the two most important personalities of my life: Nina and Romie. I could write books about them but for now, I will just say that they showed me how to appreciate life more than anyone.

Lastly, I would like to thank the CMU physics department for all the support they have provided me during my graduate years.

Contents

1 Introduction **2**

2 Effective field theory of strongly interacting cold-atomic fermions **5**
2.1 The EFT 7
2.2 The approach to Non-Fermi Liquid Behavior 9
2.3 Compressibility and Spin Susceptibility 12
2.4 Quasi-particle width 12
2.5 Conclusions 13

3 Effective field theories of Magneto-Elasticity **15**
3.1 Relevant symmetries 16
3.2 Effective actions 18
3.2.1 Spontaneous symmetry breaking pattern 20
3.2.2 Coset construction for phonons and magnons 20
3.2.3 Effective action for phonons and magnons 25
3.3 Phonons 27
3.3.1 The Elasticity equations 27
3.3.2 Phonon Spectrum 29
3.3.3 Power Counting 30
3.4 Magnons 31
3.4.1 Nonlinear Equations of Motion 31
3.4.2 Magnon Spectrum 32
3.4.3 Power counting 33
3.5 Magnon-Phonon interactions 35
3.5.1 Generalized equations of motion 35
3.5.2 Power Counting in the Mixed Theory 36
3.5.3 Magnons in a stressed sample 37
3.5.4 Magnetic Damping 38
3.6 Explicit symmetry breaking 40
3.6.1 Continuum limit of the Heisenberg model 40
3.6.2 Explicit symmetry breaking and spurions 41
3.7 Conclusions 44

4 Optimal anti-ferromagnets for dark matter detection **45**
4.1 The EFT . . . 47
4.1.1 Magnons alone . . . 47
4.1.2 Dark matter–magnon interaction . . . 48
4.2 Event rates . . . 50
4.2.1 One magnon . . . 51
4.2.2 Two magnons . . . 53
4.3 Conclusion . . . 53

5 Dynamical modes of Dislocations and their sensitivity to the UV lattice structure **55**
5.1 The String Action . . . 56
5.2 Effective field theory of solids . . . 57
5.3 Coupling of the Dislocation to bulk Phonons . . . 59
5.4 The Dislocation Action . . . 62
5.5 Conclusion . . . 65

6 Appendix **66**
6.1 WZW term for magnons . . . 66
6.2 Magnons in ferromagnets . . . 67
6.3 Magnon neutron scattering cross-section and EFT matching . . . 68
6.4 Non-relativistic limit of the dark matter interactions . . . 72
6.5 Computation of dark matter event rates . . . 74

List of Tables

3.1 Relevant symmetries of lattice of spins in three spatial dimensions in the continuum limit. Some of these symmetries may be spontaneously and/or explicitly broken. 17

3.2 Transformation properties of various symmetry generators under parity and time-reversal. Each generator X in the first column transforms as $iX \to \pm iX$ with the appropriate sign shown in the second and third column. 18

3.3 Action of the symmetries on the coordinates, the phonon fields π^i, and the magnon fields χ^a. 22

4.1 Coefficients for the anti-ferromagnets considered here. v_θ is taken from the dispersion relation, c_1 is matched from neutron scattering data (Appendix 6.3), and $\Lambda_{\rm UV}$ is estimated as the momentum for which the dispersion relation deviates from linear by 10%. The densities, $\rho_{\rm T}$, are taken from [1]. 49

List of Figures

2.1 The plot shows the phase diagram as a function of the energy and the scattering length. Our prediction for the self-energy is valid below the dilaton mass curve (orange) and above the T_c curve (green). One obtains a Non-Fermi Liquid (NFL) above the dilaton mass curve for large scattering lengths. As the scattering length decreases, the dilaton starts to decouple and one obtains a conventional Fermi Liquid (FL). 14

3.1 Schematic representation of the ground state spin configuration of (*a*) ferromagnets, (*b*) antiferromagnets, and (*c*) ferrimagnets. 19
3.2 Feynman diagram describing the emission of a phonon from a magnon 38

4.1 Projected reach at 95% C.L. for a kilogram of material and a year of exposure assuming zero background, for the magnetic dipole (**upper panel**) and pseudo-mediated (**lower panel**) models. For the latter we assume $\Omega_\chi/\Omega_{\rm DM} = 0.05$. The lowest mass region is reached via the two-magnon channel. The gray region corresponds to masses for which gapped magnons are expected to play an important role. The magnetization is taken to be parallel to the Earth's velocity. 52

To go in the dark with a light is to know the light.
To know the dark, go dark. Go without sight,
and find that the dark, too, blooms and sings,
and is traveled by dark feet and dark wings.

- Wendell Berry, To Know the Dark

Chapter 1

Introduction

The condensed matter community has seen a plenitude of exciting developments over the last decade. It has allowed us to create, control and manipulate systems involving novel interactions with great precision. This has not only opened up exciting avenues for application of quantum field theory techniques, but has also pushed the boundaries of our understanding of quantum field theories at low energies.

Condensed matter systems are characterized by finite density states and spontaneously break Poincare' invariance. The excitations in such systems usually differ from the ones commonly found in particle physics and are termed as quasi-particles. At low energies, these degrees of freedom dominate the dynamics of the system and determine their macroscopic properties. Hence understanding their interactions is crucial to predict the behavior of these systems at low temperatures. Also it can help us engineer novel devices where these modes occupy the role traditionally played by electrons.

Since the collective behavior of such systems is governed by low-energy quasiparticles and their interactions, Effective field theory (EFT) techniques are ideally suited to understand their behavior. EFT methods have been notoriously successful in the context of high-energy physics. They allow us to make robust model independent predictions about the behavior of the system. Depending on how symmetries are realized by the system, one is able to construct an effective action for the gapless modes which allows us to make systematic predictions using the methods of quantum field theory.

In this thesis, we will execute the above mentioned goal in a variety of condensed matter settings. Also we will explore an interesting idea of exploiting quasi-particles in condensed matter systems for dark matter detection. In each of the scenarios, the ground state of the system will spontaneously break a host of space-time and/or internal symmetries. After identifying the relevant goldstone modes which result from the symmetry breaking pattern, one is able to construct an effective Lagrangian that describes the long-distance physics.

The thesis is organized as follows. In Chapter 1, we discuss the EFT of cold-atomic Fermions at large scattering length. Understanding strongly correlated materials has been a long-standing interest of the condensed matter community. The simplest such systems are homogeneous cold Fermionic systems which can be created and manipulated in the lab. Understanding these systems is crucial to uncover some of the physics associated with strongly correlated materials. Here we employed EFT methods to make predictions about cold atomic systems at large scattering lengths. At large scattering lengths (unitarity), the system possesses Schrodinger symmetry which is spontaneously broken by the Fermi-sea and this results in a gapless mode (dilaton) in the spectrum. As one decreases the scattering length, the Schrodinger symmetry of the system is broken and the dilaton mode becomes massive. Using anomaly matching we were able to predict the mass of the dilaton as a function of the scattering length and the Contact parameter of the cold fermionic system. The forward scattering interaction mediated by the dilaton exchange is dominant at large scattering lengths and this allowed us to make interesting predictions in the strongly interacting regime.

In Chapter 2 of the thesis, we employed EFT techniques to study magnon-phonon interactions in magnetic insulators. These interactions have shown to play a dominant role in determining spin and heat transport in magnetic materials. We used the coset construction as a tool to systematically construct a low energy effective action for phonons and magnons by utilizing the symmetry breaking pattern of the system. We predicted the magnon decay rates and also derived the non-linear generalization of Landau-Lifshitz and the elasticity equations for ferromagnets, accounting for magneto-elastic effects. In the EFT, we also described a variety of symmetry breaking effects in the context of magnetic systems which lead to magnon-phonon mixing.

In Chapter 3 of the thesis, the EFT of magnons was implemented to study direct detection of sub-MeV dark matter (DM) particles. Collective excitations in quantum materials are a promising avenue to detect light dark matter because of their relatively low energies. If dark matter with spin-dependent interactions couples to electrons in magnetically ordered materials, it can excite magnons which can provide a novel way of detection. An EFT description provides a simple and efficient computational tool in the context of dark matter detection. We computed the single and multi-magnon excitation rates due to DM scattering within the EFT. These rates were computed for some well motivated dark matter models for multiple anti-ferromagnets. Due to higher magnon velocities in anti-ferromagnetic NiO, we found that it has the best DM mass reach for single magnon excitations. The reach is further extended by two-magnon excitations. This is particularly a useful strategy for detecting 1-100 keV mass DM as compared to ferromagnetic magnons since their reach is constrained due to absence of multi-magnon excitations.

Finally in Chapter 4 of the thesis, we studied the dynamics of dislocation modes (dislons) and their interactions with phonons in elastic solids within the context of EFT. Due to the non-locality associated with the scalar description for phonons in

the presence of a dislocation, one has to employ a gauge description to couple the phonon modes to the dislocation line. Integrating out the bulk phonon modes leads to the running of the dislocation worldsheet couplings. Utilizing relaxation conditions for the dislocation, we were able to show that the dispersion was sensitive to the UV lattice structure. For the isotropic case, the dislons have a non-analytic dispersion whereas in the anisotropic case, the non-analytic contribution are subleading in the long-wavelength limit and the dislon behaves like a type-I Goldstone.

Conventions : We work with the mostly plus metric $(-,+,+,+)$, greek (space-time) indices run $(0-3)$ while Roman capital letters $I = 1-3$ correspond to the internal degrees of freedom (or, more precisely, the co-moving coordinate system). Euclidean spatial indices are represented by small Roman letters. Note that after symmetry breaking, we can no longer distinguish between the capital and small Roman indices. Lower case indices $a, b, c..$ run over $1, 2$. We work in units where $\hbar = c = 1$.

Chapter 2

Effective field theory of strongly interacting cold-atomic fermions

The low energy description of Fermi liquids has been textbook material for many years now. Above the critical temperature one can make predictions for observables in terms of a collection of material-dependent Landau parameter(s) f_l, to leading order in an expansion in E/E_F, where E_F is the Fermi energy. Whether considering a metal, or a gas, in general, these couplings are treated as unknown parameters whose values can be determined by independent measurements. However, one might hope that for systems with enhanced symmetries, the couplings might be predictable. As such, it would seem that fermions at unitarity, where the scattering length diverges, would be a compelling system, as it manifests the maximal Schrodinger group symmetry. This group has dilatations and special conformal transformations as its symmetries in addition to Galilean transformations. These systems exhibit universal behavior as a consequence of the divergent scattering length. Recent experimental progress in producing such "uniform quantum gases" [2] via boxed traps, has opened the door to the study of such ideal systems.

However, fermions in the unitary limit can not be described by the canonical Fermi liquid EFT (as described e.g. in [3]) because there is no way to non-linearly realize the spontaneously broken conformal and boost invariance and maintain Fermi liquid behavior, as shown in [4, 5]. At present we do not know how to calculate in a systematic expansion in the unitary limit. Here we will instead calculate far enough away from unitarity that we can treat it as a Fermi liquid but close enough to keep some approximate symmetries. By doing so we will able to predict the aforementioned Landau parameters in a regime where weak coupling $k_F a$ calculations fail. Making any systematic first principle prediction for a strongly coupled theory is an extreme theoretical challenge, and we manage to do so only in a narrow range of parameter space.

To understand how to calculate near unitarity we must first ask why Fermi liquid theory breaks down at unitarity where the atomic underlying theory is invariant under

the full non-relativistic conformal (Schrodinger) group. The existence of the Fermi sea breaks a subset of symmetries: three boosts, dilatations and special conformal transformations. While the breaking of global internal symmetries leads to gapless Goldstone modes, one per broken generator, when spacetime symmetries are broken, this is no longer true [6, 7]. In such a case, the Ward identities can be saturated by excitations which can be arbitrarily wide, i.e. they need not be quasi-particles [1]. At the level of the action, invariance may be maintained despite the dearth of Goldstones. The modes for which the corresponding broken generators' commutator with unbroken translations yields another broken generator (not in the same multiplet) can be eliminated from the action. This is called the Inverse Higgs mechanism (IHM) and one can use the space-time coset construction [6, 7] to determine invariant constraints which eliminate the extra Goldstones. However, there are cases where there are no IHM's at play and yet the Goldstones, which seemingly should be in the spectrum, are not. The classic example of this is He^3 where only boosts are broken, and there are no corresponding Goldstones. In such systems, dubbed "framids" [9], the symmetry is realized by constraining the form of the interactions [5]. In fact, the famous Landau conditions on Fermi liquids is the constraint that must be imposed on the action to ensure boost invariance. Such a condition can be considered a "Dynamical Inverse Higgs Constraint" (DIHC) [5]. In [4] it was shown that in the unitary limit, in three spatial dimensions, the symmetries can be realized by either imposing another DIHC or by the inclusion of a dilaton. In either case the system cannot behave like a canonical Fermi liquid above T_c.

Fermi liquid theory starts with the assumption that quasi-particles (in our case fermionic) exist in the spectrum with widths that scale as $\Gamma \sim E^2$, due to Pauli blocking. Such systems will have two marginal couplings, the "BCS" and forward scattering channels, with the former growing strong in the IR leading to breaking of the particle number $U(1)$ symmetry. However, when interactions in the UV become strong, the Fermi liquid description can break down at which point there may no longer be any stable quasi-particles, leading to non-Fermi liquid behavior. Such is the case for fermion in the unitary limit.

In this paper we explore the approach to this non-Fermi liquid behavior by calculating how the quasi-particle width begins as a function of the scattering length (a). The starting point is the effective field theory of Fermi liquids [3] where we consider small fluctuations around the Fermi surface. We are interested in studying the normal phase of the theory where $T > T_c$. Furthermore, as will be explained below, to maintain calculational control we will keep the scattering length finite yet large, where canonical perturbative methods fail [10].

Our approach begins by utilizing the pattern of spontaneous breaking of space time symmetries. In [4] it was shown that at unitarity, non-Fermi liquid behavior emerges due to the presence of a non-derivatively coupled gapless Goldstone (the dilaton) that arises as a consequence of the symmetry breaking pattern. Typically

[1] For a recent discussion of this issue see [8].

Goldstones are derivatively coupled and therefore decouple in the far IR, however, for spontaneously broken space-time symmetries, for certain symmetry breaking patterns, Goldstone bosons, such as the dilaton, couple non-derivatively [11, 5] leading to a strong coupling in the infra-red.

When we perturb away from unitarity, the dilaton gets gapped, with its mass acting as a control parameter which can be used to study the cross-over behavior. When the mass is non-vanishing but sufficiently small, Fermi liquid behavior is expected and dilaton exchange will dominate the fermion-fermion interaction. Moreover, the dilaton mass can be determined by matching the conformal anomaly, between the UV theory (where it is exactly known) and the IR theory. Using this result, along with the fact that the dilaton coupling is fixed by symmetry, allows us to to predict the s-wave Landau parameter in terms of the scattering length, the effective mass of the fermion and the contact parameter. With this result in hand we then predict the value of the compressibility, spin susceptibility and the quasi-particle lifetime. We will be working with $m = 1$ unless otherwise states, where m is the bare quasiparticle mass.

2.1 The EFT

In the normal phase of a gas of cold atoms the only spontaneously broken symmetries are boosts. Despite this fact, the spectrum has no Goldstone bosons and the broken boosts are still non-linearly realized via the non-trivial (Landau) relation between the effective mass and the p-wave Landau parameter.

The unitary limit in the trivial vacuum is a point of enhanced symmetry realizing the full thirteen parameter Schrodinger group. The Fermi surface spontaneously breaks boosts (K), dilatations (D) and special conformal transformations(C). The way these broken symmetries can be realized was discussed in [4, 5] which for completeness we summarize here. In the case at hand, the Goldstone associated with the breaking of conformal symmetry can be eliminated using the IHC arising from the relation

$$[H, C] = iD, \tag{2.1}$$

leaving only the dilaton, the Goldstone associated with the broken scale invariance. The boost Goldstone called the framon is necessary to write down a Galilean invariant action for the dilaton. However, it was shown in [5], that one can eliminate the framon using an operator constraint called the Dynamical Inverse Higgs constraint (DIHC). In the Fermi liquid theory, the DIHC is nothing but the aforementioned Landau relation. The logical possibility remains that the action obeys further constraints, such that there is no dilaton in the action. However, as shown in [5], without a dilaton in the action the quasi-particle would have to obey a quadratic dispersion relation (as opposed to linear) and the coupling would have to undergo power law running. Moreover, independent of the choice of field variables, at unitarity there still must be a cut in the stress-energy correlation function corresponding to a highly damped

excitation. Moving away from unitarity towards a quasi-particle description, this gapped channel will be nothing but the massive dilaton.

Let us explore the consequences of the existence of a light ($m_\phi \ll E_f$) dilaton in the spectrum. We will treat the dilaton mass as the leading order perturbation in the conformal symmetry breaking, with higher order corrections being down by powers of m_ϕ/E_F. We begin by first writing down the action in the conformal/unitary limit. Since the scattering length diverges in this limit, the only scale in the theory is the Fermi energy E_F. To write down the action for quasi-particles and the dilaton, we utilize the technique of spacetime coset constructions [6, 7] which is a systematic way of non-linearly realizing the symmetries. We present here the results given in [4] and refer the reader to that paper for details.

At the unitary point, the coset element can be written as

$$U = e^{iHt} e^{-i\vec{P}.\vec{x}} e^{-i\vec{K}.\vec{\eta}} e^{-iD\phi} e^{-iC\xi} \tag{2.2}$$

where $\vec{\eta}(x,t), \phi(x,t)$ and $\xi(x,t)$ are the framon, dilaton and Goldstone of the conformal transformation respectively. In the remainder of the work, we will explicitly drop any x and t dependence from the fields. Using the Maurer-Cartan (MC) form, one can extract the covariant derivatives for the Goldstones which transform linearly under the broken group. The coupling of the dilaton ϕ in the quasi-particle action is given by

$$S_\psi = \int dt d^3x \; \psi^\dagger_\sigma (i\partial_t \psi_\sigma - e^{\frac{2\phi}{\Lambda}} \epsilon(e^{\frac{\phi}{\Lambda}} i\vec{\partial})\psi_\sigma) + \frac{f_0}{2}(\psi^\dagger_\sigma \psi_\sigma)^2], \tag{2.3}$$

We have kept only the $l = 0$ Landau parameter. The addition of higher l's will not change our predictions as we shall see.

We have introduced a scale Λ to normalize the dilaton field in the exponential. Under dilatations, the dilaton shifts by a constant $\phi \longrightarrow \phi + c\Lambda$ whereas the coordinates transform as $t \longrightarrow e^{2c}t$ and $x \longrightarrow e^c x$. The quasi-particle fields and their covariant derivatives have to transform as a linear representation of the unbroken group $\psi(x,t) \rightarrow e^{-\frac{3}{2}c}\psi(x,t)$. One is free to add an invariant term of the form $V_{dil} = Ce^{-5\phi/\Lambda}$ to the dilaton Lagrangian. Thus maintaining a light dilaton implies C must be fine tuned to be small, as its natural value is of order of the cut-off. This is analogous to the cosmological constant problem, the most egregious fine tuning in nature. However, in the context of fermions at unitarity, the appropriate fine tuning is achieved by choosing the magnetic field such that the scattering length diverges. At this point, the atoms form a zero-energy bound state, also known as Feshbach resonance.

Expanding around the Fermi surface to leading order in the dilaton field ϕ in the quasi-particle action,

$$S_\psi = \int d^3x \, dt \; \frac{\phi}{\Lambda} \psi^\dagger_\sigma \psi_\sigma (2\epsilon(k_F) - \vec{\partial}_p \epsilon(k_F) \cdot \vec{k}_F) + ... \tag{2.4}$$

where we have dropped terms sub-leading in the power expansion, since momenta normal to the Fermi surface scale as λ. It is convenient to re-express this coupling in terms the Fermi velocity $\vec{v}_F \equiv \vec{\partial}_p \epsilon(k_F)$ then

$$S_\psi = \int d^3x\, dt\, \frac{\phi}{\Lambda} \psi^\dagger_\sigma \psi_\sigma \left(2\epsilon(k_F) - v_F k_F\right) + ... \tag{2.5}$$

Notice that in the free limit, $\epsilon(k_F) = k_F^2/2m$, this coupling vanishes. For notational convenience we define

$$\delta E \equiv \left(2\epsilon(k_F) - v_F k_F\right) \tag{2.6}$$

which quantifies deviation from the canonical dispersion relation. For systems near unitarity $\delta E/E_F < 1$.

Power counting dictates that the dilaton momenta must scale homogeneously under an RG transformation in all directions ($\vec{p} \to \lambda \vec{p}$) and thus will only scatter nearby points on the Fermi surface. Any other choice of scalings would lead to a power suppression. The quasi-particle and the dilaton energies scale in the same way as we move towards the Fermi surface ($\omega \sim \lambda\omega$). From the kinetic terms in the dilaton and quasi-particle actions, we can read off the scaling of the momentum space dilaton and quasi-particle fields

$$\psi(p,t) \sim \lambda^{-1/2} \qquad \phi(p,t) \sim \lambda^{-2}. \tag{2.7}$$

The scaling of the dilaton-quasi-particle interaction is marginal as can be seen by going to momentum space and noting that, as in the four point quasi-particle interaction, the delta function enforcing the three-momentum conservation scales as $1/\lambda$ while the momentum space measure will scale as

$$d^3p_1 d^3p_2 d^3k \sim \lambda^5, \tag{2.8}$$

as all three momentum components of the dilaton, as well as the quasiparticle momenta along the direction normal to the Fermi surface, scale as λ.

2.2 The approach to Non-Fermi Liquid Behavior

As we move away from the unitary point, the scattering length becomes finite and scale invariance becomes an approximate symmetry of the effective theory. Hence the dilaton becomes a gapped pseudo-goldstone. As we will see, we can determine the mass of dilaton in terms of the scattering length and the contact parameter. We are working in the units where the fermion mass is one and $\hbar = 1$, the length dimensions will be

$$[t] = 2 \qquad [\phi] = -\frac{1}{2} \qquad [\psi] = -\frac{3}{2}. \tag{2.9}$$

Away from unitarity, the conformal symmetry is explicitly broken, however if we keep the scale of explicit symmetry breaking (the inverse scattering length) small

compared to the scale of spontaneous symmetry breaking (the Fermi wave number) we may still treat the dilaton as a pseudo-Goldstone boson. The smallness of the dilaton mass follows from the fact that the scattering length is tuned to be large. The mass of the dilaton is treated as a spurion such that the action is invariant if we scale it according to its dimensions.

$$\delta L = \frac{1}{2} m_\phi^2 \phi^2 \tag{2.10}$$

We now use a matching procedure to calculate m_ϕ. In the effective theory away from unitarity, the scale current is not conserved.

$$\partial_\mu s^\mu = m_\phi^2 \Lambda \, \phi \tag{2.11}$$

We will use current algebra to extract the mass by matching it onto the full theory result. From the Noether construction the dilatation charge is given by

$$D^0(0) = \Lambda \int d^3x \, \pi(\vec{x}, 0) \tag{2.12}$$

where $\pi(x)$ is the conjugate momentum to ϕ. Hence using (9) we have

$$\int_x [D^0(0), \partial_\mu s^\mu(\vec{x}, 0)] = \int d^3x \, m_\phi^2 \Lambda^2 \tag{2.13}$$

We match this commutator to the full theory, which is a microscopic description of the theory, in terms of fermions with action

$$S = \int dt \int d^3x \, i\chi^\dagger \partial_t \chi + \frac{1}{2} \chi^\dagger \nabla^2 \chi + g(\mu)(\chi^\dagger \chi)^2 \tag{2.14}$$

where χ is two-spinor. The Van der Waals scale(Λ_{VDW}), which describes the range of the interaction provides the upper cutoff in the theory that suppresses higher dimensional operators. In the renormalized coupling can be written in terms of the scattering length as [12]

$$g(\mu) = \frac{4\pi}{-\frac{2}{\pi}\mu + \frac{1}{a}}. \tag{2.15}$$

The four-fermion interaction defined in (5.34) explicitly breaks scale invariance. One can verify that the dilatation charge, the divergence of the scale current and their commutators are given respectively by

$$D^0(0) = \int d^3x (\frac{3}{2} \chi^\dagger(\vec{x}, 0)\chi(\vec{x}, 0) + \chi^\dagger(\vec{x}, 0)\vec{x} \cdot \vec{\partial}\chi(\vec{x}, 0)) \tag{2.16}$$

$$\partial_\mu s^\mu = (g(\mu) + \beta(g))(\chi^\dagger \chi)^2 \tag{2.17}$$

$$\int d^3x\, m_\phi^2 \Lambda^2 \;=\; 3\int d^3x\, (g(\mu)+\beta(g))\,(\chi^\dagger\chi)^2. \tag{2.18}$$

Where in (2.18) we have matched the commutators in the full and the effective theory using (2.13). Note that the RHS of (2.18), is an RG invariant, and the dilaton mass is independent of the scale μ. The coupling and the four-fermion operator both depend on the scale μ but the dependence cancels exactly in (2.18) to give a scale independent mass as required. Evaluating the beta function and taking the expectation value, we have

$$m_\phi^2\Lambda^2 \;=\; \frac{3}{4\pi a}\langle g^2\,\chi_\uparrow^\dagger\chi_\uparrow\chi_\downarrow^\dagger\chi_\downarrow\rangle \equiv \frac{3}{4\pi a}\,\mathcal{C}(a) \tag{2.19}$$

where we have now made the spin state explicit and $\mathcal{C}(a)$ is the contact density [13] whose vacuum expectation value is a measure of the local pair density of the fermions and is independent of the RG scale μ. For any system consisting of fermions with two spin states and large scattering length, one can define universal relations which depend on the contact. Note that Λ is still an undetermined free parameter. However, we will see that it will cancel in the calculation of the Landau parameter f_0.

If the dilaton mass is sufficiently small it will dominate the quasi-particles interactions, as other contributions to the interaction, arising from integrating out other modes, will be parametrically suppressed by powers of m_ϕ/E_F, where $E_F = \frac{k_F^2}{2m}$. We integrate out the dilaton to generate net interaction

$$L_{int} = \frac{1}{2}\Big(f_0 + \frac{4\pi a\,\delta E^2}{3\tilde{\mathcal{C}}(a)k_F^4}\Big)(\psi_\sigma^\dagger\psi_\sigma)(\psi_{\sigma'}^\dagger\psi_{\sigma'}) \tag{2.20}$$

δE is defined in eq.(2.6). The corrections to this expression are suppressed by powers of $(E^2,T^2)_{max}/m_\phi^2 = \frac{\pi}{3}k_F a\frac{(E^2,T^2)_{max}}{\tilde{\mathcal{C}}(a)E_F^2}$ and we have taken $\Lambda \sim k_F^{1/2}$ as the symmetry breaking scale. $\tilde{\mathcal{C}}(a) = \frac{\mathcal{C}(a)}{k_F^4}$ is the dimensionless contact parameter [14].

Thus if we are in the regime

$$\tilde{\mathcal{C}}(a)\left(\frac{E_F}{(E,T)_{max}}\right)^2 \gg ak_F \gg \tilde{\mathcal{C}}(a)\left(\frac{E_F}{\delta E}\right)^2 k_F f_0 \tag{2.21}$$

then the dilaton exchange dominates so that we have an effective coupling

$$f_D = \frac{4\pi a\,\delta E^2\, m}{3\tilde{\mathcal{C}}(a)p_F^4}, \tag{2.22}$$

where we have re-introduced the factors of $\hbar$ and the atomic mass m. It is important to keep in mind that δE as defined in (2.6) depends upon a itself in non-perturbative way that can be determined from experiment or possibly simulations. We will make

some estimates for this dependence below to get a handle on the region of validity of the prediction.

Note that since the coupling to the dilaton is scalar in nature, higher angular momentum interactions will be sub-leading in our expansion. Since we are working in the unbroken phase $T_{min} = T_c$, where T_c is the superfluid transition temperature.

2.3 Compressibility and Spin Susceptibility

We can now make a prediction for the compressibility (κ) in terms of f_D, again, as this contribution dominates in the strongly interacting region. We may extract κ from a canonical calculation in the effective theory of the number density response function and it is given by

$$\kappa = \frac{\kappa_0}{1 - \hbar^2 N_F f_D} = \frac{\kappa_0}{1 - \frac{1}{3\pi}\frac{m^\star}{m}\frac{k_F a\, \delta E^2}{\tilde{C}(a) E_F^2}} \tag{2.23}$$

where $N_F = \frac{m^\star p_F}{\hbar^3 \pi^2}$ is the density of states at the Fermi surface and κ_0 is the compressibility of the free Fermi gas. One can obtain $m^\star$ from the measurement of the specific heat of the Fermi gas via the relation $C_v = \frac{m^\star p_F}{3\hbar^3} k_B^2 T$. From (2.23) we find an additional limit of our EFT if we assume the compressibility must be positive

$$a k_F < 3\pi \left(\frac{E_F}{\delta E}\right)^2 \frac{m}{m^\star} \tilde{\mathcal{C}}(a). \tag{2.24}$$

Since the compressibility is a zero frequency observable, this is the appropriate bound on the validity of this particular prediction, as opposed to the upper bound stemming from the LHS[2] of (2.21).

One can also consider the response of the Fermi liquid to an external magnetic field and calculate the spin susceptibility χ. This can be computed straightforwardly in the effective theory and is given by

$$\chi = \frac{\chi_0}{1 + \hbar^2 N_F f_D} = \frac{\chi_0}{1 + \frac{1}{3\pi}\frac{m^\star}{m}\frac{k_F a\, \delta E^2}{\tilde{C}(a) E_F^2}} \tag{2.25}$$

where χ_0 is the susceptibility of the free Fermi gas. Note that the validity bound in (2.24) need not hold for the above prediction. The regime of validity for the spin susceptibility can only be clarified from experiments.

2.4 Quasi-particle width

We may also calculate the quasi-particle width using our result for f_D. The self-energy only gets contributions from the forward scattering coupling, as the other marginal

[2]Note that there is no thermal mass for the dilaton, due to quasi-particle loops, in the large T limit [15], though the width will scale with $\frac{\delta E}{\Lambda} T$.

coupling (BCS) is restricted to back-to-back interactions. The imaginary part of the self energy of a fermi-liquid due to S-wave interaction is $\Gamma_{FL}(E,T) = f_0^2 I(E,T)$, where $I(E,T) = \frac{m_\star^3}{4(2\pi)^3}(E^2 + (\pi kT)^2)$ is the imaginary part of the two-loop self energy diagram at finite temperature[15]. Using our result (2.22) we can then calculate the quasi-particle width

$$\Gamma(E,T) = f_D^2 I(E,T). \tag{2.26}$$

such that,

$$\Gamma(E,T) = \frac{m^\star}{18\pi\,\tilde{\mathcal{C}}(a)^2}\left(\frac{m^\star}{m}\frac{a\,\delta E^2}{4\hbar E_F^2}\right)^2 (E^2 + (\pi kT)^2) \tag{2.27}$$

This prediction is valid in the range defined by eq.(2.21).

The theoretical errors in this predictions are of order

$$\frac{\Delta\Gamma_T}{\Gamma} \sim O\left(\frac{1}{k_F a}\right) + O\left(k_F a\left(\frac{E^2}{E_F^2}\right)\right). \tag{2.28}$$

2.5 Conclusions

It is known that degenerate fermionic systems cross over from Fermi to non-Fermi liquids as unitarity is approached. Symmetry requires that Fermi gases at unitarity manifest a gapless excitation in response to external stress. This "dilaton" mode will look like an over damped sound mode, but it might be hoped to be isolated since we are working in the attractive regime where there is no zero sound. Furthermore, by working below the hydrodynamic limit, there will be no contamination from second sound.

Perturbing away from the unitary limit gaps this mode. For energy scales large compared to the gap, the quasiparticle excitations are expected to behave as in a non-Fermi liquid with a width that scales linearly with the energy. However, as the energy of the quasi-particle drops below the gap the dilaton mediated interaction localizes and Fermi liquid behavior with the width scaling quadratically with energy is expected. The behavior of the system as a function of energy and scattering length is depicted in figure one.

The key insight noted here is that the mass of the dilaton can be fixed by matching the effective theory current algebra to that of the full theory, the result of which leads to a prediction for the mass in terms of the scattering length and contact parameter, which in turn allows us to make a prediction for the quasi-particle lifetime including the normalization. The width is predicted to scale quadratically with the ratio of scattering length to the contact parameter. Note also that the dilaton, because its not derivatively coupled, will only generate the $l = 0$ Landau parameter. Thus we have the additional prediction that the $l = 0$ Landau parameter will dominate all other

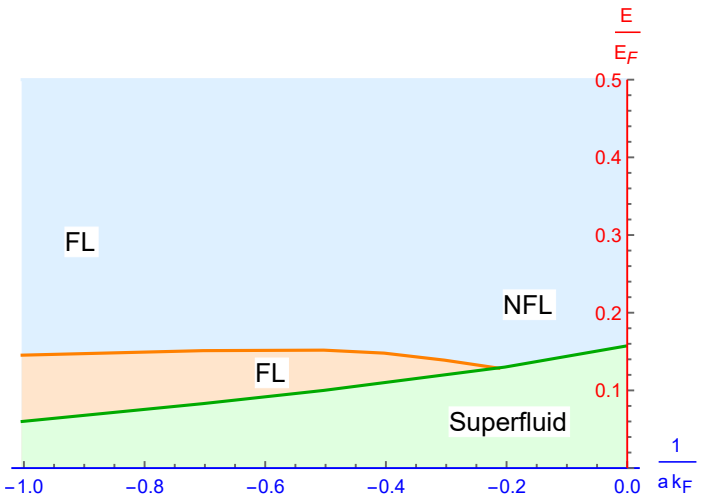

Figure 2.1: The plot shows the phase diagram as a function of the energy and the scattering length. Our prediction for the self-energy is valid below the dilaton mass curve (orange) and above the T_c curve (green). One obtains a Non-Fermi Liquid (NFL) above the dilaton mass curve for large scattering lengths. As the scattering length decreases, the dilaton starts to decouple and one obtains a conventional Fermi Liquid (FL).

channels. We also calculate the compressibility and the spin susceptibilty of the Fermi liquid as a function of the scattering length. These predictions have a limited range of validity. The energy must be small enough that the dilaton exchange can still be treated as a local interaction. This limitation also implies our EFT breaks down when the scattering length, which is inversely proportional to the dilaton mass, becomes large i.e. in the NFL region. However, our method/prediction is non-perturbative in the sense that it is valid up to scattering lengths of order $k_F a \sim 1$ where perturbative EFT techniques [10] fail. Figure one summarizes the bounds on the range of validity of the EFT. For typical, model, values of $\tilde{C}$ and T_c [16, 17], this gives $k_F a < 5$ for the prediction for the width to be valid.

Chapter 3

Effective field theories of Magneto-Elasticity

In this chapter we utilize effective field theory (EFT) techniques to investigate magneto-elastic phenomena in insulators in the long wavelength limit. The interaction between phonons and magnons is a well developed subject. For earlier theoretical work on phonon-magnon interactions, see for instance [18, 19, 20, 21, 22, 23, 24, 25, 26] and for experimental work, see [27, 28, 29]. Here, we will be utilizing the coset construction [30, 31, 32, 33] which, to the best of our knowledge, has yet to be applied to magneto-elastic systems. A primary, but not limited, goal of this paper is to set the stage for understanding the interactions of Skyrmionic with magnons and phonons [34].

Within our EFT approach, the action is completely dictated by the spontaneous symmetry breaking pattern. In the absence of gapless modes which carry conserved quantum numbers (e.g. itinerant electrons), the relevant degrees of freedom at sufficiently low energies are the Goldstone bosons associated with the spontaneously broken global symmetries. The latter act non-linearly on the Goldstone fields, and therefore are not always manifest. The coset construction [31, 30, 32, 33] is a powerful algorithmic tool to generate an effective action for the Goldstone modes which is invariant under all the symmetries, including the ones that are realized non-linearly. The action will be organized as a derivative expansion valid up to a cutoff energy of the order of the spontaneous symmetry breaking scale. We also use this formalism to capture systematically the consequences of a small explicit breaking of certain symmetries–e.g. due to an external magnetic field, or the presence of Dzyaloshinsky-Moriya (DM) interactions among spins.

Solids break a multitude of space-time symmetries, including translations, rotations and boosts. Moreover, homogeneous and isotropic solids possess emergent internal translational and rotational symmetries (see e.g. [35, 36, 37]), which are also spontaneously broken in the ground state, as will be discussed below. We should stress that the assumption of isotropy is convenient but by no means necessary. It is straightforward to relax this assumption and consider instead a finite subgroup of rotations (for

a relativistic solid, this was done for instance in [38]). The relevant symmetries and the associated generators are given in Table 3.1. The resulting symmetry breaking pattern is summarized in Eq. (3.2).

Magneto-elastic interactions are characterized by a multitude of scales, and the derivative expansion can be implemented in different ways depending upon whether or not there are hierarchies among them. We will refer to these possible choices as different *power counting schemes*. For simplicity of presentation we will make a simple choice of scales. Exploring other hierarchies can be achieved by minor variations. Our EFT approach can in principle predict a large number of effects from first principles. Here, we will only focus on a set of illustrative observables calculated in a particular power counting scheme.

3.1 Relevant symmetries

Given the non-relativistic nature of the system we are considering, the appropriate space-time symmetry group is the Galilean group, which is comprised of time and spatial translations, spatial rotations, Galilean boosts, and total mass (or, equivalently, particle number). As we will discuss at length below, the *spontaneous* breaking of Galilean invariance, places non-trivial constraints on the dynamics of the system, which in turn enhances predictive power.

Our system also admits a number of internal symmetries including spin rotations and, if we restrict ourselves to homogeneous and isotropic systems, an emergent internal $ISO(d)$ symmetry [37] (in d spatial dimensions) whose implementation will be discussed in the next section.

All these continuous symmetries and their corresponding generators are summarized in Table 3.1. The generators satisfy an algebra whose only non-vanishing commutators are

$$\begin{aligned} [L_i, K_j] &= i\epsilon_{ijk} K_k, & [L_i, P_j] &= i\epsilon_{ijk} P_k, \\ [K_i, H] &= -iP_i, & [K_i, P_j] &= -iM\delta_{ij}, \\ [Q_i, T_j] &= i\epsilon_{ijk} T_k, & [Q_i, Q_j] &= i\epsilon_{ijk} Q_k \\ [S_A, S_B] &= i\epsilon_{ABC} S_C \ . & [L_i, L_j] &= i\epsilon_{ijk} L_k \end{aligned} \tag{3.1}$$

Notice in particular that the internal symmetry generators Q_i, S_A and T_i, commute with all the generators of the Galilei group, as befits the generators of internal symmetries.

Symmetries	**Generators**
Time translations:	H
Spatial translations:	P_i
Spatial rotations:	L_i
Galilean boosts:	K_i
Total mass:	M
Spin rotations:	S_A
Homogeneity:	T_i
Isotropy:	Q_i

Table 3.1: Relevant symmetries of lattice of spins in three spatial dimensions in the continuum limit. Some of these symmetries may be spontaneously and/or explicitly broken.

Generators	Parity	Time-reversal
H	$+$	$-$
P_i	$-$	$+$
L_i	$+$	$+$
K_i	$-$	$-$
M	$+$	$-$
S_A	$+$	$+$
T_i	$-$	$+$
Q_i	$+$	$+$

Table 3.2: Transformation properties of various symmetry generators under parity and time-reversal. Each generator X in the first column transforms as $iX \to \pm iX$ with the appropriate sign shown in the second and third column.

Discrete symmetries such as parity and time-reversal will also play an important role in what follows. The transformation properties of the above generators under these symmetries are listed in Table 3.2. Under parity and time-reversal, each generator X in the first column transforms as $iX \to \pm iX$ with the appropriate sign shown in the second and third column. A factor of "i" was included in these transformation rules for later convenience, to more easily account for the fact that time-reversal is implemented in a way that is anti-linear and anti-unitary (as opposed to parity, which is linear and unitary). Notice however that our transformation rules are equivalent to the ones that some readers may already be familiar with. For instance, the transformation rule of the spin S_A under time reversal, which we write as $iS_A \to iS_A$, is equivalent to $S_A \to -S_A$ owing to the anti-linear nature of time-reversal.

3.2 Effective actions

In this section, we will discuss the way in which the symmetries are realized in (anti-)ferromagnets and ferrimagnets. We first address how some of these symmetries are spontaneously broken, and derive the effective action for the ensuing Goldstone modes. A discussion of explicit symmetry breaking is postponed until Section 3.6.

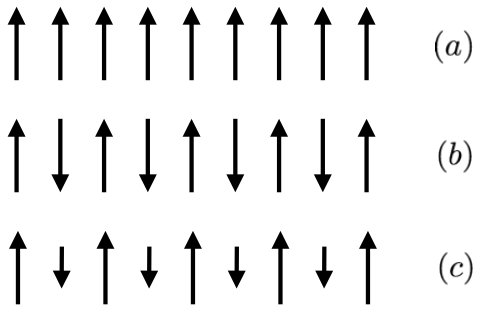

Figure 3.1: Schematic representation of the ground state spin configuration of (a) ferromagnets, (b) antiferromagnets, and (c) ferrimagnets.

3.2.1 Spontaneous symmetry breaking pattern

The full symmetry group will be denoted by G with elements g, while the unbroken subgroup will be denoted by H with elements h. The vacuum manifold corresponds to the coset G/H. (Anti-)ferromagnets and ferrimagnets have the same symmetry breaking pattern save for time reversal, as depicted in Figure 3.1. Including lattice effects, all three cases possess the following spontaneous breaking pattern:

$$unbroken = \begin{cases} H \\ P_i + T_i \equiv \bar{P}_i \\ L_i + Q_i \equiv \bar{L}_i \\ S_3 \\ M \end{cases}, \quad broken = \begin{cases} K_i \\ T_i \\ Q_i \\ S_1, S_2 \equiv S_a \end{cases}, \tag{3.2}$$

where we have assumed the spins to be oriented along the "3" direction. This pattern describes all the spin configurations in Figure 3.1. The distinction between these cases can be understood by recalling that $S_A \to -S_A$ under time-reversal. Thus, the first configuration (ferromagnets) maximally breaks time-reversal invariance, the second one (antiferromagnets) preserves it, and the last one (ferrimagnets) once again breaks it, but in a more "gentle way", as the amount of breaking is controlled by the difference between the magnitude of the spins pointing upward and those pointing downwards. In other words, time-reversal gets restored in the limit where these spins have the same magnitude. As is well known, the fate of time-reversal invariance turns out to have a significant effect on the spectrum of gapless modes (see *e.g.* [39]), which will be discussed in Section 3.4.2.

At this stage, it is worth pointing out that, since T_i and Q_i are spontaneously broken, P_i and L_i must be as well in order for the linear combinations $\bar{P}_i$ and $\bar{L}_i$ to remain unbroken. In fact, broken generators are always defined only up to the addition of unbroken ones. The broken generators listed above are just one particular choice of bases for the coset space of broken symmetries. Moreover, since some of these are space-time symmetries, not all the broken generators in our basis will give rise to Goldstone modes [40]. As we will see, phonons and magnons are the only Goldstone modes associated with the symmetry breaking pattern in Eq. (3.2).

3.2.2 Coset construction for phonons and magnons

Starting from the symmetry breaking pattern (3.2), there exists a systematic procedure, known as the *coset construction*, [31, 30, 33, 32] to write down a low energy effective action for the Goldstone modes. A modern and concise review of this technique can be found for instance in Sec. 2 of [41]. We will now apply it to the problem at hand

to write down an effective action for phonons and magnons.[1]

The starting point of a coset construction is a choice of parametrization of the vacuum manifold. The parametrization that we will work with is

$$\Omega = e^{-iHt} e^{ix^i \bar{P}_i} e^{i\eta^i K_i} e^{i\pi^i T_i} e^{i\theta^i Q_i} e^{i\chi^a S_a}. \tag{3.3}$$

There is a considerable amount of freedom involved in choosing this parameterization, as the order of the exponentials and the basis of broken generators are to a large extent arbitrary. However, different choices are connected to each other by a field redefinition and thus generate identical predictions for physical quantities. One can think of Ω as the most general broken symmetry transformation, supplemented by an unbroken spatial and time translation.

The fields η^i, π^i, θ^i and χ^a in Eq. (3.3) are the Goldstone modes associated with the spontaneous breaking of K_i, T_i, Q_i and S_a respectively and their transformation rules under the action of G is defined by the equation [33]

$$g\,\Omega(t, x, \Phi) = \Omega(t', x', \Phi')\, h(\Phi, g), \tag{3.4}$$

where $\Phi = \{\eta^i, \pi^i, \theta^i, \chi^a\}$, and h is some element of the unbroken subgroup that generically depends on the Goldstone fields as well as the group element g.

As previously mentioned, not all of these modes are physically independent of each other. In fact, we will see in a moment that the fields η^i and θ^i can be removed while preserving all the symmetries by imposing certain "inverse Higgs" constraints [47]. The remaining fields, π^i and χ^a, will respectively describe phonon and magnon excitations. The transformation properties of coordinates, phonon fields, and magnon fields are summarized in Table 3.3.

Starting from the coset parametrization Ω, one can calculate the Maurer-Cartan form defined as $\Omega^{-1}d\Omega$:

$$\begin{aligned}\Omega^{-1}d\Omega = i\Big\{ &- H dt + \bar{P}^i(\eta^i dt + dx^i) - M(\eta^i dx^i + \tfrac{1}{2}\vec{\eta}\cdot\vec{\eta}\, dt) + Q^i \tfrac{1}{2}\epsilon^{ijk}\left[R^{-1}(\theta)dR(\theta)\right]_{jk} \\ &+ K^i d\eta^i + T^j\left[(dx^i + d\pi^i)R^{ij}(\theta) - \eta^j dt - dx^j\right] + S^a \tfrac{1}{2}\epsilon^{aBC}\left[O^{-1}(\chi)dO(\chi)\right]^{BC}\Big\},\end{aligned} \tag{3.5}$$

where we have introduced the matrices $R_{ij} \equiv \left(e^{i\theta^i Q_i}\right)_{ij}$ and $O_{AB} \equiv \left(e^{i\chi^a S_a}\right)_{AB}$. Note that this result follows using only the algebra in Eq. (3.1), and as such, can be obtained without committing to any particular representation for the group generators.

[1] For separate discussions of magnons and (relativistic) phonons based on the coset construction, see respectively [39, 42] and [37]. The low-energy effective theory of (anti-)ferromagnets was also discussed in [43, 44, 45, 46].

	t'	$\vec{x}'$	$\pi_i'(t', \vec{x}')$	$\chi_a'(t', \vec{x}')$
H	$t + c$	$\vec{x}$	$\pi_i(t, \vec{x})$	$\chi_a(t, \vec{x})$
$\bar{P}_i$	t	$\vec{x} + \vec{a}$	$\pi_i(t, \vec{x})$	$\chi_a(t, \vec{x})$
$\bar{L}_i$	t	$R_{ij}^{-1}(\vec{\theta})x_j$	$R_{ij}^{-1}(\vec{\theta})\pi_j$	$\chi_a(t, \vec{x})$
S_3	t	$\vec{x}$	$\pi_i(t, \vec{x})$	$R_{ab}^{-1}(\theta_3)\chi_b(t, \vec{x})$
M	t	$\vec{x}$	$\pi_i(t, \vec{x})$	$\chi_a(t, \vec{x})$
K_i	t	$\vec{x} - \vec{v}t$	$\pi_i + v_i t$	$\chi_a(t, \vec{x})$
Q_i	t	$\vec{x}$	$R_{ij}^{-1}(\vec{\theta})\phi_j - x_i$	$\chi_a(t, \vec{x})$
T_i	t	$\vec{x}$	$\pi_i + c_i$	$\chi_a(t, \vec{x})$
S_a	t	$\vec{x}$	$\pi_i(t, \vec{x})$	$\chi_a(t, \vec{x}) + \omega_a + ...$
$\mathbf{P}$	t	$-\vec{x}$	$-\pi_i(t, \vec{x})$	$\chi_a(t, \vec{x})$
$\mathbf{T}$	$-t$	$\vec{x}$	$\pi_i(t, \vec{x})$	$\chi_a(t, \vec{x})$

Table 3.3: Action of the symmetries on the coordinates, the phonon fields π^i, and the magnon fields χ^a.

Even though we are considering a non-relativistic system, it is convenient to use the relativistic notation where $x^\mu = (t, x^i)$, and define $\bar{P}_t \equiv -H$. We should stress that this is just a matter of notational convenience, and we are not imposing Lorentz invariance. With this notation, we can rewrite the Maurer-Cartan form as follows:

$$\begin{aligned}\Omega^{-1}d\Omega \;\equiv\; & i dx^\nu e_\nu{}^\mu \big(\bar{P}_\mu + \nabla_\mu \pi^i T_i + \nabla_\mu \theta^i\, Q_i + \nabla_\mu \eta^i K_i \\ & + \nabla_\mu \chi^a S_a + A_\mu M + A'_\mu S_3\big). \end{aligned} \tag{3.6}$$

This equation *defines* the "covariant derivatives" of the Goldstones $\nabla_\mu \pi^i, \nabla_\mu \theta^i, \nabla_\mu \eta^i$ and $\nabla_\mu \chi^a$, as well as the "connections" A_μ and A'_μ and vierbein $e_\nu{}^\mu$, which read:

$$e_0{}^0 = 1, \quad e_i{}^j = \delta^i_j, \quad e_i{}^0 = 0, \quad e_0{}^i = \eta^i \tag{3.7a}$$
$$\nabla_t \pi^i = (\partial_t \phi^j - \eta^k \partial_k \phi^j) R_j{}^i(\theta) \tag{3.7b}$$
$$\nabla_j \pi^i = \partial_j \phi^k R_k{}^i(\theta) - \delta^i_j \tag{3.7c}$$
$$\nabla_t \theta^i = \tfrac{1}{2}\epsilon^{ikl}\left[R^{-1}(\theta)(\partial_t - \eta^j \partial_j) R(\theta)\right]_{kl} \tag{3.7d}$$
$$\nabla_j \theta^i = \tfrac{1}{2}\epsilon^{ikl}\left[R^{-1}(\theta)\partial_j R(\theta)\right]_{kl} \tag{3.7e}$$
$$\nabla_t \eta^i = \partial_t \eta^i - \eta^j \partial_j \eta^i \tag{3.7f}$$
$$\nabla_j \eta^i = \partial_j \eta^i \tag{3.7g}$$
$$\nabla_t \chi^a = \tfrac{1}{2}\epsilon^{aBC}\left[O^{-1}(\chi)(\partial_t - \eta^j \partial_j) O(\chi)\right]_{BC} \tag{3.7h}$$
$$\nabla_j \chi^a = \tfrac{1}{2}\epsilon^{aBC}\left[O^{-1}(\chi)\partial_j O(\chi)\right]_{BC} \tag{3.7i}$$
$$A_t = \tfrac{1}{2}\vec{\eta}^2 \tag{3.7j}$$
$$A_i = -\eta_i \tag{3.7k}$$
$$A'_t = \tfrac{1}{2}\epsilon^{ab}\left[O^{-1}(\chi)(\partial_t - \eta^j \partial_j) O(\chi)\right]_{ab} \tag{3.7l}$$
$$A'_j = \tfrac{1}{2}\epsilon^{ab}\left[O^{-1}(\chi)\partial_j O(\chi)\right]_{ab} \tag{3.7m}$$

where we have defined $\phi^i \equiv x^i + \pi^i$ to streamline the notation. ϕ^i's are the comoving coordinates of the solid, which at equilibrium (i.e. when $\pi^i = 0$), can be chosen to be aligned with the physical coordinates x^i [35].

The fields η^i and θ^i can now be removed from the theory in a way that is compatible with all the symmetries by solving the inverse Higgs constraints [47]

$$\nabla_t \pi^i \equiv 0, \qquad\qquad \nabla_{[i}\pi_{j]} \equiv 0. \tag{3.8}$$

The first constraint can be solved immediately for η^i and yields $\eta^i = \partial_t \pi^j (D^{-1})_j{}^i$, with $D_{ij} \equiv \partial_i \phi_j$. The second constraint can instead be solved for $R_{ij}(\theta)$ using the same strategy employed for instance in Sec. V of [37]. After substituting both solutions back into the remaining covariant derivatives, the low-energy effective action will only

depend on the phonon field π^i and the magnon field χ^a through the combinations:[2]

$$\nabla_{(i}\pi_{j)} = (D\sqrt{D^T D}D^{-1})_{ij} - \delta_{ij} \tag{3.9a}$$

$$\nabla_t \chi^a = \frac{1}{2}\epsilon^{aBC}\left\{O^{-1}[\partial_t - \partial_t \pi^k (D^{-1})_k{}^j \partial_j] O\right\}_{BC} \tag{3.9b}$$

$$\nabla_i \chi^a = \frac{1}{2}\epsilon^{aBC}(O^{-1}\partial_i O)_{BC}\,, \tag{3.9c}$$

where $D_{ij} = \partial_i \phi_j = \delta_{ij} + \partial_i \pi_j$ and, once again, $O_{AB} \equiv \left(e^{i\chi^a S_a}\right)_{AB}$.

Covariant derivatives of η's and θ's, once expressed solely in terms of the fields π^i and χ^a, turn out to have a higher number of derivatives per field compared to the ones in Eqs. (3.9). Thus, these quantities can be neglected at lowest order in the derivative expansion. Moreover, the coset connections A_μ and A'_μ are needed only if one is interested in higher covariant derivatives of the π's and χ's, or in couplings with additional fields. In this paper we won't be interested in either, and therefore these connections won't play any role for our purposes.

By combining the building blocks (3.9) in a way that preserves the unbroken symmetries in Eq. (3.2), one can write down all the terms in the low-energy effective action that are *exactly* invariant under all the symmetries, including the ones that are broken spontaneously. However, the latter are realized non-linearly and thus are not manifest. Therein lies the power of the coset construction.

There are also some terms that we can write down that are invariant only up to a total derivative. Following the high-energy physics terminology (see e.g. [48]), we will generically refer to these terms as Wess-Zumino-Witten (WZW) terms, even though they do not have a topological origin and their coefficient is not quantized. These kind of terms can be obtained systematically by combining the 1-forms that appear in front of the various generators in Eq. (3.5) to build 5-forms α that are exact, i.e. $\alpha = d\beta$, and manifestly invariant under all unbroken transformations.[3] Once again, the coset construction ensures that any α built this way is actually invariant under all the symmetries—including the broken ones. Therefore, the 4-form β is in principle allowed to shift by a total derivative under a symmetry transformation [49, 48, 50], and its integral is in general a WZW term.[4] Using the solutions to the inverse Higgs constraints (3.8), we can always express these WZW terms solely in terms of π's and χ's.

For the system under consideration, there are two WZW terms that we should include in our effective Lagrangian. In particular, note that if we were restricted to our building blocks (3.9) our action would not have time derivatives acting on the

[2]Notice that, although it's not obvious, the tensor $(D\sqrt{D^T D}D^{-1})$ that appears in (3.9a) is actually symmetric. This can be checked explicitly by working perturbatively in the fields π^i.

[3]More generally, in d space-time dimensions one would need to consider a $(d+1)-$form α that is exact.

[4]More precisely, not all the terms built this way will be WZW terms, since they could turn out to be accidentally exactly invariant. However, all WZW terms can be built this way [49].

phonon field. In order to write down WZW terms, it is convenient to denote with ω_X the 1-form associated with the generator X in the Maurer-Cartan form (3.5) up to an over all factor of "i". Hence, with this notation we have for instance $\omega_H = -dt$, and so on. The two exact 5-forms that we we can write down are then

$$\begin{aligned}\alpha_\pi &= \epsilon_{ijk}\delta_{\ell m}\omega_{K_m} \wedge \omega_{\bar{P}_\ell} \wedge (\omega_{\bar{P}_i} + \omega_{T_i}) \wedge (\omega_{\bar{P}_j} + \omega_{T_j}) \wedge (\omega_{\bar{P}_k} + \omega_{T_k}) \\ &= d\left[\left(\eta_\ell dx^\ell + \tfrac{1}{2}\bar{\eta}^2 dt\right) \wedge d\phi^i \wedge d\phi^j \wedge d\phi^k \epsilon_{ijk}\right] \qquad (3.10a) \\ \alpha_\chi &= \epsilon_{ijk}\epsilon_{ab}\,\omega_{S_a} \wedge \omega_{S_b} \wedge (\omega_{\bar{P}_i} + \omega_{T_i}) \wedge (\omega_{\bar{P}_j} + \omega_{T_j}) \wedge (\omega_{\bar{P}_k} + \omega_{T_k}) \\ &= d\left[2\epsilon^{ab}(O^{-1}dO)_{ab} \wedge d\phi^i \wedge d\phi^j \wedge d\phi^k \epsilon_{ijk}\right]. \qquad (3.10b)\end{aligned}$$

The derivation of the RHS of Eq. (3.10b) is summarized in Appendix 6.1. Once again, notice that the 5-forms above are fully invariant under all the symmetries, even though they are manifestly invariant only under the unbroken ones. The 4-forms that give rise to the relevant WZW terms are the ones in square brackets on the RHS of Eqs. (3.10). Using the solutions to the inverse Higgs constraints, we can then write down the WZW terms explicitly as follows:

$$\mathcal{L}^\pi_{WZW} \equiv \frac{c_1}{2}\det(D)\,[\partial_t \pi^j (D^{-1})_j{}^i]^2 \qquad (3.11a)$$

$$\mathcal{L}^\chi_{WZW} \equiv \frac{c_2}{2}\det(D)\,\epsilon^{ab}\left[(O^{-1}\partial_t O)_{ab} - \partial_t \pi^k (D^{-1})_k{}^j (O^{-1}\partial_j O)_{ab}\right] \qquad (3.11b)$$

with c_1, c_2 arbitrary coefficients.

Up until now we have only concerned ourselves with invariance under continuous symmetries. However, time-reversal plays a crucial role in determining the spectrum of low-energy excitations in magnetic systems. It is straightforward to derive how space-time coordinates and Goldstone fields transform under parity and time-reversal. To this end, we require that the coset parametrization Ω remains invariant when the broken generators transform according to the rules summarized in Table 3.2. This leads to the transformation rules shown in Table 3.3.

Using these results, we infer that $\nabla_{(i}\pi_{j)}, \nabla_t\chi^a$, $\mathcal{L}^\pi_{WZW}, \mathcal{L}^\chi_{WZW}$ $(\nabla_i\chi^a)$ are even (odd) under parity, whereas $\nabla_{(i}\pi_{j)}, \nabla_i\chi^a, \mathcal{L}^\pi_{WZW}$, $(\nabla_t\chi^a, \mathcal{L}^\chi_{WZW})$ are even (odd) under time-reversal.

Finally, we should point out that, although the quantities in Eqs. (3.9) and (3.11) have been derived in three dimensions, they can be used in any number of spatial dimensions d, provided one lets the lowercase indices $i, j, k, ...$ run from 1 to d. In the remainder of this paper we will mostly restrict ourselves to the $d = 3$ case, unless otherwise stated.

3.2.3 Effective action for phonons and magnons

At low-energies and large distances, the most relevant terms in the Lagrangian will be those with the least number of derivatives. In practice, this requirement means

something slightly different for the phonon field π^i and the magnon field χ^a, i.e. the derivative expansion is implemented differently on the two fields. This can be easily seen from the fact that, unlike the χ's, each π in Eqs. (3.9) and (3.11) appears with a derivative.[5] Therefore at lowest order in the derivative expansion, anharmonic corrections to the free Lagrangian for phonons and magnons are suppressed by higher powers of $\partial_i \pi^j$ and χ^a (which, with our conventions, are both dimensionless). When these quantities are small, one can safely expand the terms in Eqs. (3.9) and (3.11) in powers of $\partial\pi$ and χ and keep only the first few terms. This is certainly the appropriate thing to do if we are interested in studying small fluctuations around a particular ground state of the system—as we will do for instance in Secs. 3.3.2 and 3.4.2.

It is however not necessary to perform such an expansion at this stage. In fact, by keeping intact the non-linear structures in (3.9) and (3.11) we will be able to also describe non-trivial field configurations where the first derivative of the phonon field is of order one, with second derivatives being suppressed. A similar approach is taken in General Relativity where the Einstein-Hilbert action can be derived starting from spin-2 perturbations around a particular ground state—the Minkowski vacuum—and then resumming all non-linear interactions that are dictated by symmetry, locality, and self-consistency [51]. This action can then be used to describe spacetimes other than Minkowski as long as higher derivative curvature invariants for these solutions remain small in units of the cutoff.

Since magnons do not carry one derivative per field, we allow the field itself to vary at the order one level, but its first derivatives must remain small in units of the cutoff. We can systematically include higher derivative corrections at the cost of introducing additional unknown Wilson coefficients.

Thus, we are going to use the full expression for our Goldstone covariant derivatives and WZW terms, and write down the most general effective Lagrangian that contains one derivative on each π, and the least possible number of derivatives on the χ's. For ferromagnets, this requirement leads to the following effective Lagrangian:

$$\mathcal{L}_{\text{ferromagnets}} = \mathcal{L}^{\pi}_{WZW} + \mathcal{L}^{\chi}_{WZW} - F_1(u) - \tfrac{1}{2} F_2^{ij}(u)\, \nabla_i \chi_a \nabla_j \chi^a, \tag{3.12}$$

where we have defined $u_{ij} \equiv \nabla_{(i}\pi_{j)}$ for notational convenience, F_1 and F_2^{ij} admit an *a priori* arbitrary series expansion in powers of u_{ij}. Notice that the i-type indices and a-type indices cannot be contracted with each other, because the former transform under $\bar{L}_i$, whereas the latter under S_3. Moreover, we have not included a term of the form $\nabla_t \chi_a \nabla_t \chi^a$ which would contain a term quadratic in χ with two time derivatives, because for ferromagnets it is subleading compared to $\mathcal{L}^{\chi}_{WZW}$ which contains a quadratic term with only one time derivative. The latter, in turn, is allowed only because time-reversal is broken. Hence, this term cannot appear in the effective Lagrangian for anti-ferromagnets, which reads:

$$\mathcal{L}_{\text{antiferromagnets}} = \mathcal{L}^{\pi}_{WZW} - F_1(u) - \tfrac{1}{2} F_2^{ij}(u) \nabla_i \chi_a \nabla_j \chi^a + \tfrac{1}{2} F_3(u) \nabla_t \chi_a \nabla_t \chi^a. \tag{3.13}$$

[5]The reason for this is that the phonons are associated with a broken Abelian group.

The leading kinetic term for the χ's now comes from the last term in Eq. (3.13) rather than from $\mathcal{L}^{\chi}_{WZW}$, and this leads to a different dispersion relation for magnons [39], as we will see in a moment.

Finally, the low-energy excitations in ferrimagnets derive their kinetic term from an interplay between the term $\nabla_t\chi_a\nabla_t\chi^a$ and $\mathcal{L}^{\chi}_{WZW}$. The coefficient c_2 in $\mathcal{L}^{\chi}_{WZW}$ is much smaller than in ferromagnets since its size is determined by the scale at which time reversal is spontaneously broken, which in ferrimagnets is parametrically smaller than the scale at which all other symmetries are broken. Thus, the effective action for ferrimagnets is:

$$\mathcal{L}_{\text{ferrimagnets}} = \mathcal{L}^{\pi}_{WZW} + \mathcal{L}^{\chi}_{WZW} - F_1(u) - \tfrac{1}{2}F_2^{ij}(u)\nabla_i\chi_a\nabla_j\chi^a + \tfrac{1}{2}F_3(u)\nabla_t\chi_a\nabla_t\chi^a. \tag{3.14}$$

3.3 Phonons

Let us start by turning off the magnon field and focusing on the phonons. Then, our effective Lagrangian reduces to

$$\mathcal{L} \to \frac{c_1}{2}\det(D)\,[\partial_t\phi^j(D^{-1})_j{}^i]^2 - F_1(u), \tag{3.15}$$

where, as the reader may remember, we have previously defined $D_{ij} = \partial_i\phi_j$ and $u_{ij} = (D\sqrt{D^TD}D^{-1})_{ij} - \delta_{ij}$.

3.3.1 The Elasticity equations

It is convenient to exploit the fact that, in an isotropic system, the function F_1 depends only on the $SO(3)$-invariant contraction of the tensor u_{ij}. In any such contraction, the outermost tensors D and D^{-1} drop out. This means that F_1 can also be regarded as an arbitrary function of $\sqrt{D^TD}$ or, equivalently, $(D^TD)_{ij} = \partial_k\phi_i\partial^k\phi_j \equiv B_{ij}$, which is the metric in the co-moving coordinate system. Therefore, we can work with the Lagrangian

$$\mathcal{L} \to \frac{c_1}{2}\det(D)\,[\partial_t\phi^j(D^{-1})_j{}^i]^2 - F_1(B), \tag{3.16}$$

where, with a slight abuse of notation, we have replaced $F_1(u) \to F_1(B)$.

This action admits a simple physical interpretation if we think of the ϕ^i's as comoving coordinates—meaning that $\phi^i(x)$ labels the volume element at position x. Denoting by $\rho(\phi^i)$ the mass density in the comoving frame, the mass density in the lab frame is [35]

$$\rho(x) = \rho(\phi^i)\det(\partial_i\phi_j). \tag{3.17}$$

This quantity is actually the zero component of the identically conserved current[6]

$$J^\mu = \frac{\rho(\phi)}{3!}\epsilon^{\mu\nu\rho\sigma}\partial_\nu\phi^i\partial_\rho\phi^j\partial_\sigma\phi^k\epsilon_{ijk}. \tag{3.18}$$

From this current, we can deduce the velocity at which volume elements move around in the lab frame:

$$v^i = \frac{J^i}{J^0} = -(\partial_t\phi^j)(D^{-1})_j{}^i. \tag{3.19}$$

With this identification, the equation $\partial_\mu J^\mu = 0$ reproduces the standard continuity equation, $\partial_t\rho + \partial_i(\rho v^i) = 0$. Notice that this result for v^i is consistent with the covariant derivative in eq. (3.9b), where the time derivative becomes the "fisherman derivative".

Moreover, homogeneity implies that the comoving mass density must be a constant, i.e. $\rho(\phi^i) = \bar{\rho}$. This can be deduced more formally by noting that the symmetry generators T_i act on the fields ϕ^i as constant shifts: $\phi^i \to \phi^i + c^i$. As a result, we see that the first term in the Lagrangian (3.16) is just the usual kinetic energy $\frac{1}{2}\rho v^2$ with the identification $c_1 \equiv \bar{\rho}$; the second term can be thought of as a potential energy contribution.

The equations of motion can be obtained as usual from the Euler-Lagrange equations for π^i, or equivalently ϕ^i, that follow from the Lagrangian (3.16). However, as is usually the case for Goldstone fields, their equation of motion are also equivalent to the conservation equations for the associated broken generators. In our case, the equations for the phonons follow from the conservation equations for the "homogeneity generators" T_i. Equivalently, we can also consider the equations for momentum conservation, since the momentum generators P_i and the T_i's are equivalent up to an unbroken generator: $T_i = \bar{P}_i - P_i$. We therefore consider

$$\partial_\mu T^{\mu i} = 0, \tag{3.20}$$

with

$$T^{\mu i} = \frac{\partial L}{\partial(\partial_\mu\phi^j)}\partial^i\phi^j - \eta^{\mu i}L. \tag{3.21}$$

An explicit calculation of $T^{\mu i}$ yields

$$T^{0i} = \bar{\rho}(\det D)(\partial_t\phi^k(D^{-1})^i_k) = -\rho v^i \tag{3.22a}$$

$$T^{ij} = \frac{\partial L}{\partial D^{ik}}D^{jk} - \delta^{ij}L = -\rho v^i v^j + \sigma^{ij}. \tag{3.22b}$$

where we have identified the *stress tensor*

$$\sigma_{ij} \equiv \tilde{F}_1\delta_{ij} - 2\frac{\partial\tilde{F}_1}{\partial B^{k\ell}}\partial_i\phi^k\partial_j\phi^\ell. \tag{3.23}$$

[6]By identically conserved we mean that this is not a Noether current that follows from a symmetry of the Lagrangian (3.16).

Then, leveraging the conservation of the current (3.18), Eq. (3.20) reduces to the familiar elasticity equations:

$$\rho(\partial_t + v^j\partial_j)v^i = \partial_j\sigma^{ji}, \tag{3.24}$$

3.3.2 Phonon Spectrum

Let us now expand the Lagrangian (3.16) up to quadratic order in the π fields to derive the existence of phonon excitations in the static unstressed ground state $\langle\phi^I\rangle = x^I$. Expanding B_{ij} in the phonon fields π's, we find

$$B_{ij} = \delta_{ij} + \partial_i\pi_j + \partial_j\pi_i + \partial_k\pi_i\partial^k\pi_j \tag{3.25}$$

At quadratic order in the π fields the Lagrangian is then given by

$$\mathcal{L}^{(2)}_\pi = \tfrac{c_1}{2}\partial_t\pi^i\partial_t\pi_i - \tfrac{c_4+c_5}{2}(\partial_i\pi^i)^2 - \tfrac{c_5+c_3}{2}\partial_i\pi_j\partial^i\pi^j \tag{3.26}$$

where the coefficients c_3, c_4 and c_5 are defined by the relations:

$$\left.\frac{\partial F_1}{\partial B^{ij}}\right|_{\delta_{ij}} \equiv \frac{c_3}{2}\delta_{ij} \tag{3.27}$$

$$\left.\frac{\partial^2 F_1}{\partial B^{ij}\partial B^{kl}}\right|_{\delta_{ij}} \equiv \frac{c_4}{4}\delta_{ij}\delta_{kl} + \frac{c_5}{4}(\delta_{ik}\delta_{jl} + \delta_{jk}\delta_{il}). \tag{3.28}$$

where we have utilized the isotropy of the background. Given the assumption of isotropy, we can decompose the strains into their irreducible components

$$\partial_i\pi_j = (S_{ijkl} + A_{ijkl} + T_{ijkl})\partial_k\pi_l \tag{3.29}$$

where S_{ijkl}, A_{ijkl} and T_{ijkl} are the projectors onto the symmetric-traceless, anti-symmetric and the trace parts.

$$\begin{aligned} S_{ijkl} &= \frac{1}{2}(\delta_{ik}\delta_{jl} + \delta_{il}\delta_{jk}) - \frac{1}{3}\delta_{ij}\delta_{kl} \\ A_{ijkl} &= \frac{1}{2}(\delta_{ik}\delta_{jl} - \delta_{il}\delta_{jk}) \\ T_{ijkl} &= \frac{1}{3}\delta_{ij}\delta_{kl} \end{aligned} \tag{3.30}$$

It is easy to see that the anti-symmetric part is just the θ goldstone and can be set to zero since we have integrated it out. The irreducible components of the strains are orthogonal to each other. The decomposition in (3.29) allows us to re-write the action in (3.26) as

$$\mathcal{L} = \frac{c_1}{2}(\partial_t\pi^i)^2 - \frac{c_5+c_3}{2}(S_{ijkl}\partial^k\pi^l)^2 - \frac{4c_5+3c_4+c_3}{2}(T_{ijkl}\partial^k\pi^l)^2 \tag{3.31}$$

This puts constraints on the coefficients of the Lagrangian

$$G \equiv c_5 + c_3 > 0 \quad 3K \equiv 2c_5 + 3c_4 - c_3 > 0 \tag{3.32}$$

where we have identified the coefficients with the shear G and bulk modulus K. This is straightforward to see since the trace part only contributes to pure compression whereas the traceless symmetric part contributes to pure shear of the material. It is now convenient to decompose π^i into the sum of a longitudinal part π^i_L and a transverse part π^i_T, such that

$$\vec{\nabla} \cdot \vec{\pi}_T = 0, \qquad \vec{\nabla} \times \vec{\pi}_L = 0. \tag{3.33}$$

It follows from the Lagrangian (3.31) that these two components satisfy two different wave equations, which admit solutions—the sound waves, or phonons—with linear dispersion relations $\omega^2 = v^2_{L,T} k^2$, and longitudinal and transverse speeds given by

$$v_L^2 = \frac{4G + 3K}{3\bar{\rho}} \qquad v_T^2 = \frac{G}{\bar{\rho}} \tag{3.34}$$

From (3.32), this implies that $v_L^2 > \frac{4}{3} v_T^2$.[7]

3.3.3 Power Counting

The effective Lagrangian (3.16) is the leading term in a suitably defined derivative expansion. This means that the elasticity equations we derived from it are only valid to the extent that higher derivative corrections are negligible. Similarly, the quadratic Lagrangian (3.26) can be trusted only if it is safe to neglect the non-linear corrections that arise by expanding (3.16) to higher orders in π^i. Under what circumstances are these good approximations?

To address this question, we will make the simplifying assumption that v_L and v_T are of the same order, which we will schematically denote with v_π. Then, the effective action (3.16) can be written as

$$\frac{S}{\hbar} = \int dt d^3r \, \frac{\bar{\rho}\, v_\pi^2}{\hbar} \, \mathcal{L}(\dot{\pi}/v_\pi, \partial_i \pi_j), \tag{3.35}$$

where we have momentarily reintroduced an explicit factor of $\hbar$ to make dimensional analysis more transparent. On naturalness grounds, we will assume that the Lagrangian density $\mathcal{L}$—which is a dimensionless function of dimensionless arguments—only contains coefficients of order one. This implies immediately that quadratic Lagrangian (3.26) is a good approximation for field configurations such that $\dot{\pi}/v_\pi, \partial_i \pi_j \ll 1$.

It is convenient to introduce a new time variable $t' \equiv v_\pi t$. This is equivalent to introducing new units such that time is measured in the same units as lengths, and

[7] See however [52] for an interesting UV model that violates this bound.

the sound speeds are dimensionless numbers of $\mathcal{O}(1)$. In these new units, the action above becomes

$$\frac{S}{\hbar} = \int dt' d^3r \, \frac{\bar{\rho}\, v_\pi}{\hbar} \, \mathcal{L}(\partial_{t'}\pi, \partial_i \pi_j). \tag{3.36}$$

This action now depends on a single length scale, $L_\pi \equiv (\bar{\rho} v_\pi/\hbar)^{-1/4}$, which therefore should be identified with the length cutoff of our effective theory. This means that higher derivative corrections to (3.36) must appear in the combinations $L_\pi \partial_i$ and $L_\pi \partial_{t'} = (L_\pi/v_\pi)\partial_t$. Hence, our effective action can reliably describe phonon excitations with frequencies $\omega \ll v_\pi/L_\pi$ and wave-numbers $|\vec{k}| \ll 1/L_\pi$.

3.4 Magnons

In the incompressible limit one can neglect the phonon field, and the effective Lagrangian for the magnon fields reduces to

$$\mathcal{L} \to \frac{c_2}{2}\epsilon^{ab}(O^{-1}\partial_t O)_{ab} + \frac{c_6}{2}(\nabla_t \chi_a)^2 - \frac{c_7}{2}(\nabla_i \chi_a)^2, \tag{3.37}$$

where we have defined $F_3(u=0) \equiv c_6$ and $F_2^{ij}(u=0) \equiv c_7 \delta^{ij}$. The coefficient c_2 is $\sim (c_6 c_7)^{3/4}$ for ferromagnets, $\ll (c_6 c_7)^{3/4}$ for ferrimagnets, and vanishes for antiferromagnets.

3.4.1 Nonlinear Equations of Motion

As we did for the phonons in the previous section, we can easily derive the non-linear equations of motion for the magnons. This will allow us to make contact with the standard literature on magnetism. To this end, it is convenient to perform the following field redefinition:

$$\chi_1 \equiv \theta \sin\phi, \qquad \chi_2 \equiv -\theta\cos\phi\,, \tag{3.38}$$

and to introduce the unit-norm vector

$$\hat{n} = O(\chi)\hat{x}_3 = (\sin\theta\cos\phi, \sin\theta\sin\phi, \cos\theta). \tag{3.39}$$

In terms of these new fields, after some algebra, the Lagrangian (3.37) becomes

$$\mathcal{L} \to \; -c_2\,\dot{\phi}\cos\theta + \tfrac{c_6}{2}(\partial_t \hat{n})^2 - \tfrac{c_7}{2}(\partial_i \hat{n})^2. \tag{3.40}$$

Note that the first term doesn't admit a simple expression in terms of $\hat{n}$ because, unlike the other ones, it is only invariant up to a total derivative. This can be easily checked using the fact that $\hat{n}$ transform linearly under spin rotations, and hence that its change under infinitesimal spin rotations is $\delta\hat{n} = \vec{\omega} \times \hat{n}$. This implies that

$$\begin{aligned} \delta\theta &= \omega_y \cos\phi - \omega_x \sin\phi \\ \delta\phi &= \omega_z - \omega_x \cot\theta\cos\phi - \omega_y \cot\theta \sin\phi, \end{aligned} \tag{3.41}$$

or, equivalently, that the χ fields must transform as

$$\begin{aligned}\delta\chi_1 &= -\frac{\omega_x}{1+\chi_1^2/\chi_2^2}(\chi_1^2/\chi_2^2 + \sqrt{\chi_1^2+\chi_2^2}\cot\sqrt{\chi_1^2+\chi_2^2}) \\ \delta\chi_2 &= -\frac{\omega_y}{1+\chi_1^2/\chi_2^2}(1+\chi_1^2/\chi_2^2\sqrt{\chi_1^2+\chi_2^2}\cot\sqrt{\chi_1^2+\chi_2^2}).\end{aligned} \tag{3.42}$$

It is then easy to check that the Lagrangian (3.40) changes by a total time derivative under a spin rotation:

$$\delta\mathcal{L} = -\frac{d}{dt}\left[\frac{1}{\sin\theta}\left(\omega_y\sin\phi + \omega_x\cos\phi\right)\right]. \tag{3.43}$$

Once again, rather than deriving the equations of motion by varying the Lagrangian (3.37) with respect to our fields, we will resort to the conservation of the Noether currents associated with spin rotations. In order to calculate the currents, we must account for the fact that the WZ term is only invariant up to a total time derivative. Including this contribution leads to

$$J_a^\mu = (-n_a, (\vec{\nabla}n\times\hat{n})_a). \tag{3.44}$$

The equations of motion, for θ and ϕ can now be written in a very compact form in terms of $\hat{n}$ by imposing $\partial_\mu J_a^\mu = 0$ to find:

$$c_2\,\partial_t\hat{n} = -(c_6\partial_t^2\hat{n} - c_7\nabla^2\hat{n})\times\hat{n}\,. \tag{3.45}$$

When $c_6\partial_t \ll c_2$, the first term on the righthand side can be neglected, and our result reduces to the well-known *Landau-Lifshitz equation* for ferromagnets [53, 39].

The informed reader will notice that these equations are missing the so-called "Gilbert damping" term, induced by the magnon finite lifetime. As is well known, an action formalism, from which we have derived our equations of motion, is inherently time symmetric. To account for damping one should work within the so-called "in-in" formalism. In section (3.5.4) we will calculate the magnon damping using our formalism. To generate the Gilbert damping would entail using these results in conjunction with the in-in formalism [54].

3.4.2 Magnon Spectrum

Let us now turn our attention to the spectrum of long-wavelength excitations around the ground state. For simplicity, we will work with the Lagrangian (3.37), which strictly speaking is appropriate for ferrimagnets; (anti-)ferromagnets can be easily recovered by taking appropriate limits. These limits will in turn affect the power counting, as we will discuss in the next section.

Expanding (3.37) up to quadratic order in the χ's, we find

$$\mathcal{L}_\chi^{(2)} = \frac{c_2}{2}\epsilon_{ab}\chi^a\partial_t\chi^b + \frac{c_6}{2}\partial_t\chi_a\partial_t\chi^a - \frac{c_7}{2}\partial_i\chi_a\partial^i\chi^a, \tag{3.46}$$

The dispersion relations for the magnon modes then follow by demanding that the determinant of the quadratic kernel vanishes in Fourier space. If the coefficient c_2 doesn't vanish, as is the case for ferri- and ferro-magnets, then one finds that, in the small k limit,

$$\omega_+^2 \simeq \Delta^2 + \mathcal{O}(k^2), \qquad \omega_-^2 \simeq \left(\frac{k^2}{2m}\right)^2 + \mathcal{O}(k^6), \tag{3.47}$$

where we have introduced the gap $\Delta = c_2/c_6$ and the effective mass $m = c_2/(2c_7)$. The gapped modes with dispersion relation ω_+^2 are physical provided c_2 is small enough that the energy gap Δ falls below the cutoff of the effective theory. This is the case for ferrimagnets, but not ferromagnets, as we discuss in the following section and further elaborate on in Appendix 6.2.

When $c_2 = 0$, one instead finds two modes with identical linear dispersion relation:

$$\omega_\pm^2 = v_\chi^2 k^2, \tag{3.48}$$

with the phase velocity equal to $v_\chi^2 = c_7/c_6$. Note that the three parameters that appear in the dispersion relations above are not all independent: they are related to each other by $\Delta = 2mv_\chi^2$. The mechanism by which a term with a single time derivatives can turn a pair of gapless modes with linear dispersion relation into a gapped mode and a mode with quadratic dispersion relation has been studied extensively in the literature—see e.g. [55, 56, 57] and references therein.

3.4.3 Power counting

Let us first consider anti-ferromagnets, where $c_2 = 0$; in this case, the low-energy effective Lagrangian (3.37) acquires an accidental symmetry. Although Galilean boosts appear to be explicitly broken in the incompressible limit, when the phonon fields are neglected, the Lagrangian for antiferromagnets is formally invariant under Lorentz transformations with "speed of light" $v_\chi^2 = c_7/c_6$; indeed, it has the same form as the Lagrangian for a relativistic nonlinear sigma model $SO(3)/SO(2)$. This additional symmetry ensures that the coefficients $c_{6,7}$ get renormalized by nonlinearities in (3.37) in such a way that their ratio remains constant. Higher derivative corrections to (3.37) won't generically preserve this accidental symmetry—even though it would be technically natural for them to do so—and can therefore affect the ratio c_7/c_6.

Because of this accidental symmetry, the power counting scheme for anti-ferromagnets is virtually identical to that for a relativistic theory, with the speed of light replaced by v_χ. Keeping length and time scales separate, we find that the only length scale

that can be built out of c_6 and c_7 is $L_\chi = (c_6 c_7)^{-1/4}$, and the only time scale is L_χ/v_χ. In the absence of fine-tunings, these must be the scales that suppress higher derivative corrections to the effective Lagrangian (3.37) (as usual, up to loop factors of 4π and coefficients of order one).[8] In other words, observables in the effective theory can be calculated in an expansion in powers of $\omega L_\chi/v_\chi$ and kL_χ. Furthermore, non-linearities in (3.37) are suppressed compared to the quadratic terms as long as $\chi^a \ll 1$.

Let us now turn our attention to the case of ferromagnets, where $c_2 \sim L_\chi^{-3}$. The gap Δ becomes comparable to the energy cutoff of the effective theory, i.e. $\Delta \sim v_\chi/L_\chi$ [9], and therefore the corresponding mode exits the regime of validity of the effective theory. An equivalent viewpoint is that the second term in the quadratic Lagrangian (3.46) becomes negligible compared to the first one for $\omega \ll v_\chi/L_\chi$. By themselves, the first and third term describe a single propagating mode with a non-relativistic dispersion relation—the second mode in Eq. (3.47). In fact, combining the χ^a in a single complex field $\Psi = \chi_1 + i\chi_2$, the Lagrangian (3.46) with $c_6 = 0$ reduces to the standard Lagrangian for a non-relativistic field Ψ. Thus, in this case the power counting is implemented exactly like in a theory for non-relativistic point particles (see e.g. [58, 41]).[10]

Finally, let us discuss the case of ferrimagnets, where c_2 is non-zero but small in units of the cutoff, i.e. $c_2 L_\chi^3 \ll 1$. This ratio introduces an additional expansion parameter that controls the soft breaking of time reversal [42]. The low-energy excitations are akin to a light relativistic particle and a heavy non-relativistic particle interacting with each other (of course, the interactions that are not invariant under Galilei nor Lorentz boosts). At energies $\Delta \ll \omega \ll v_\chi/L_\chi$, the gap is negligible and one is left with an essentially gapless mode interacting with a heavy non-relativistic particle; explicit power counting can then be implemented as in non-relativistic QED and QCD [59, 58, 41]. At energies $\omega \ll \Delta$, one can treat also the gapped mode as non-relativistic, and switch to a new effective theory with cutoff Δ that describes soft interactions of two non-relativistic particles with widely separated masses Δ and m. Note that there is no distinction between the various cases

As in the case of the solid we may relate the cut-off to the UV parameters of the theory. There is one fundamental energy scale J, the exchange energy (see section 3.6) and one length scale, the lattice spacing a. Therefore, these must be the length ($L_\chi = a$) and time ($L_\chi/v_\chi = \hbar/J$) scales which suppress higher dimensional operators.

[8] Of course, one can always *engineer* materials where this assumption fails, i.e. higher derivative terms are suppressed by unnaturally small coefficients. In this case, the power counting must be adjusted accordingly.

[9] Here we have used the relation $c_2 \sim (c_6 c_7)^{3/4}$ valid for ferromagnets.

[10] One technical difference compared to ordinary non-relativistic particles is that all magnon self-interactions are suppressed by at least two derivatives.

3.5 Magnon-Phonon interactions

We will finally turn our attention to the coupled system of phonons and magnons. Magnetoelastic effects have already been studied in ferromagnets [60, 61, 26, 62, 63], ferrimagnets [64], and antiferromagnets [65, 66]. However, the focus has been on particular effects (e.g. Spin Seebeck effect [67, 68, 69]) or particular materials (e.g. Yttrium Iron Garnet [28, 63]). In contrast, we are interested in universal low-energy phenomena that follow directly from symmetries. In this section we will derive a few such results.

3.5.1 Generalized equations of motion

We will start by deriving the coupled equations of motion for magnon and phonon fields, which generalize the elasticity and Landau-Lifshitz equations discuss previously. In order to obtain the most general form of these equations, we work with the Lagrangian for ferrimagnets. Using the definition for $\hat{n}$, ρ and $\vec{v}$ we can rewrite Eq. (3.14) as

$$\mathcal{L} = \tfrac{1}{2}\rho v^2 + \mathcal{L}^{\chi}_{WZW} - F_1(B) - \tfrac{1}{2}F_2^{ij}(B)\,\partial_i\hat{n}\cdot\partial_j\hat{n} + \tfrac{1}{2}\rho\tilde{F}_3(B)D_t\hat{n}\cdot D_t\hat{n} \tag{3.49}$$

where in the last term we have used eq. (3.9b) and defined $D_t \equiv (\partial_t + v^i\partial_i)$ and redefined $F_3 = \rho\tilde{F}_3$. Varying this Lagrangian with respect to the magnon fields, we obtain

$$\rho\frac{c_2}{c_1}D_t\hat{n} - \rho\hat{n}\times D_t(\tilde{F}_3 D_t\hat{n}) + \rho\tilde{F}_3\partial_i v^i\hat{n}\times D_t\hat{n} + \hat{n}\times\partial_i(F_2^{ij}\partial_j\hat{n}) = 0, \tag{3.50}$$

while varying with respect to the phonon fields yields:

$$\rho\, D_t\Big[v_i + \frac{c_2}{2c_1}\epsilon^{ab}(O^{-1}\partial_i O)_{ab} + \tilde{F}_3 D_t\hat{n}\cdot\partial_i\hat{n}\Big] = \partial_j(\sigma_{ji} + \bar{\sigma}_{ji} + \tilde{\sigma}_{ji}), \tag{3.51}$$

where

$$\bar{\sigma}_{ji} = (\partial_m\hat{n})\cdot(\partial_p\hat{n})\left[\frac{\delta_{ij}}{2}F_2^{mp} - \frac{\partial F_2^{mp}}{\partial B^{kl}}\partial_k\phi_i\partial_l\phi_j\right] \tag{3.52}$$

$$\tilde{\sigma}_{ji} = -\rho(D_t\hat{n})\cdot(D_t\hat{n})\left[\frac{\delta_{ij}}{2}\tilde{F}_3 - \frac{\partial\tilde{F}_3}{\partial B_{lk}}\partial_i\phi_l\partial_j\phi_k\right]. \tag{3.53}$$

These equations are a generalization of previous works on magneto-elastic equations [70, 71, 72, 73]. Notice that we have used the continuity equation $\partial_t\rho + \partial_i(\rho v^i) = 0$ to simplify Eqs. (3.50) and (3.51). We can recover the equations for ferromagnets (anti-ferromagnets) by setting $\tilde{F}_3 = 0$ ($c_2 = 0$). Interestingly, when the stresses on the right-hand side of Eq. (3.51) are negligible, the quantity that is conserved in a

comoving sense is no longer the local velocity of the solid, but in fact a combination that also involves the magnons. To the best of our knowledge the results for the fully non-linear equations of motion, to leading order in derivatives, (3.50) and (3.51) are novel.

3.5.2 Power Counting in the Mixed Theory

Once we consider both magnons and phonons at the same time, the power counting becomes much more complex. Consider, for instance, the case of antiferromagnets, for which $\mathcal{L}^{\chi}_{WZW} = 0$. We now have two characteristic length scales, L_χ and L_π (which need not be of the same order as their ratio is dictated by the micro-physics), and at least two independent speeds, v_χ and v_π (assuming that longitudinal and transverse speeds are of the same order, which need not be the case). Based on our previous discussions on power counting, the natural expectation is that the functions appearing in the Lagrangian (3.49) scale like

$$F_1 \sim \frac{v_\pi}{L_\pi^4}, \qquad F_2^{ij} \sim \frac{v_\chi}{L_\chi^2}, \qquad \tilde{F}_3 \sim \frac{v_\pi L_\pi^4}{v_\chi L_\chi^2}, \tag{3.54}$$

and that higher powers of $\dot{\pi}$ are suppressed by v_π. Observables should now be calculated in an expansion in powers of $\omega L_</v_>$, $kL_<$, $L_</L_>$, and $v_</v_>$, where $L_>$ ($L_<$) is the largest (smallest) between L_π and L_χ, and similarly for the speeds.

Unfortunately, one cannot associate *a priori* a definite scaling to each term in the Lagrangian (3.49). This is because, when vertices are combined into Feynman diagrams, internal lines can be off-shell but an amount that is controlled by one or more of the expansion parameters listed above. A similar problem occurs in non-relativistic QED and QCD, and it's handled by resorting to the method of regions (see e.g. [74, 59, 58, 41]). Ferro- and ferri-magnets[11] presents a similar challenge, except that the relevant kinematical regions are different compared to those of ferromagnets.

Ultimately, these subtleties related to power counting become relevant only if one wants to calculate higher order corrections in a systematic way. At lowest order, it is usually straightforward to drop subleading corrections and zero in on the leading contribution to whatever process one is interested in. To illustrate this, in what follows we will consider the leading corrections to the propagation of magnons due to couplings with the phonons. At leading order, these effects are captured by interactions in the Lagrangian (3.49) that are quadratic in χ and linear in π

$$\begin{aligned}\mathcal{L}_{\text{int}} =& \frac{c_2}{2}\partial_i\pi^i\epsilon_{ab}\chi^a\partial_t\chi^b - \frac{c_2}{2}\epsilon_{ab}\chi^a\partial_t\pi^i\partial_i\chi^b - \frac{c_8}{2}\partial_k\pi^k\partial_i\chi^a\partial^i\chi^a - c_9\partial_i\chi^a\partial_j\chi^a\partial^{(i}\pi^{j)} \\ &+ \frac{c_{10}}{2}(\partial_i\pi^i)(\partial_t\chi^a)^2 - c_6\dot{\chi}_a\dot{\pi}^k\partial_k\chi_a,\end{aligned} \tag{3.55}$$

[11] As we discussed in the previous section, ferrimagnets feature yet another expansion parameter, $c_2 L_\chi^3$, controlling the amount of time reversal breaking.

where we have defined

$$\frac{\delta F_2^{ij}}{\delta B_{kl}} \equiv \frac{c_8}{2}\delta_{ij}\delta_{kl} + \frac{c_9}{2}(\delta_{ik}\delta_{jl} + \delta_{il}\delta_{jk}), \tag{3.56a}$$

$$\frac{\delta F_3}{\delta B_{ij}} \equiv \frac{c_{10}}{2}\delta_{ij}. \tag{3.56b}$$

It is straightforward to estimate the natural size of the coefficients in (3.55) in terms of $L_{\chi,\pi}$ and $v_{\chi,\pi}$.

3.5.3 Magnons in a stressed sample

Consider now a magnetic material under the application of a constant stress (normal and shear). This causes the atoms to displace from their equilibrium positions, which is captured by a non-zero expectation value for the phonon fields. We will denote the linear strain tensor in the sample by $\gamma_{ij} = \langle \partial_{(i}\pi_{j)} \rangle$. In the limit where the strain is small (note that γ_{ij} is dimensionless), the leading corrections to the quadratic Lagrangian for magnons in Eq. (3.46) will come from the interactions shown in Eq. (3.55) with the phonon fields replaced by their expectation value:

$$\mathcal{L}_{\text{int}} \to \frac{c_2\gamma}{2}\epsilon_{ab}\chi^a\partial_t\chi^b - \frac{c_8\gamma}{2}\partial_i\chi^a\partial^i\chi^a - c_9\gamma^{ij}\partial_i\chi^a\partial_j\chi^a + \frac{c_{10}\gamma}{2}(\partial_t\chi^a)^2, \tag{3.57}$$

where we used the fact that the shear is by assumption time-independent, and we defined $\gamma = \delta^{ij}\gamma_{ij}$.

Assuming moreover that the stress is homogeneous, i.e. that γ_{ij} is just a constant tensor, we can easily derive the corresponding modification to the dispersion relations of magnons. Once again, the case of ferro- and ferri-magnets need to be treated separately from the case of antiferromagnets, for which $c_2 = 0$. The final outcome is that the magnon dispersion relations retain the same qualitative form, but the parameters Δ, m and v_χ^2 get modified as follows:

$$\Delta \to \Delta' = \Delta\left[1 + \gamma\left(1 - \frac{c_{10}}{c_6}\right)\right], \tag{3.58a}$$

$$m \to m' = m\left[1 + \gamma\left(1 - \frac{c_8}{c_7}\right) - 2\frac{c_9}{c_7}\gamma^{ij}\hat{k}_i\hat{k}_j\right], \tag{3.58b}$$

$$v_\chi^2 \to v_\chi^{2\prime} = v_\chi^2\left[1 + \gamma\left(\frac{c_8}{c_7} - \frac{c_{10}}{c_6}\right) + 2\frac{c_9}{c_7}\gamma^{ij}\hat{k}_i\hat{k}_j\right]. \tag{3.58c}$$

Interestingly, it remains true that $\Delta' = 2m'v_\chi^{2\prime}$. We should also emphasize that the full action (3.49) can also be used to calculate the magnon dispersion relations in regimes where $\gamma_{ij} \sim \mathcal{O}(1)$. In that case, however, one needs to take into account the full non-linear structure of the functions $F_i(B)$. The advantage of focusing on small strains is that the coefficients appearing in (3.57) will also control other phenomena, such as the magnetic damping we are about to discuss. The effect of straining the lattice on anti-ferromagnetic magnons has also been studied in [75].

3.5.4 Magnetic Damping

As previously mentioned our analysis has not included the Gilbert damping, which is typically added as a phenomenological term, but for magnetic insulators the damping arises due to magnon decay mediated by the interaction Lagrangian in Eq. (3.55). The decay width can be calculated from the cut diagram, which is the square of the amplitude shown in Fig. 3.2. This process induces a torque on the lattice that contributes to the Einstein-de Haas effect [76]. The converse process, where a phonon emits a magnon, is not allowed unless some of the symmetries are explicitly broken, as will be discussed in the next section. For simplicity, in what follows we are going to focus on (anti-)ferromagnets. Our analysis can be easily extended to the case of ferrimagnets.

Ferromagnets. On general grounds, we would expect interactions with the lowest number of derivatives to give the dominant low-energy contribution to the process shown in Fig. (3.2). In ferromagnets, where $c_2 \neq 0$, this suggests that we focus on the term in the first line of Eq. (3.55). In fact, when the derivatives are estimated on-shell using the dispersion relation appropriate for ferromagnets, we find that

$$\frac{\frac{c_2}{2}\partial_i\pi^i\epsilon_{ab}\chi^a\partial_t\chi^b}{\frac{c_2}{2}\epsilon_{ab}\chi^a\partial_t\pi^i\partial_i\chi^b} \sim \frac{k^3/m}{v_\pi k^2} = \frac{k}{mv_\pi}. \tag{3.59}$$

This means that the second interaction in (3.55) is actually the leading one, i.e.

$$\mathcal{L}_{\rm int} \to -\frac{c_2}{2}\epsilon_{ab}\chi^a\partial_t\pi^i\partial_i\chi^b. \tag{3.60}$$

The corresponding amplitude is given by

$$i\mathcal{M} = -\frac{i}{2\sqrt{c_1}}\,\omega_\lambda(k)\hat{\epsilon}^\star_\lambda(k)\cdot(\vec{p}+\vec{p}') \tag{3.61}$$

where $\omega_\lambda(k)$ and $\hat{\epsilon}_\lambda(k)$ are respectively the dispersion relation and the polarization vector associated with a phonon of polarization λ. Notice also that the amplitude associated with the interaction (3.60) includes a factor of $(1/\sqrt{c_1})(1/\sqrt{c_2})^2$ that accounts for the non-canonical normalization of the phonon and magnon fields.

The total decay rate can be obtained as usual by integrating the amplitude squared over all possible final states that conserve momentum, with a relativistic

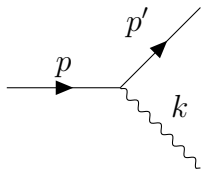

Figure 3.2: Feynman diagram describing the emission of a phonon from a magnon

(nonrelativistic) normalization for the phonon (magnon) states. The explicit results for longitudinal and transverse phonons are:

$$\begin{aligned}\Gamma_L =&\frac{1}{4c_1}\int\frac{d^3p'}{(2\pi)^3}\frac{d^3k}{2\omega_L(k)(2\pi)^3}\omega_L(k)^2\frac{[(\vec{p}+\vec{p}')\cdot\vec{k}]^2}{\vec{k}^2}(2\pi)^4\delta^3(\vec{p}-\vec{p}'-\vec{k})\delta(\omega(p)-\omega(p')-\omega_L(k))\\ =&\frac{2m^3v_L^3}{3\pi\bar{\rho}p}(p-mv_L)^3\theta(p-mv_L),\end{aligned} \tag{3.62}$$

and

$$\begin{aligned}\Gamma_T =&\frac{1}{4c_1}\int\frac{d^3p'}{(2\pi)^3}\frac{d^3k}{2\omega_T(k)(2\pi)^3}\omega_T(k)^2\left\{(\vec{p}+\vec{p}')^2-\frac{[(\vec{p}+\vec{p}')\cdot\vec{k}]^2}{\vec{k}^2}\right\}\\ &\times(2\pi)^4\delta^3(\vec{p}-\vec{p}'-\vec{k})\delta(\omega(p)-\omega(p')-\omega_T(k))\\ =&\frac{mv_T}{15\pi\bar{\rho}p}(p-mv_T)^4\,(4p+mv_T)\,\theta(p-mv_T),\end{aligned} \tag{3.63}$$

where in final results we have used the fact that c_1 is equal to the background density $\bar{\rho}$.

Anti-Ferromagnets. In the antiferromagnetic case, $c_2 = 0$ and the power counting is such that the momentum and energy scale in the same way. This is because both phonons and magnons now have linear dispersion relations: $\omega_{L,T}^2 = v_{L,T}^2k^2$ and $\omega^2 = v_\chi^2p^2$, respectively. Thus all the terms in (3.55) contribute at the same order, and the expressions for the decay rates become more complicated:

$$\Gamma_T = \frac{2p^5(1-\hat{v}_T)\hat{v}_T\,(\hat{v}_T^3+6\hat{v}_T^2+14\hat{v}_T+14)\,(c_6+c_9)^2}{105\pi c_1c_6^2(\hat{v}_T+1)^5}\Theta(1-\hat{v}_T), \tag{3.64}$$

$$\begin{aligned}\Gamma_L =&\frac{p^5}{210\pi c_1c_6^2\hat{v}_L(\hat{v}_L+1)^5}(4c_6^2\hat{v}_L^6+20c_6^2\hat{v}_L^5+32c_6^2\hat{v}_L^4-56c_6c_{10}\hat{v}_L^2+8c_6c_8\hat{v}_L^4+40c_6c_8\hat{v}_L^3\\ &+8c_6c_8\hat{v}_L^2+8c_6c_9\hat{v}_L^6+40c_6c_9\hat{v}_L^5+72c_6c_9\hat{v}_L^4+40c_6c_9\hat{v}_L^3-48c_6c_9\hat{v}_L^2+14c_{10}^2\hat{v}_L^2\\ &-35c_{10}^2\hat{v}_L+35c_{10}^2+28c_{10}c_8\hat{v}_L^2-70c_{10}c_8\hat{v}_L+14c_{10}c_8-140c_{10}c_9\hat{v}_L+84c_{10}c_9\\ &+18c_8^2\hat{v}_L^2-15c_8^2\hat{v}_L+11c_8^2+8c_8c_9\hat{v}_L^4+40c_8c_9\hat{v}_L^3+72c_8c_9\hat{v}_L^2-100c_8c_9\hat{v}_L+36c_8c_9\\ &+4c_9^2\hat{v}_L^6+20c_9^2\hat{v}_L^5+40c_9^2\hat{v}_L^4+40c_9^2\hat{v}_L^3+12c_9^2\hat{v}_L^2-120c_9^2\hat{v}_L+60c_9^2)\Theta(1-\hat{v}_L)\end{aligned}$$

,

(3.65)

where $\hat{v}_{L,T} \equiv v_{L,T}/v_\chi$.

The purpose of this calculation is only illustrative. For one thing the result is a function of the unknown quantities $(v_{L,T}, v_\chi, c_6, c_8, c_9, c_{10})$, all of which would have to be fit from data. Furthermore, phenomenologically, one would typically be more interested in the finite temperature decay rate as as well as the transport lifetime. This analysis was performed for the special case of Yttrium Iron Garnet in [63]. It is straightforward exercise to calculate these quantities in the effective field theory.

3.6 Explicit symmetry breaking

Explicitly breaking internal spin rotations leads to a broad range of interesting phenomena. To gain some physical intuition for how explicit symmetry breaking can arise, we shall begin by recalling the microscopic origin of the symmetric Lagrangian in the incompressible limit, Eq. (3.37).

3.6.1 Continuum limit of the Heisenberg model

The strong coupling expansion of the half filled Hubbard model reduces to the Heisenberg model,

$$H = -J \sum_{\langle ij \rangle} \vec{\mathcal{S}}_i \cdot \vec{\mathcal{S}}_j. \tag{3.66}$$

Since the Hubbard model only involves spin independent nearest neighbor interactions, this Hamiltonian is independent of the magnetic moment. i.e. J only depends upon the matrix element of the Coulomb interaction between electrons centered on neighboring atoms. In this way we can think of the Heisenberg model as an effective theory of the Hubbard model where we have integrated out the atomic orbits. At higher orders in the strong coupling expansion, the Hamiltonian (3.66) gets corrected by the so-called "bi-quadratic" terms of the form

$$\Delta H = -\tilde{J} \sum_{\langle ij \rangle} (\vec{\mathcal{S}}_i \cdot \vec{\mathcal{S}}_j)^2. \tag{3.67}$$

While such terms, if numerically significant, can have considerable effects on the phase transition [77] the low energy theory of Goldstones below the critical point is unchanged by their presence.

Starting from the Heisenberg Hamiltonian (3.66), we can obtain (minus) the static limit of the Lagrangian density (3.40) by taking to the continuum limit. This is accomplished by parameterizing the spins as $\vec{\mathcal{S}}_i \equiv \mathcal{S}\hat{n}_i$, where the magnitude $\mathcal{S}$ is constant and replacing $i \to \vec{r}, j \to \vec{r} + \vec{\delta}$, where $\vec{r}$ is the position of the ith spin with some choice of origin. The sum over nearest neighbors becomes an integral over $\vec{r}$. We

then coarse grain by averaging over the $\vec{\delta}$'s,[12] and take the limit $\vec{\delta} \to 0, \mathcal{S} \to \infty$ with $\delta^2\mathcal{S}^2$ fixed.

The final result is

$$-\mathcal{L}_{\text{static}} = \frac{c_7}{2}(\partial_i \hat{n})^2, \tag{3.68}$$

and $c_7 \sim J\delta^2\mathcal{S}^2$.

3.6.2 Explicit symmetry breaking and spurions

To properly capture the long distance physics of explicit symmetry breaking we utilize a spurion analysis (see e.g. [78]). We will assume that the associated length and time scales are much longer than those at which spontaneous symmetry breaking occurs, so that explicit breaking can be treated perturbatively using spurion fields. The symmetry breaking parameter (in cut-off units) is treated as an additional expansion parameter, whose relative size compared to other corrections will depend upon the energy/length scale of interest.

Zeeman Interactions

Arguably the simplest source of explicit symmetry breaking is the Zeeman coupling between spins and a constant external magnetic field. At the microscopic level, this is described by supplementing the microscopic Hamiltonian with a term

$$\Delta H = -\mu \sum_i \vec{\mathcal{B}} \cdot \vec{\mathcal{S}}_i. \tag{3.69}$$

This interaction explicitly breaks the spin $SO(3)$ down to the $SO(2)$ subgroup that leaves $\vec{\mathcal{B}}$ invariant

The spurion technique amounts to treating the explicit symmetry breaking as if it were a *spontaneous* breaking due to an operator $\vec{\Psi}$—the spurion field—that develops a small expectation value $\langle\vec{\Psi}\rangle = \mu\vec{\mathcal{B}}$. The advantage of this approach is that the spurion can be treated like any other matter field and coupled to the Goldstone modes following the standard rules of the coset construction [79, 33]. The spurion transforms in a linear representation of the full symmetry group (G), $\vec{\Psi} \to g\,\vec{\Psi}$. However, to form invariant using the coset construction we are interested in objects which transform under the unbroken subgroup H. The field $\vec{\Psi}' = \Omega^{-1}\vec{\Psi}$ is such an object as it transforms as $\vec{\Psi}' \to h(\Phi, g)\vec{\Psi}'$, where Φ stands for all the Goldstone fields. However, $\vec{\Psi}'$ transforms reducibly under H so we decompose $\vec{\Psi}'$ into irreducible representations of the unbroken group, i.e. Ψ'_a and Ψ'_3. Finally we add to the effective action terms that depend on these irreps and are manifestly invariant under the unbroken group. To this end it is

[12] By isotropy, we must have $\langle\delta_i\delta_j\rangle \sim \delta^2\delta_{ij}$.

helpful to notice that the microscopic interaction preserves time reversal if the spurion is assumed to be odd, i.e. to transform as $\vec{\Psi} \to -\vec{\Psi}$.

In a ferromagnet, where time reversal is spontaneously broken, we are allowed to write terms involving the spurion that are not invariant under time reversal. Consequently, at leading order in $\mu\mathcal{B}L_\chi/v_\chi$ we have

$$\mathcal{L}_{\text{spurion}} = F(B)\,\Psi'_3 = F(B)\,O^{-1}_{3A}(\chi)\Psi^A = F(B)\hat{n}\cdot\vec{\Psi} \to F(B)\mu\hat{n}\cdot\vec{\mathcal{B}}, \tag{3.70}$$

where in the last step we have replaced the spurion with its expectation value. Since, in the continuum limit, an external magnetic field couples to the Noether density of spin [39], the function $F(B)$ is constrained [13]. More precisely, since the Ferromagnetic spin density is given by $\vec{s} = c_2\text{det}(D)\hat{n}$ for a ferromagnet, this fixes $F(B) = c_2\text{det}(D)$. The operator in (3.70) introduces mixing between magnons and longitudinal phonons when $\vec{\mathcal{B}}$ is not aligned with the unbroken spin direction (the 3 direction, in our notation)[14] . Of course, the incompressible limit ($F(B) =$ constant) of this result could have also been obtained more easily by taking the continuum limit of the microscopic interaction (3.69).

In the case of an antiferromagnet, the leading interaction with the spurion must be invariant under time reversal, and therefore we have

$$\mathcal{L}_{\text{spurion}} = F(B)\,\Psi'_a\nabla_t\chi^a \to F(B)\,O^{-1}_{aA}(\chi)\,\mu\mathcal{B}^A\nabla_t\chi^a. \tag{3.71}$$

Of course, the interaction (3.71) is also allowed for ferromagnets. But in the incompressible limit, this is not the leading correction to the effective action for ferro-magnons. The functional form of $F(B)$ is also constrained in this case from the anti-ferromagnetic spin density to be $\rho\tilde{F}_3(B)$. As in (3.70), this also results in phonon-magnon mixing when $\vec{\mathcal{B}}$ is not aligned with the unbroken spin direction. Interestingly, Zeeman interactions cannot introduce mixing between magnons and transverse phonons—a result that follows straightforwardly from our spurion analysis.

The Dzyaloshinsky-Moriya (DM) interactions

At the microscopic level the Dzyaloshinsky-Moriya (DM) interaction [80, 81] takes the form:

$$H = \sum_{\langle ij\rangle}(\vec{\mathcal{S}}_i \times \vec{\mathcal{S}}_j)\cdot\vec{D}_{ij}, \tag{3.72}$$

where the vector $\vec{D}_{ij}$ depends on two neighboring lattice points, and in perturbation theory can be expressed as a linear combination of matrix elements of the orbital angular momentum operator [82]. This interaction occurs when the inversion symmetry is broken in a material, and leads to the canting of the spins in the ground state. It

[13] We thank Tomas Brauner for pointing this out to us.

[14] When $\vec{\mathcal{B}}$ is not aligned with the magnetization, the system will precess around the field. Damping will eventually lead to alignment on longer time scales.

explicitly breaks spin and spatial rotations down to the diagonal subgroup, generated by $\vec{J} \equiv \vec{S} + \vec{L}$.

At the microscopic level, one can distinguish between two types of DM interactions depending on whether $\vec{D}_{ij}$ is parallel or perpendicular to the lattice vector $\vec{r}_{ij}$ connecting the sites i and j. In the continuum limit, the first case yields the so-called *Bloch-type* DM interactions, which arise for instance in non-centrosymmetric bulk materials [83]. In the second case, the resulting DM interaction is dubbed *Néel-type*. This interaction is anisotropic, and it occurs for example when a thin film ferromagnet is placed on top of a non-magnetic material with a large spin-orbit interaction (interfacial DM interaction) [84]. Significant theoretical and experimental attention has been recently devoted to DM interactions, as they provide a mechanism to stabilize magnetic Skyrmions [85, 86, 87, 88, 89, 90, 91, 92, 93, 94, 95, 96, 97, 98].

Instead of taking the continuum limit of the microscopic interactions (3.72), we are going to use the spurion technique to infer the corresponding terms in the effective action for magnons and phonons. In order to break spatial and spin rotations down to the diagonal subgroup, we need a spurion field that transforms in a non-trivial representations of both symmetries, which we will take to be the fundamental representations for simplicity, i.e. we will use a field Ψ_i^A. There are two distinct ways of implementing the desired explicit breaking by giving a vev to the spurion, and they correspond to the two types of DM interactions mentioned above:

$$\text{Bloch:} \quad \langle \Psi_i^A \rangle = \delta_i^A D_\parallel, \tag{3.73a}$$

$$\text{Néel:} \quad \langle \Psi_i^A \rangle = \epsilon^A{}_{ij} D_\perp^j. \tag{3.73b}$$

In order to couple the spurion to phonon and magnons, we will follow the blueprint outlined for the Zeeman interaction: we first introduce a new field $\Psi' \equiv \Omega^{-1}\Psi$, then break it up into its irreducible representations under the (spontaneously) unbroken group, $\Psi_i'^3$ and $\Psi_i'^a$. The leading symmetry breaking term in the effective Lagrangian is then

$$\mathcal{L}_{\text{spurion}} = F(B)\, \Psi_i'^a \nabla^i \chi_a \to F(B)\, O^{-1}(\chi)^a{}_A \langle \Psi_i^A \rangle \nabla^i \chi_a. \tag{3.74}$$

It is easy to show that, after replacing the spurion with the appropriate expectation values in (3.73) and taking the incompressible limit ($F(B) = \text{constant}$), this spurion action reproduces the familiar expressions for the Bloch and Néel DM interactions:

$$\text{Bloch:} \quad D_\parallel \epsilon_{ijk} \hat{n}^i \partial^j \hat{n}^k, \tag{3.75a}$$

$$\text{Néel:} \quad D_\perp^j (\hat{n}_j \partial_i \hat{n}^i - \hat{n}^i \partial_i \hat{n}^j). \tag{3.75b}$$

Away from the incompressible limit, the coupling (3.74) gives rise to a kinetic mixing between the longitudinal phonon and either $\partial_a \chi^a$ (Bloch) or $\epsilon^{ab}\partial_a \chi_b$ (Néel). This however is not the only source of kinetic mixing, since one should also consider the operator

$$\mathcal{L}'_{\text{spurion}} = F'(B)\, \Psi_i'^a \nabla^{(i} \pi^{j)} \nabla_j \chi_a. \tag{3.76}$$

which additionally generates a kinetic mixing between magnons and the transverse phonons. See e.g. [99, 100, 101, 102] for recent work on phonon-magnon mixing.

3.7 Conclusions

We have demonstrated how to build an effective field theory for magneto-elastic interactions using the space-time coset construction. The action non-linearly realizes all of the broken symmetries in a long wavelength approximation. The action includes all orders in the fields with a fixed number of derivatives, which makes the theory valid for any background where $\partial^2\chi/\Lambda_\chi^2 \ll 1$. We have also shown how to systematically include the effects of explicit symmetry breaking due to Zeeman and DM interactions. Other symmetry breaking terms can be included using the same line of reasoning as presented in the last section. We have presented several new results most important of which are eqs. (3.50) and (3.51) that generalized the Landau-Lifshitz equations to allow for incompressibility. Applications of our formalism to Skyrmionic physics will follow in a subsequent publication.

Chapter 4

Optimal anti-ferromagnets for dark matter detection

There is today overwhelming evidence that most of the matter in the Universe is dark. Despite that, the question about its nature arguably remains among the biggest ones in fundamental physics. In particular, the possible dark matter mass spans a range of several orders of magnitude. In light of stringent constraints on heavy WIMPs [103, 104, 105, 106, 107, 108], recent years have witnessed an increasing interest in models for sub-GeV dark matter [109, 110, 111, 112, 113, 114, 115, 116, 117, 118, 119, 120], also motivating new detection ideas. In particular, dark matter candidates in the keV to GeV range, while still heavy enough to be considered as particles, cannot release appreciable energy via standard nuclear recoil. They therefore require detectors with low energy thresholds, such as semiconductors [121, 122, 123, 124, 125, 126, 127, 128], superconductors [129, 130, 131, 132, 133], Dirac materials [134, 135, 136], lower dimensional materials [137, 138, 139, 140], and so on (see also [141, 142, 143]).

Among these, the proposals based on superfluid ^{4}He [144, 145, 146, 147, 148, 149, 150, 151, 152, 153, 154, 155, 156] and solid crystals [157, 158, 159, 160, 161] aim at detecting the collective excitations (phonons) produced by the spin-*independent* interaction of dark matter with the nuclei in the material—for an overview see [162, 163, 164]. These collective modes have typical energies below $\mathcal{O}(100$ meV), and are therefore sensitive to particles as light as $m_\chi \sim \mathcal{O}(\text{keV})$. Different proposals for the detection of single phonons have been recently put forth [165, 166, 167, 168].

The targets above are, however, not the most suitable ones to probe possible scenarios where spin-*dependent* interactions of dark matter with the Standard Model are dominant over the spin-independent ones. In this regard, it has been proposed to use ferromagnets [169, 170, 171], i.e. materials that exhibit a non-zero macroscopic magnetization in their ground state.[1] The dark matter can interact with the individual spins in the target, exciting their local precession: a propagating collective mode

[1]The materials presented in [169, 170] are actually insulating ferrimagnets. This makes no difference in our discussion [172]. We refer to ferromagnets, which are conceptually simpler.

called magnon. The proposals to detect single magnons involve either calorimetric readout [169], using TES or MKID, or quantum sensors, which instead couple the magnon mode to a superconducting qubit [173, 174, 175]. A generic ferromagnet features several magnon types (branches). However, for sufficiently light dark matter ($m_\chi \lesssim 10$ MeV, for the typical material [169]), the momentum transfer becomes smaller than the inverse separation between the spins. In this regime the event rate is dominated by the emission of gapless magnons which, for ferromagnets, are characterized by a quadratic dispersion relation, $\omega(q) = q^2/(2m_\theta)$, with m_θ a mass scale set by the properties of the material under consideration. Moreover, as we argue below, conservation of total magnetization implies that, when only gapless magnons are allowed, no more than one can be produced in each event. Thus, for $m_\chi \lesssim 10$ MeV, the maximum energy that can be released to a ferromagnet is $\omega_{\rm max} = 4T_\chi x/(1+x)^2$, with T_χ the dark matter kinetic energy and $x \equiv m_\theta/m_\chi$. Typically, $m_\theta \sim \mathcal{O}(\text{MeV})$ (e.g., $m_\theta \simeq 3.5$ MeV for $Y_3Fe_5O_{12}$ [169], see also [176, 177]), and a sub-MeV dark matter will not deposit all its energy to the target.

In this work, we show that, instead, *anti*-ferromagnets are optimal materials to probe the spin-dependent interactions of light dark matter. Similarly to ferromagnets, they also exhibit magnetic order in the ground state, but the spins are anti-aligned, leading to a vanishing macroscopic magnetization. This leads to two crucial differences: (1) gapless magnons have a linear dispersion relation, $\omega(q) = v_\theta q$, and (2) the interaction with the dark matter can excite any number of them. If only one magnon is emitted, the maximum energy that can be transferred to the anti-ferromagnet is $\omega_{1,\rm max} = 4T_\chi y(1-y)$, with $y \equiv v_\theta/v_\chi$. One of the anti-ferromagnets we consider here, nickel oxide, features magnons with a propagation speed surprisingly close to the typical dark matter velocity, which allows it to absorb most of the kinetic energy even through a single magnon mode. This is a well-known and well-studied material, which makes it a particularly ideal target. Moreover, the possibility of exciting several magnons in a single event relaxes the kinematic constraints above, allowing any anti-ferromagnet to absorb the totality of the dark matter kinetic energy, hence being sensitive to masses down to $m_\chi \sim \mathcal{O}(\text{keV})$.

In what follows, we describe anti-ferromagnets and their interaction with dark matter via an effective field theory (EFT) [39, 178, 172]. This elucidates the role played by conservation laws in allowing multi-magnon emission and allows the computation of the corresponding event rates in a simple way, bypassing the difficulties encountered with more traditional methods [179, 180, 181].

4.1 The EFT

4.1.1 Magnons alone

One can often picture an atom in a magnetic material as having a net spin coming from the angular momentum of the electrons localized around it. The Coulomb interaction between electrons pertaining to different atoms induces a coupling between different spins which, in turns, causes magnetic order in the ground state [182]. In an anti-ferromagnet these interactions are such that the spins are anti-aligned along one direction (Figure 3.1), which from now on we take as the z-axis. One can then define an order parameter, the so-called Néel vector, as $\boldsymbol{\mathcal{N}} \equiv \sum_i (-1)^i \boldsymbol{\mathcal{S}}_i$, where $\boldsymbol{\mathcal{S}}_i$ is the i-th spin and $(-1)^i$ is positive for those sites pointing 'up' in the ordered phase, and negative for those pointing 'down'. In the ground state the Néel vector acquires a non-zero expectation value, $\langle \boldsymbol{\mathcal{N}} \rangle \neq 0$ [39].

In the non-relativistic limit, a system of 3-dimensional spins enjoys an internal $SO(3)$ symmetry. The ground state described above breaks it spontaneously down to only the rotations around the z-axis, $SO(3) \to SO(2)$, and the gapless magnons are nothing but the associated Goldstone bosons. As such, at sufficiently low energies, they are described by a universal EFT, very much analogous to the chiral Lagrangian in QCD. A convenient way of parametrizing the magnons is as fluctuations of the order parameter around its equilibrium value, $\hat{\boldsymbol{n}} \equiv e^{i\theta^a S_a} \cdot \hat{\boldsymbol{z}}$, with $a = 1, 2$. Here $\theta^a(x)$ is the magnon field and S_a are the broken $SO(3)$ generators.

The EFT Lagrangian is derived purely from symmetry considerations. First of all, one notes that under time reversal each spin changes sign, $\boldsymbol{\mathcal{S}}_i \to -\boldsymbol{\mathcal{S}}_i$. If combined with a translation by one lattice site, which swaps spin 'up' with spin 'down', this leaves the ground state unchanged. The effective Lagrangian for anti-ferromagnets must then be invariant under the joint action of these two symmetries. At large distances, translations by one lattice site do not affect the system, and the only requirement is time reversal: the Lagrangian must feature an even number of time derivatives [39]. Moreover, the underlying crystal lattice spontaneously breaks boosts. Assuming, for simplicity, that the material is homogeneous and isotropic at long distances, this implies that there must be explicit invariance under spatial translations and rotations, but that space and time derivatives can be treated separately.[2] Since $|\hat{\boldsymbol{n}}| = 1$, the most general low-energy Lagrangian for the gapless magnons in an anti-ferromagnet is then [39, 172],

$$\begin{aligned} \mathcal{L}_\theta &= \frac{c_1}{2}\left(\partial_t \hat{\boldsymbol{n}}\right)^2 - \frac{c_2}{2}\left(\partial_i \hat{\boldsymbol{n}}\right)^2 \\ &= \frac{c_1}{2}\left(\dot{\theta}^a\right)^2 - \frac{c_2}{2}\left(\partial_i \theta^a\right)^2 + \dots \,, \end{aligned} \tag{4.1}$$

[2] We treat the underlying solid as a background which spontaneously breaks some spacetime symmetries. The corresponding Goldstone bosons, the phonons, realize these symmetries non-linearly and can be included in the description if necessary [172].

where in the second equality we expanded in small fluctuations around equilibrium. The coefficients $c_{1,2}$ depend on the details of the anti-ferromagnet under consideration, and cannot be determined purely from symmetry.

One recognizes Eq. (4.1) as the real representation of the Lagrangian of a complex scalar, corresponding to two magnons with linear dispersion relation, $\omega(q) = v_\theta q$, and propagation speed $v_\theta^2 = c_2/c_1$. The two magnons are completely analogous to relativistic particle and anti-particle, and they carry opposite charge under the unbroken $SO(2)$. As shown in [39, 172], the action for a ferromagnet, instead, contains only one time derivative and it is analogous to that of a non-relativistic particle, which does not feature excitations with opposite charge. This is the reason why, when coupled to light dark matter, anti-ferromagnets allow for the emission of more than one magnon in each event, while ferromagnets do not. We discuss this more in Section 4.1.2.

As far as our application is concerned, a central role is played by the spin density, which is the time-component of the Noether current associated to the original $SO(3)$ symmetry [39, 172]. This rotates the $\hat{\boldsymbol{n}}$ vector (i.e., $\hat{n}_i \to R_{ij}\hat{n}_j$), and the current can be computed with standard procedures, giving the spin density:

$$s_i = c_1\big(\hat{\boldsymbol{n}} \times \partial_t \hat{\boldsymbol{n}}\big)_i = c_1\Big(\delta_{ia}\dot{\theta}^a + \delta_{i3}\epsilon_{ab}\theta^a\dot{\theta}^b + \dots\Big)\,. \tag{4.2}$$

From the equation above we also deduce that, while the ratio c_2/c_1 can be determined from the magnon speed, the coefficient c_1 can be found from an observable sensitive to the spin density of the anti-ferromagnet. One such quantity is the neutron scattering cross section, which we discuss in detail in Appendix 6.3.

Finally, our EFT breaks down at short wavelengths, when the dark matter is able to probe the microscopic details of the material. In other words, it loses validity for momenta larger than a certain strong coupling scale, $\Lambda_{\rm UV}$. The latter can be estimated, for example, as the momentum for which the dispersion relation sensibly deviates from linearity, which indicates that higher derivative terms in the Lagrangian (4.1) become relevant. In this work we consider three anti-ferromagnets: nickel oxide (NiO), manganese oxide (MnO) and chromium oxide (Cr_2O_3). In Table 4.1 we report their values of v_θ, c_1, $\Lambda_{\rm UV}$, and of their density, $\rho_{\rm T}$.

4.1.2 Dark matter–magnon interaction

We now study how a dark matter particle couples to the magnon modes introduced in the previous section. To do that, one starts from a specific model for the interaction of dark matter with the Standard Model. This is then computed in the non-relativistic limit, and matched with low-energy quantities, as we now show. For concreteness, we focus on two well motivated models, which serve as benchmarks to our general point. These were also studied in the context of ferromagnets [169, 183]. They are the magnetic dipole (m.d.) and the pseudo-mediated (p.m.) dark matter, which interact

	v_θ	c_1 [MeV/A]	$\Lambda_{\rm UV}$ [keV]	$\rho_{\rm T}$ [g/cm^3]
NiO [193]	1.3×10^{-4}	0.5	0.6	6.6
MnO [194]	2.5×10^{-5}	4.2	0.5	5.2
Cr_2O_3 [195]	3.5×10^{-5}	0.3	0.9	4.9

Table 4.1: Coefficients for the anti-ferromagnets considered here. v_θ is taken from the dispersion relation, c_1 is matched from neutron scattering data (Appendix 6.3), and $\Lambda_{\rm UV}$ is estimated as the momentum for which the dispersion relation deviates from linear by 10%. The densities, $\rho_{\rm T}$, are taken from [1].

with the Standard Model electron respectively as [184, 185, 186, 187, 188, 189, 190, 191, 192],

$$\mathcal{L}_\chi^{\rm m.d.} = \frac{g_\chi}{\Lambda_\chi} V_{\mu\nu}\bar\chi\sigma^{\mu\nu}\chi + g_e V_\mu \bar e\gamma^\mu e\,, \tag{4.3a}$$

$$\mathcal{L}_\chi^{\rm p.m.} = g_\chi\phi\,\bar\chi\chi + g_e\phi\, i\,\bar e\gamma^5 e\,, \tag{4.3b}$$

where ϕ and V_μ are ultra-light vector and pseudo-scalar mediators, χ and e are the dark matter and electron fields, and Λ_χ is a UV scale pertaining to the dark sector. Moreover, $V_{\mu\nu} = \partial_\mu V_\nu - \partial_\nu V_\mu$ and $\sigma^{\mu\nu} = [\gamma^\mu, \gamma^\nu]$.

To compute the dark matter–magnon interaction one can integrate out the mediator and perform the non-relativistic limit for both the dark matter and electron fields. This can be done either at the level of the matrix elements or integrating out anti-particles, similarly to the Heavy Quark Effective Theory procedure [196]. For the interested reader, we review this in Appendix 6.4. After this, the dark matter–magnon interaction in the two instances is,

$$\begin{aligned}\mathcal{L}_{\rm int}^{\rm m.d.} =& -\frac{4g_\chi g_e}{\Lambda_\chi m_e}\left(\chi_{\rm nr}^\dagger\frac{\sigma^i}{2}\chi_{\rm nr}\right)\left(\delta^{ij}-\frac{\nabla^i\nabla^j}{\nabla^2}\right)\left(e_{\rm nr}^\dagger\frac{\sigma^j}{2}e_{\rm nr}\right)\\ &\xrightarrow{\rm IR} -\frac{4g_\chi g_e}{\Lambda_\chi m_e}\left(\chi_{\rm nr}^\dagger\frac{\sigma^i}{2}\chi_{\rm nr}\right)\left(\delta^{ij}-\frac{\nabla^i\nabla^j}{\nabla^2}\right)s^j\,,\end{aligned} \tag{4.4a}$$

$$\mathcal{L}_{\rm int}^{\rm p.m.} = -\frac{g_\chi g_e}{m_e}\chi_{\rm nr}^\dagger\chi_{\rm nr}\nabla^{-2}\boldsymbol{\nabla}\cdot\left(e_{\rm nr}^\dagger\frac{\boldsymbol{\sigma}}{2}e_{\rm nr}\right)\xrightarrow{\rm IR} -\frac{g_\chi g_e}{m_e}\chi_{\rm nr}^\dagger\chi_{\rm nr}\nabla^{-2}\boldsymbol{\nabla}\cdot\boldsymbol{s}\,, \tag{4.4b}$$

where $\chi_{\rm nr}$ and $e_{\rm nr}$ are non-relativistic fields, and $\boldsymbol{\sigma}$ are Pauli matrices. We also used the fact that $e_{\rm nr}^\dagger\boldsymbol{\sigma}e_{\rm nr}/2$ is the electron spin density operator. When running towards low-energies, it will remain such, except that it must be expressed in terms of the correct low-energy degrees of freedom: the magnons rather than the single electrons.

One can now understand why anti-ferromagnets allow for multi-magnon emission while ferromagnets do not. As shown in Eqs. (4.4), dark matter interacts with magnons via the spin density, whose components, $(s_x \pm i s_y, s_z)$, have at most charge 1 under the

unbroken $SO(2)$. In a ferromagnet this charge can be carried only by a single magnon mode. In an anti-ferromagnet, instead, there are two magnon modes carrying opposite charges. Hence any coupling to the spin density operator will allow multi-magnon emission.

Given the Lagrangians in Eqs. (4.4) and the spin density in Eq. (4.2), one derives Feynman rules for the dark matter–magnon interaction, obtaining,

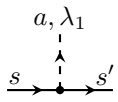

$$= -\frac{g_\chi g_e \sqrt{c_1}}{m_e}\omega \times \begin{cases} \frac{4}{\Lambda_\chi} P_{ia}(\boldsymbol{q})\sigma^i & \text{m.d.} \\ q^a/q^2 & \text{p.m.} \end{cases},$$

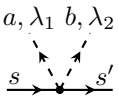

$$= \frac{g_\chi g_e}{m_e}(\omega_1 - \omega_2)\epsilon_{ab} \times \begin{cases} \frac{4}{\Lambda_\chi} P_{iz}(\boldsymbol{q})\sigma^i & \text{m.d.} \\ q^z/q^2 & \text{p.m.} \end{cases}.$$

Solid lines represent a dark matter with polarization $s^{(\prime)}$, and dashed ones represent magnons with momenta $\boldsymbol{q}_{1,2}$, energies $\omega_{1,2}$, polarizations $\lambda_{1,2}$, and carrying an index $a, b = 1, 2$. The total momentum and energy carried by the magnons are $\boldsymbol{q}$ and ω, with $P_{ij}(\boldsymbol{q}) \equiv \delta_{ij} - q_i q_j/q^2$. External dark matter lines come with standard non-relativistic bi-spinors, while external magnon lines come with a polarization vector, $\hat{\boldsymbol{\varepsilon}}_\pm = (1, \pm i)/\sqrt{2}$ [172].

With this at hand, one can compute matrix elements for the emission rate of any number of gapless magnons with simple diagrammatic methods, exactly as one would do for relativistic particles. In particular, the matrix element for the emission of *any* number of low energy magnons is completely fixed by symmetry and by a single effective coefficient, c_1. In a more traditional formulation, the computation of multi-magnon scattering is substantially complicated by the failure of the Holstein–Primakoff approach, which mandates for a more involved treatment [**?**, e.g.,]]dyson1956general.

4.2 Event rates

We now have everything we need to compute the expected event rates for the emission of one and two magnons by a dark matter particle. For a target material with density $\rho_{\rm T}$, the total event rate per unit target mass can be evaluated by averaging the magnon emission rate over the dark matter velocity distribution, $f(\boldsymbol{v}_\chi + \boldsymbol{v}_{\rm e})$:

$$R = \frac{\rho_\chi}{\rho_{\rm T} m_\chi} \int d^3 v_\chi f(\boldsymbol{v}_\chi + \boldsymbol{v}_{\rm e}) \Gamma(v_\chi)\,. \tag{4.5}$$

The local dark matter density is taken to be $\rho_\chi = 0.4$ GeV/cm^3 [197]. The velocity distribution in the Milky Way is instead considered as a truncated Maxwellian given by the standard halo model, with dispersion $v_0 = 230$ km/s, escape velocity $v_{\rm esc} = 600$ km/s and boosted with respect to the galactic rest frame by the Earth velocity, $v_{\rm e} = 240$ km/s [197, 198]. In the following, we present the projected reach for the case of single and two-magnon emission for the anti-ferromagnets NiO, MnO and Cr_2O_3.

4.2.1 One magnon

Using the Feynman rules presented in Section 4.1.2, we compute the rates for the emission of a single gapless magnon. For the two benchmark models they read,

$$\frac{d\Gamma}{d\omega} = \frac{g_\chi^2 g_e^2 c_1}{\pi v_\chi m_e^2} \times \begin{cases} \frac{1+\langle\cos^2\eta\rangle}{2v_\theta^2\Lambda_\chi^2}\omega^2 & \text{m.d.} \\ \frac{\langle\sin^2\eta\rangle}{4} & \text{p.m.} \end{cases}, \tag{4.6}$$

where η is the angle between the Néel vector, $\boldsymbol{\mathcal{N}}$, and the magnon momentum, $\boldsymbol{q}$, and $\langle\cdots\rangle$ represents an average over the direction of the latter. The decay rate is then a function of the relative angle between the magnetization and the direction of the incoming dark matter. Moreover, the magnon is emitted at fixed Cherenkov angle with respect to the incoming dark matter, $\cos\theta = q/(2m_\chi v_\chi) + v_\theta/v_\chi$. The final event rate, Eq. (4.5), depends on the relative angle between $\boldsymbol{v}_\mathrm{e}$ and $\boldsymbol{\mathcal{N}}$. This leads to a daily modulation, which can possibly be used for background discrimination. To reduce the computational burden, we fix the two vectors to be parallel. More details can be found in Appendix 6.5.

To obtain the decay rate, one integrates Eq. (4.6) over magnon energies between ω_min and ω_max. The first one is set by the detector energy threshold. For the case of calometric readout, the best sensitivities that have been envisioned are of $\mathcal{O}(\mathrm{meV})$ [199]. We thus set $\omega_\mathrm{min} = 1$ meV. The maximum magnon energy is instead set by either the cutoff of the EFT or by kinematics. Specifically, $\cos\theta < 1$ limits the possible momentum transfer, implying $\omega_\mathrm{max} = \mathrm{min}(v_\theta\Lambda_\mathrm{UV}, 2m_\chi v_\theta(v_\chi - v_\theta))$.

Our projected reach for the three target materials are shown in Figure 4.1, as compared to the following dark matter–electron cross sections, obtained from the interactions in Eqs. (4.3) in vacuum evaluated at the reference momentum $q_0 = \alpha\, m_e$ [169]:

$$\bar{\sigma}_e = \frac{g_\chi^2 g_e^2}{\pi} \times \begin{cases} \frac{1}{\Lambda_\chi^2}\frac{6m_\chi^2+m_e^2}{(m_\chi+m_e)^2} & \text{m.d.} \\ \frac{1}{4\alpha^2 m_e^2}\frac{m_\chi^2}{(m_\chi+m_e)^2} & \text{p.m.} \end{cases}. \tag{4.7}$$

Moreover, to avoid white dwarf cooling and self-interacting dark matter constraints, we impose χ to be a 5% sub-component of dark matter for the pseudo-mediated model [169]. Following convention, and for a simpler comparison with other proposals, we also assume zero background.

Importantly, NiO is sensitive to masses down to $m_\chi \simeq 5$ keV, even in the single magnon channel. This, as mentioned in the Introduction, is due to the good matching between the magnon and dark matter velocities. For $m_\chi \gtrsim 1$ MeV, the rate starts receiving contributions from momenta above the cutoff, indicating that gapped magnons, not captured by the EFT, become relevant.

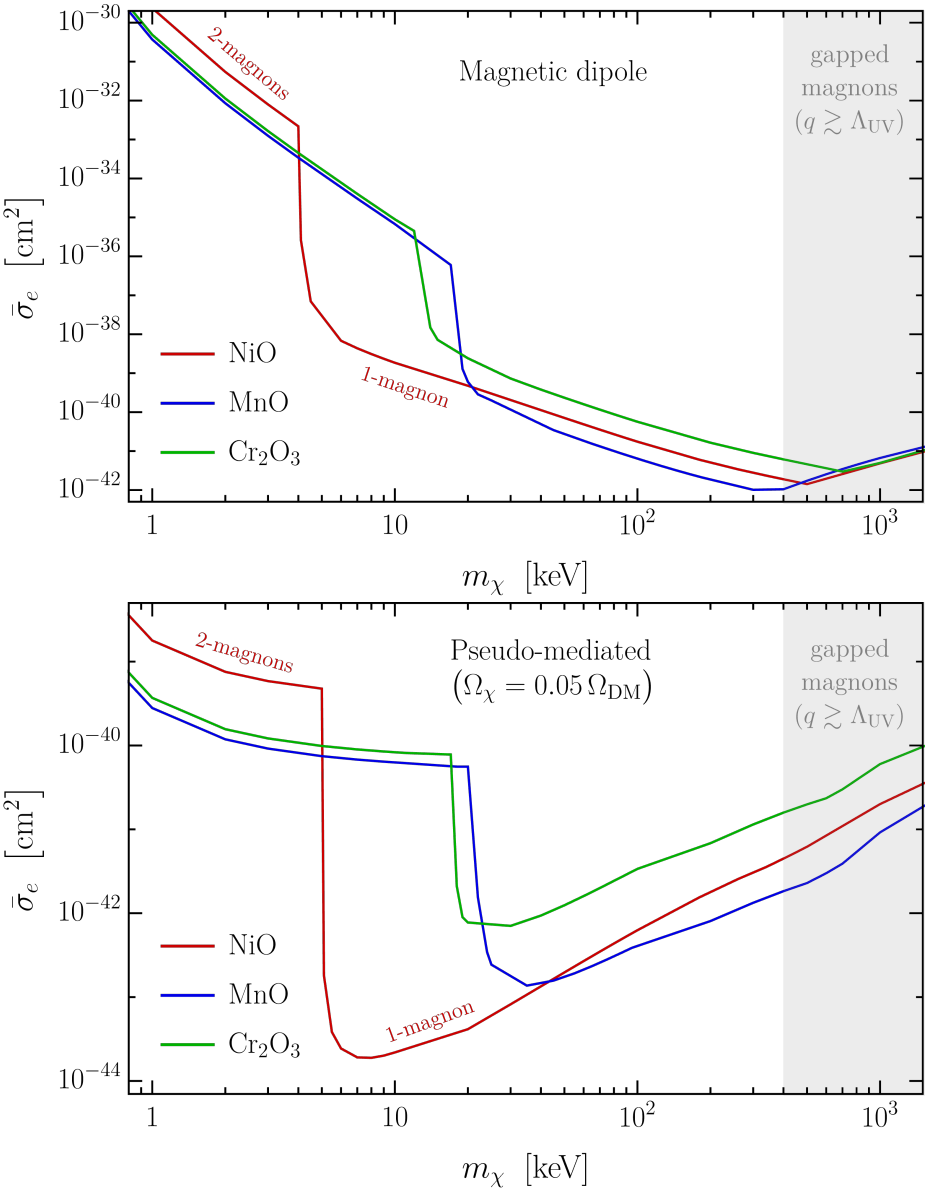

Figure 4.1: Projected reach at 95% C.L. for a kilogram of material and a year of exposure assuming zero background, for the magnetic dipole (**upper panel**) and pseudo-mediated (**lower panel**) models. For the latter we assume $\Omega_\chi/\Omega_{\rm DM} = 0.05$. The lowest mass region is reached via the two-magnon channel. The gray region corresponds to masses for which gapped magnons are expected to play an important role. The magnetization is taken to be parallel to the Earth's velocity.

4.2.2 Two magnons

We consider now the emission of two magnons of energies and momenta $\omega_{1,2}$ and $\boldsymbol{q}_{1,2}$, and total energy and momentum ω and $\boldsymbol{q}$, by a dark matter of initial and final momentum $\boldsymbol{k}$ and $\boldsymbol{k}'$. Using conservation of energy and momentum, the decay rate can be written as

$$\Gamma = \int \frac{k'^2 dk' d\cos\psi dq_1}{4(2\pi)^3 v_\theta^3 \, q} |\mathcal{M}|^2 = \int \frac{d\omega dq dq_1}{4(2\pi)^3 v_\theta^3 v_\chi} |\mathcal{M}|^2 \,, \tag{4.8}$$

were ψ denotes the angle between $\boldsymbol{k}$ and $\boldsymbol{k}'$. In the second equality we also used $k'^2 dk' \, d\cos\psi = (q/v_\chi) dq \, d\omega$. Conservation of energy and momentum further implies $q_1 \leq (\omega + v_\theta q)/(2v_\theta)$. Thus, including also the EFT cutoff, the integral above is performed over $\omega_{\rm min} \leq \omega \leq \min\left(v_\theta \Lambda_{\rm UV}, \frac{1}{2} m_\chi v_\chi^2\right)$, $0 \leq q \leq \min\left(\Lambda_{\rm UV}, 2 m_\chi v_\chi\right)$, and $0 \leq q_1 \leq \min\left(\Lambda_{\rm UV}, (\omega + v_\theta q)/(2v_\theta)\right)$. Again, we assume ideal calorimetric readout and set $\omega_{\rm min} = 1$ meV.

The projected reach for the two-magnon case is again shown in Figure 4.1. This process allows to explore an even larger parameter space, by going down to masses as low as $m_\chi \sim 1$ keV. Due to improved kinematic matching, the mass reach is now almost independent of the target material. For the lightest dark matter, the momentum transfer is much smaller than the energy transfer, and the two magnons are emitted almost back-to-back, with possible interesting implications for background rejection [152]. Similar to the one magnon case, the EFT predictions are unreliable for masses above 1 MeV.

4.3 Conclusion

We have shown how well-assessed anti-ferromagnets can be used as optimal probes for sub-MeV dark matter with spin-dependent interactions. At low energies, these materials feature gapless magnons with two different polarizations, hence allowing for the emission of an arbitrary number of excitations. This, in turns, extends the potential reach down to $m_\chi \sim \mathcal{O}(\text{keV})$. As compared to ferromagnets [169], they have similar sensitivites on the dark matter couplings, but they probe masses more than an order of magnitude lighter. Interestingly, one of these anti-ferromagnets, nickel oxide, sustains magnon modes with a propagation speed accidentally close to the typical dark matter velocity, which allows it to absorb most of the dark matter energy already via the (dominant) one-magnon channel. These results complements what already proposed for dark matter with spin-independent interactions [145, 146, 148, 157, 159], allowing to cover the same mass region.

Moreover, the introduction of an EFT treatment to the problem opens the possibility for the evaluation of more involved observables as, for example, multi-magnon events with strong directionality and the potential for background discrimination [152].

Finally, a simple extension of our EFT would allow the description of the magnon–phonon coupling [172]. This could be used to probe both spin-dependent and spin-independent interactions with a single target. Finally, it is interesting to study the prospect of our materials for axion absorption, and compare with the proposal in [200, 201, 170, 171, 178] (see also, [202, 203, 204]). We leave these and other questions for future work.

Chapter 5

Dynamical modes of Dislocations and their sensitivity to the UV lattice structure

In this work, we explore the dynamics of dislocations in solids using an effective field theory approach. The physics of dislocations is obviously quite mature (see e.g.[205]) but it is perhaps fair to say that highly relevant pieces of the puzzle have yet to be explored. In particular, the dynamics of the excitations of the dislocation itself has only more recently begun to be investigated [206], though we believe that a first principles theoretical underpinning is still lacking, which is a hole we wish to fill herein.

The excitations of dislocations, which were termed "dislons" in [206], are Goldstone bosons for systems with spontaneously broken space-time symmetries. When space-time symmetries are broken, the Goldstone bosons will have either a linear or quadratic dispersion relations, corresponding what what are called type I and type II respectively [1]. For broken internal symmetries, the number of type I and II Goldstones obeys $n_I + 2n_{II} = n_{BG}$ [207, 208, 209], where n_{BG} is the number of broken generators. However, at the moment there is no such equality known for the Goldstones arising from the breaking of space-time symmetries [2].

One would expect that the excitations of dislocations would correspond to canonical phonons which are type I. However, it turns out that, for embedded solids, the dispersion for these modes becomes non-analytic in the momenta. This non-analyticity results from integrating out gapless bulk phonon modes, analogous to what happens in the case of kelvin waves in (super)-fluids. In addition to this, the dispersion turns out to be sensitive to the boundary conditions of the solid. In particular, if we consider a one dimensional solid in vacuum, then if the ends are open, the tension will relax to zero, which leads to the vanishing of the quadratic spatial gradient term for the

[1] More generally type I/II correspond to odd/even powers of the momentum. Furthermore, when rotational invariance is broken one can generate dispersion relations of the form $E = \sqrt{\sum_i c_i k_i^2}$.

[2] For a derivation of the inequality in the context of translational symmetry breaking see [210].

transverse modes in the action. This well known fact, can be understood from the point of view of effective field theory as an example of a generic relaxation mechanism of a Wilson coefficients when the target space is bounded [211]. What we will show here is that the dispersion relation for the transverse modes of a one dimensional defect, will depend upon the nature of the symmetry of the underlying crystal lattice. This distinction will lead to phenomenological differences.

To study the phenomenology of dislocations we need to understand the interaction with bulk phonons [3]. However such interactions are non-local [4] when the phonon is described by $\pi^I(x)$, defined as the displacement of an atom away from its equilibrium position, becomes multi-valued in the presence of a dislocation. This leads to an ambiguity as it is no longer clear which atom "belongs" to which position in the lattice. However, whichever choice is made to fix this ambiguity, the physics should remain unchanged, which is nothing more than a gauge theory description of the physics [212]. For three dimensional solids, which we focus upon, dislocations are co-dimension two objects and, as such, couple topologically to anti-symmetric two form fields. Furthermore, it is known that derivatively coupled scalars, such as ϕ^I, have a dual description in terms of an anti-symmetric two form gauge field [213], which couples locally to the dislocation. This dual description of elasticity theory in three dimensions has been explored in [214], which concentrated on the nature of the melting phase transition. Here we will only be interested in the solid phase, though excitations of the dislocations modes we study here should be expected to play a roll in the transition as well.

The goal of this paper is to develop a first principles theory for the dynamics of dislocations in solids. In particular we will write down an effective field theory of the dislocation excitations which interact with the bulk phonons. A complete analysis of the non-linearities will be left for future work.

5.1 The String Action

To determine the action for the dislocation excitations we will build an effective field theory for an embedded solid. Dislocations share commonalities with fundamental strings as well as with vortices in superfluids, with the important distinctions being the space-time and, in the case of vortices, internal symmetry breaking patterns. The effective field theory of vortices and their interactions in superfluids was worked out in the elegant paper [215], upon which we have leaned. There are some crucial distinctions however, as one might expect, between such vortices and dislocations, that distinguishes our analysis from [215].

[3] It is also known that electron quasi-particle interactions with dislocations can play an important role in determining the superconducting temperature. This topic goes beyond the scope of this paper.

[4] In [206] this non-locality is manifest. It is not clear to the authors how to power count in such a circumstance.

We begin by considering the action of a physical/matter string in vacuum, and then will embed the string into a solid. The two scenarios will be distinguished by their space-time symmetry breaking patterns. A physical string is distinguished from a fundamental string in that they lack reparameterization invariance (RPI) along the world sheet since we can now label the matter elements along the string. Put another way, the matter string breaks boost invariance along the directions of the string, and as such, the system includes an additional dynamical degree of freedom corresponding to a longitudinal mode. We choose to work in a covariant language, despite our eventual goal of calculating in the non-relativistic limit, for ease of notation. Thus we will retain RPI and add an additional mode to the action which is given by

$$S = \int d^2\sigma \sqrt{g}\, F(B) \tag{5.1}$$

where g is the induced metric

$$g_{\alpha\beta} = \eta_{\mu\nu}\partial_\alpha X^\mu \partial_\beta X^\nu \tag{5.2}$$

and

$$B = g^{\alpha\beta}\partial_\alpha\phi\partial_\beta\phi. \tag{5.3}$$

This action contains three physical degrees of freedom, which by appropriate choice of gauge corresponds to the transverse modes X^a and ϕ.

A dislocation is a string embedded in a solid. It is a topological defect which is characterized by a "Burgers vector" which is analogous to the vorticity of a line defect in a superfluid and describes the holonomy of the embedding. We will return to this point when we discuss the coupling of the dislocation to the phononic bulk modes, to which we now turn.

5.2 Effective field theory of solids

A solid breaks space-time symmetries but simultaneous non-linearly realizes emergent internal symmetries. The details of the symmetry breaking pattern are discussed in [216, 37]. For our purposes it will suffice to recall that all of the Ward identities can be saturated with just the three Goldstone bosons π^I associated with broken translations. The action for these Goldstones can be fixed in a derivative expansion using a coset construction [172] or via a Landau-Ginsburg construction [217], which we follow here.

A solid is defined as a system for which the action is invariant under shifts of the co-moving coordinates, $\phi^I \to \phi^I + a^I$. These shifts may be taken to be continuous in the long distance limit. Invariance under $SO(3)$ rotations, which act on the capital Roman letters of these coordinates, will not however, be manifest for crystals, but only for "Jelly like" objects. The action is then given by some arbitrary function of the quantity $B^{IJ} = \partial_\mu\phi^I\partial^\mu\phi^J$. In the ground state we may align the comoving coordinates with the space-time coordinates, i.e. $\langle\phi^I\rangle = x^I$. Thus our power counting will be such

that the first derivatives of the field ϕ^I can be of order one, and subsequent derivatives will be suppressed. This vev breaks both the space-time and internal translations but preserves the diagonal subgroup. For crystalline systems, there will be unbroken discrete rotations which will play an important role below.

With an eye on the fact that we will eventually be interested in taking the non-relativistic limit, we will follow [218] and write the action in the following form

$$S = -\int d^{D+1}x\, n(m + U(B^{IJ})), \tag{5.4}$$

where $n = \sqrt{\text{Det}(B^{IJ})}$ is the number density, m is interpreted as the mass of the atoms sitting at the lattice sights and U is the internal energy functional.

The number density n can be defined via the current J^μ for the comoving coordinates

$$J^\mu = \frac{\bar{n}}{6}\epsilon^{\mu\nu\rho\sigma}\epsilon_{IJK}\partial_\nu\phi^I\partial_\rho\phi^J\partial_\sigma\phi^k \tag{5.5}$$

where $\bar{n}$ is the ground state number density in the rest frame. The current obeys

$$d * J = 0, \tag{5.6}$$

i.e. it is algebraically conserved (off-shell) and expresses the matter conservation. We can write an invariant expression for the number density which reduces to $\det(B^{IJ})$ in the local rest frame

$$n = \sqrt{-J^\mu J_\mu}. \tag{5.7}$$

The corresponding velocity field is given by

$$u^\mu = J^\mu/\sqrt{-J^2}. \tag{5.8}$$

such that $u^2 = -1$ and in the local rest frame $u^0 = 1$. We can thus rewrite the action in (5.4) as

$$S = \int d^4x\ -J^0\sqrt{1-\vec{u}^2}\,(m + U(B^{IJ})) \tag{5.9}$$

In the NR limit, one can expand the above action in $\vec{u}$ and take the $c \to \infty$ to obtain

$$S = J^0\int d^4x\,\frac{m\vec{u}^2}{2} - U(B^{IJ}) \tag{5.10}$$

In the above action we have dropped the contributions from the term $J^0 m$ since it does not contribute to the equations of motion, which can be seen from the fact that the current J^μ can be written as a total derivative $J^\mu = \partial_\nu(J^\nu x^\mu)$.

We may now consider excitations around the ground state via

$$\phi^I(\vec{x},t) = x^I + \pi^I(\vec{x},t) \tag{5.11}$$

where $\pi^I(\vec{x},t)$ are the phonons. To obtain the action for the phonons, one can expand the function eq.(5.4) around the background $B^{IJ}=\delta^{IJ}$. Expanding to quadratic order leaves

$$S=\bar{n}\int d^4x\,\frac{1}{2}m\dot{\vec{\pi}}^2-\lambda_{IJ}(2\partial^I\pi^J+\partial_\mu\pi^I\partial^\mu\pi^J)-2\,\mathcal{C}^{IJKL}(\partial^I\pi^J)(\partial^K\pi^L)+.... \quad (5.12)$$

We have Taylor expanded the functional $U(B^{IJ})=U(\delta_{IJ})+\frac{\partial U}{\partial B_{IJ}}(B^{IJ}-\langle B^{IJ}\rangle)+....$

$$U(B^{IJ})=\lambda_{IJ}(2\partial^I\pi^J+\partial_\mu\pi^I\partial^\mu\pi^J)+2\mathcal{C}^{IJKL}(\partial^I\pi^J)(\partial^K\pi^L)+... \quad (5.13)$$

We have defined $\frac{\partial U}{\partial B_{IJ}}\equiv\lambda_{IJ}$ and the elastic moduli tensor

$$C_{IJKL}\equiv\frac{\partial U}{\partial B_{IJ}\partial B_{KL}}. \quad (5.14)$$

The form of λ_{IJ} and C^{IJKL} depends upon the lattice symmetries. For a cubic lattice $\lambda_{IJ}\sim\delta_{IJ}$, but to achieve isotropy at rank four we need icosohedral symmetry [219], in which case we would write

$$C^{IJKL}=c_2\delta^{IJ}\delta^{KL}+c_3(\delta^{IK}\delta^{JL}+\delta^{IL}\delta^{JK}). \quad (5.15)$$

For a general crystal one would need to decompose C^{IJKL} into the proper invariant tensors for the crystal group of interest. Nonetheless one may have completely isotropic solids if they embody many crystalline domains or are glassy [220], in which case dislocations may no longer be relevant. However, no matter the crystal structure it will always be true that λ_{IJ} will be symmetric and C_{IJKL} will be symmetric in IJ and KL as well as in the interchange of the pair.

Notice that at this point the action depends upon both the symmetric as well as the anti-symmetric pieces of the phonon gradients $\partial_I\pi_J$ at quadratic order and above. For a finite sample, under the assumption that any external applied stresses are isotropic, the anti-symmetric part can be set to zero at the cost of adding boundary terms [211]. This is equivalent to setting $\lambda^{IJ}=0$ in the above action, which we will assume throughout this work since we will be working with open boundary conditions.

5.3 Coupling of the Dislocation to bulk Phonons

It is interesting to contemplate the phenomenological distinctions between the type I and type II realizations. In addition to changing the thermodynamics, interactions between bulk phonons and dislocations will affect the phonon lifetime in the solid since the phonon will scatter off of the dislocation and will be dissipated into dislocation excitations.

Until now we have discussed the effective field theory for solids in terms of the co-moving coordinates $\phi^I(\vec{x},t)$ of the individual particles. However, as previously mentioned, the coupling of $\phi^I(\vec{x},t)$ to these defects is non-local in this canonical description. Something similar happens in the case of superfluids, where it was shown that the non-locality can be eliminated by going to a dual (gauged) description [213, 215]. In 3+1 solids, one may introduce an anti-symmetric two-form fields $b^I_{\mu\nu}$ with $I = 1, 2, 3$ to describe the low energy dynamics [214] in such as way as to leave local couplings to the dislocation.

The idea [213] is that when the theory is derivatively coupled we may change variables from $\partial_\mu\phi^I$ to F^I_μ via a Legendre transformation. Given an action $\mathcal{F}(B^{IJ})$ we may write

$$\mathcal{G}(Y^{IJ}) = \partial^\mu\phi^I \frac{\delta\mathcal{F}(B^{IJ})}{\delta\partial^\mu\phi^J} - \mathcal{F}(B^{IJ}), \tag{5.16}$$

where $Y^{IJ} = F^I_\mu F_{\mu J}$ and

$$F^I_\mu = \frac{\delta\mathcal{F}(B^{IJ})}{\delta\partial^\mu\phi^J}, \tag{5.17}$$

and the inverse is given by

$$\mathcal{F}(B^{IJ}) = \frac{\delta\mathcal{G}(Y^{IJ})}{\delta F^{\mu I}} F^{\mu I} - \mathcal{G}(Y^{IJ}) \tag{5.18}$$

$$\partial_\mu\phi^I = \frac{\delta\mathcal{G}(Y^{IJ})}{\delta F^{\mu I}}. \tag{5.19}$$

The equations of motion for ϕ^I leads to the condition $\partial_\mu F^{\mu I} = 0$, which can be solved by defining

$$F^I_\mu = \epsilon_{\mu\nu\rho\sigma}\partial^\nu b^{\rho\sigma I} \tag{5.20}$$

and $b^{\rho\sigma I}$ is the anti-symmetric vector valued two form field. F^I_μ is invariant under the gauge transformation

$$b^I_{\mu\nu} \to b^I_{\mu\nu} + \partial_\mu\xi^I_\nu - \partial_\nu\xi^I_\mu. \tag{5.21}$$

It can be shown [213] that the Hamiltonian involves only one conjugate pair of variables as required to describe a scalar theory.

Now using our action $\mathcal{F}$ in (5.12) in the presence of open boundaries, we find that at linear order

$$\begin{aligned} F^{IJ} &= -4\bar{n}\mathcal{C}^{IJKL}\partial^K\pi^L \\ F^{0I} &= m\bar{n}\dot{\pi}^I \end{aligned} \tag{5.22}$$

Thus to leading order we have

$$\begin{aligned} \partial^K\pi^L &= -\frac{1}{4\bar{n}}\mathcal{C}^{(-1)KLIJ}F^{IJ} \\ \dot{\pi}^I &= \frac{1}{\bar{n}m}F^{0I}. \end{aligned} \tag{5.23}$$

Notice that at this order the action $\mathcal{G}$ will be insensitive to the anti-symmetry part of $\partial_I \pi_J$, which will only arise once we include non-linearities.

Using the above relations, we may now write (5.16) at leading order as

$$\mathcal{G}^{\mathcal{LO}} = \frac{1}{\bar{n}m}(F^{0I})^2 - \frac{1}{4\bar{n}} C^{(-1)IJKL} F^{IJ} F^{KL} - \mathcal{F}^{LO}(F^{\mu I}). \tag{5.24}$$

where

$$\begin{aligned} \mathcal{F}^{LO}(F^I_\mu) &= \frac{1}{2\bar{n}m}(F^I_0)^2 - \frac{1}{8\bar{n}} \mathcal{C}^{(-1)IJKL} F^{IJ} F^{KL} \end{aligned} \tag{5.25}$$

which gives the leading order dual action

$$\mathcal{G}^{\mathcal{LO}} = \frac{1}{2\bar{n}m}(F^{0I})^2 - \frac{1}{8\bar{n}} C^{(-1)IJKL} F^{IJ} F^{KL}. \tag{5.26}$$

We have the action in terms of $\delta F^I_\mu = \frac{1}{2}\epsilon_{\mu\nu\rho\sigma}\partial^\nu b^{\rho\sigma I}$, but we can clarify the physics [215] by decomposing the two form in terms of two vector fields A^a_i and B^a_i via

$$b^I_{jk} = \epsilon_{ijk} B^I_i \qquad b^I_{0k} = A^I_k. \tag{5.27}$$

We then find

$$\begin{aligned} \delta F^I_0 &= \vec{\partial} \cdot \vec{B}^I \\ \delta F^I_A &= -\dot{B}^I_A + (\vec{\nabla} \times \vec{A})^I_A. \end{aligned} \tag{5.28}$$

Since the action is written in terms of gauge invariant variables it is invariant under the transformations $b^I_{\mu\nu} \to b^I_{\mu\nu} + \partial_\mu \lambda^I_\nu - \partial_\nu \lambda^I_\mu$. The gauge transformation parameter itself has a further redundancy $\lambda_\mu \to \lambda_\mu + \partial_\mu \eta$. We will gauge fix by choosing the Coulomb gauge, which is not covariant, but since we will be interested in the non-relativistic case, this is of no consequence. To do this we include a term in the action

$$S_{GF} = \frac{1}{2\zeta} \int d^4x (\partial^i b^I_{i\nu})^2 \tag{5.29}$$

the limit $\zeta \to 0$ the fields A and B become longitudinal and transverse respectively obeying $\vec{\nabla} \cdot \vec{A}^I = 0$ and $\vec{\nabla} \times \vec{B}^I = 0$ respectively. These correspond to nine conditions that reduces the number of degrees of freedom down to three.

The leading order Lagrangian in terms of these fields is then given by

$$\begin{aligned} L^{LO} &= \frac{1}{2\zeta}[(\partial_i A^I_i)^2 + (\partial_a B^I_a)^2 - (\partial_i B^I_a)(\partial_i B^I_a)] \\ &+ \frac{1}{2\bar{n}m}(\partial_i B_{iI})^2 - \frac{1}{8\bar{n}} C^{-1}_{KLIJ}(\dot{B}_{IJ}\dot{B}_{KL} \\ &+ (\vec{\nabla} \times \vec{A})_{IJ}(\vec{\nabla} \times \vec{A})_{KL} - 2\dot{B}_{IJ}(\vec{\nabla} \times \vec{A})_{KL}) \end{aligned} \tag{5.30}$$

Similarly one can derive the interactions in the bulk using the legendre transform.

As we have emphasized the central point of using the dual description is to construct a local effective action which captures the coupling of the phonons to the dislocation fields, which is encoded in the Kalb-Ramond action. The Kalb-Ramond action describes the leading coupling between the dislocation and the phonon gauge fields. The current associated with a p-dimensional defect is a $p+1$ form and hence a dislocation current in 3+1 dimensions is a two-form given by

$$J_I^{\mu\nu}(x) = n_I \int d\rho\, d\tau\, \partial_\tau X^{[\mu} \partial_\rho X^{\nu]}\, \delta^{(4)}(x - X(\tau,\rho)) \tag{5.31}$$

where $v^\mu = \partial_\tau X^\mu$ is the velocity of the dislocation line.

As was shown in [221] the form of this current along with the particle number conservation leads to the glide constraint, which states the the dislocation is limited to motion in the direction parallel to the Burgers vector. The Kalb-Ramond action takes the form

$$S_{KR} = n^I \int d\tau\, d\rho\, \partial_\rho X^\mu \partial_\tau X^\nu b^I_{\mu\nu} \tag{5.32}$$

which is manifestly gauge invariant and unique. One can notice that this term has no derivatives acting on the two-form $b^I_{\mu\nu}$ which leads to a long range field. This should be contrasted with the scalar field theory for phonons where ϕ^I always comes with a derivative acting on it, and the long range field can then only arise if the couplings are non-local as previously mentioned.

5.4 The Dislocation Action

Let us return to the action for a dislocation embedded in a solid. In this context, we now have at our disposal some bulk metric $G_{\mu\nu}$ in place of the minkowski metric.

Thus we may define the world-sheet metric as

$$g_{\alpha\beta} = G_{\mu\nu} \partial_\alpha X^\mu \partial_\beta X^\nu. \tag{5.33}$$

To determine the dispersion relation for the transverse modes X^a, we choose the defect to lie on the z-axis and work in the gauge $X^0 = \sigma_1$, and $X^3 = \sigma_2 = z$. The solid string coordinate will then be expanded around this configuration, that is $\phi = z$. Expanding out to quadratic order in the fluctuations we have

$$S^{(0)} = \int dt dz \sqrt{G_{zz}} \left[\frac{f_0}{2} G_{ab} \dot{X}^a \dot{X}^b - \frac{1}{2}\left(f_0 - 2\frac{f_1}{G_{zz}} \right) \frac{G_{ab}}{G_{zz}} (\partial_z X^a)(\partial_z X^b) - \frac{1}{2} f_2 \Big(\frac{G_{az}}{G_{zz}} \partial_z X^a \Big)^2 \right], \tag{5.34}$$

where f_i are the coefficients of the taylor expansion of $F(B)$ and we have taken $G_{tt} = -1$.

It would seem that this is the end of the story in the sense that these modes will be of type I. However, the dislon modes mix with the bulk modes as can be seen from re-writing the Kalb-Ramond action in terms of the stress photon and phonon fields in the gauge $X^0 = \tau = t$ and $X^3 = \rho = z$,

$$S_{KR} = n^I \int dt\, dz\, \partial_z X^k A^I_k + \partial_t X^k \partial_z X^i \epsilon_{ikj} B^I_j \tag{5.35}$$

Integrating out the bulk modes leads to a correction to the effective action in (5.34). Since we are essentially interested in the behavior of transverse dislon modes, let us compute these corrections using the above action. In doing so, we will expand the propagators in small frequencies and hence neglect the frequency dependence. Though this may seem a bit cavalier, we will see that it leads to a self-consistent solution.

$$S^{(1)} = n^I n^J \int \frac{d\omega}{2\pi} \int \frac{d^3k}{(2\pi)^3} X^a_{-\omega,-k_z} \left[\epsilon_{ac}\epsilon_{bd}\, (G_B(k))^{IJ}_{cd}\, \omega^2 + (G_A(k))^{IJ}_{ab}\, k_z^2\right] X^b_{\omega,k_z} \tag{5.36}$$

where $G_A(k)$ and $G_B(k)$ are the propagators for the A and B fields evaluated at zero frequency. Integrating over the transverse momenta will induce a logarithmic running of the coefficients in (5.34). Let us consider the isotropic case for simplicity. The propagators for the A and the B field in the zero frequency limit are then given by

$$(G_A(p))^{IJ}_{ij} = -\frac{c_T^2}{p^2}\left[2c_3(2P_T^{ij}P_T^{IJ} - P_T^{iI}P_T^{jJ}) + \frac{8c_2c_3}{2c_3+c_2}(P_T^{ij}P_T^{IJ} - P_T^{iJ}P_T^{jI})\right] \tag{5.37}$$

$$(G_B(p))^{IJ}_{ij} = 2c_3\frac{p^i p^j}{p^4}\delta^{IJ} \tag{5.38}$$

where P_T^{ij} are the transverse projectors. Using these propagators, the integrals over the A and B propagators turn out to be

$$\begin{aligned}
\int \frac{d^2k_\perp}{(2\pi)^2}(G_B(k))^{IJ}_{ab} &= \frac{c_3}{4\pi}\delta_{ab}\delta^{IJ}\left[\frac{2}{\varepsilon} + \ln\left(\frac{\mu^2}{k_z^2}\right) + \ln(4\pi) - \gamma\right] \\
\int \frac{d^2k_\perp}{(2\pi)^2}(G_A(k))^{IJ}_{ab} &= \frac{c_3(c_3+c_2)}{\pi(2c_3+c_2)}c_T^2\delta_{ab}\delta^{I3}\delta^{J3}\left[\frac{2}{\varepsilon} + \ln\left(\frac{\mu^2}{k_z^2}\right) + \ln(4\pi) - \frac{3}{2} - \gamma\right] \\
&\quad + \frac{c_3}{16\pi}D^{IJ}_{ab}\left[\frac{2}{\varepsilon} + \ln\left(\frac{\mu^2}{k_z^2}\right) + \ln(4\pi) - \frac{3}{2}\right]
\end{aligned} \tag{5.39}$$

where

$$D^{IJ}_{ab} = (3\delta_{a1}\delta_{b1} + \delta_{a2}\delta_{b2})\delta^{I1}\delta^{J1} + (\delta_{a1}\delta_{b1} + 3\delta_{a2}\delta_{b2})\delta^{I2}\delta^{J2} \tag{5.40}$$

We have performed these integrals using dimensional regularization with μ acting as the renormalization scale. Also, we have assumed that the dislocations are either screw or edge type and there are no mixed ones.

Let us consider screw dislocations as an illustration. The burgers vector points in the 3-direction and hence $\vec{n} = (0, 0, n)$. The one-loop effective action re-normalizes the effective couplings in (5.34). In the $\bar{MS}$, one can cancel the poles and the constant terms using counter-terms. Thus we are left with

$$S_{eff} = \sqrt{\bar{G}} \int \frac{d\omega}{2\pi} \int \frac{dk}{2\pi} X^a_{-\omega,-k} \Bigg[\left(\bar{G} \frac{f_0(\mu)}{2} + \frac{n^2}{\sqrt{\bar{G}}} \frac{c_3}{2\pi} \ln\left(\frac{\mu}{k}\right) \right) \omega^2 \\ - \left(\frac{f_0(\mu)}{2} - \frac{f_1(\mu)}{\bar{G}} + \frac{n^2}{\sqrt{\bar{G}}} \frac{2c_3(c_3+c_2)}{\pi(2c_3+c_2)} c_T^2 \ln\left(\frac{\mu}{k}\right) \right) k^2 \Bigg] X^a_{\omega,k} \tag{5.41}$$

Note that we have considered this for an isotropic solid where $G_{ij} = \bar{G}\delta_{ij}$ and hence the last term in (5.34) vanishes. We see that the effect of the effective action is to make the world-sheet couplings run with the scale μ.

$$\begin{aligned} f_0(\mu) &= \frac{n^2}{\bar{G}^{3/2}} \frac{c_3}{\pi} \ln\left(\frac{\mu_0}{\mu}\right) \\ f_1(\mu) &= n^2 \sqrt{\bar{G}} \frac{c_3}{2\pi} \left(\frac{1}{\bar{G}} \ln\left(\frac{\mu}{\mu_1}\right) + \frac{2(c_3+c_2)}{(2c_3+c_2)} c_T^2 \ln\left(\frac{\mu}{\mu_1}\right) \right) \end{aligned} \tag{5.42}$$

where μ_0 and μ_1 are some reference UV scales, typically of the order of the inverse dislocation radius $1/r_0$. This leads us with the following effective action.

$$S_{eff} = n^2 \frac{c_3}{2\pi} \int \frac{d\omega}{2\pi} \int \frac{dk}{2\pi} X^a_{-\omega,-k} \left[\ln\left(\frac{\mu_0}{k}\right) \omega^2 - 2 \left(\frac{1}{\bar{G}} \ln\left(\frac{\mu_0}{\mu_1}\right) + c_T^2 \frac{2(c_3+c_2)}{(2c_3+c_2)} \ln\left(\frac{\mu_1}{k}\right) \right) k^2 \right] X^a_{\omega,k} \tag{5.43}$$

However, for a physical, finite solid, we must choose a set of boundary conditions. In particular, we must specify whether not the sample is stressed. For an unstressed sample we may take the boundary conditions to be be open such that in the ground state $\langle \mathcal{T}_{zz} \rangle = 0$, which imposes conditions on the Wilson coefficient of the gradient term in (5.43) via the relation

$$\mathcal{T}_{zz} = \frac{2}{G_{zz}} f_1(L) - f_0(L) = 0 \tag{5.44}$$

which implies

$$\frac{1}{\bar{G}} \ln\left(\frac{\mu_0}{\mu_1}\right) + c_T^2 \frac{2c_3 + 2c_2}{2c_3 + c_2} \ln\left(\frac{\mu_1}{L}\right) = 0 \tag{5.45}$$

Imposing the above condition, one obtains the following dislon action in the isotropic case.

$$S_{eff} = n^2 \frac{\mu}{2\pi} \int \frac{d\omega}{2\pi} \int \frac{dk}{2\pi} X^a_{-\omega,-k} \left[\ln\left(\frac{\mu_0}{k}\right)\omega^2 - 4c_T^2 \frac{c_3 + c_2}{2c_3 + c_2} \ln(kL)\, k^2 \right] X^a_{\omega,k} \quad (5.46)$$

One can see that the dislon has a non-analytic dispersion as opposed to the phonons. One can see that for long-wavelength modes $k \sim 1/L$, the second term in the above action is suppressed. Thus for on-shell modes, one obtains $\omega \ll k$, which is why the assumption of expanding the bulk propagators in small frequencies is consistent. One can calculate the group velocity of the dislons from the above action.

$$v(k) = \frac{d\omega}{dk} = 2c_T \sqrt{\frac{c_3 + c_2}{2c_3 + c_2}} \sqrt{\frac{\log(kL)}{\log(\mu_0/k)}} \left[1 + \frac{1}{2\sqrt{\log(\mu_0/k)}} + \frac{1}{2\log(kL)} \right] \quad (5.47)$$

For long wavelength modes, the last term dominates which results in a velocity $v^2 \sim c_T^2 \log(1/\mu_0 L)$ which is much smaller than the bulk phonon velocity.

Until now, we have restricted our attention to the isotropic case. Let us briefly discuss what happens in an non-isotropic lattice. Analogous to the isotropic case, the exchange of bulk modes renormalizes the couplings in (5.34) and thus leads to a logarithm running of the Wilson coefficients. The relaxation condition (5.44) involves a relation between f_0 and f_1 but in the non-isotropic case, one has additional Wilson coefficient f_2 which is unaffected by the presence of the boundary. At long-wavelengths, this term dominates since f_2 scales a $\log(\mu_0/k) \gg \log(kL)$. Since the coefficient of the kinetic term also scales as $\log(\mu_0/k)$, one obtains a linear dispersion for the dislon mode with corrections scaling as $\frac{\log(kL)}{\log(\mu_0/k)} c_T k$.

5.5 Conclusion

In this work, we have presented an effective field theory of dislocations in solids. We have emphasized the interesting fact that the dispersion relation for the excitations of dislocations, called "dislons", depends upon the UV physics through the discrete symmetries of the lattice. For lattices with at least cubic symmetry the dispersion is non-local in the momenta while less symmetric lattices lead to a linear dispersion relation. The boundary conditions play a crucial roll in leading to this effect, which disappears when the solid is stressed. The distinction between these two cases will show up, among other experiments, in the phonon lifetime.

Chapter 6

Appendix

6.1 WZW term for magnons

In this short appendix, we provide a few more details about the derivation of the RHS of Eq. (3.10b). To this end, we'll focus our attention on the 2-form $\omega_2 \equiv \epsilon_{ab}\,\omega_{S_a} \wedge \omega_{S_b}$, which can be written more explicitly as

$$\omega_2 = \tfrac{1}{2}\epsilon^{aBC}[O^{-1}dO]_{a3} \wedge [O^{-1}dO]_{BC}. \tag{6.1}$$

Using the fact that $O^{-1} = O^T$, and writing explicitly the sums over the indices $B = b, 3$ and $C = c, 3$, we find

$$\omega_2 = \epsilon^{ab} O_{Aa} O_{Bb}\, dO_{A3} \wedge dO_{B3}. \tag{6.2}$$

At this point, it is convenient to think of the matrix elements O_{AB} as a triplet of mutually orthogonal unit vectors defined by

$$\hat{m}^{(a)}_A \equiv O_A{}^a, \qquad \hat{n}_A \equiv O_{A3} \tag{6.3}$$

Then,

$$\epsilon^{ab} O_{Aa} O_{Bb} = (\hat{m}^{(1)}_A \hat{m}^{(2)}_B - \hat{m}^{(2)}_A \hat{m}^{(1)}_B) = \epsilon_{ABC}\hat{n}^C. \tag{6.4}$$

The result on the RHS follows from the fact that the expression in the intermediate step must be antisymmetric, orthogonal to $\hat{n}^A$ and $\hat{n}^B$, and its contraction with $\epsilon^{ABC}\hat{n}_C$ must be equal to 2. Thus, the 2-form in Eq. (6.2) can be written as

$$\omega_2 = \epsilon_{ABC}\,\hat{n}^A\, d\hat{n}^B \wedge d\hat{n}^C. \tag{6.5}$$

Now, if we parametrize the unit vector as in Eq. (3.39), we can calculate ω_2 explicitly to obtain

$$\omega_2 = 2\sin\theta\, d\theta \wedge d\phi = d[-2\cos\theta\, d\phi]. \tag{6.6}$$

However, the discussion in Sec. 3.4.1 shows that this is also equivalent to

$$\omega_2 = d[\epsilon^{ab}(O^{-1}dO)_{ab}]. \tag{6.7}$$

6.2 Magnons in ferromagnets

In the ferromagnetic case, the term in the action with one time derivative is the leading order kinetic term. Therefore, we may eliminate the term with two time derivatives via a field redefinition such that

$$\partial_t \chi_a \partial_t \chi^a \to (\partial^2 \chi_a)^2 + ... \tag{6.8}$$

where the remaining terms involves sub-leading operators (see e.g. [58]). Recall that our power counting for the FM case dictates that time derivatives scale like two spatial derivatives, based on the dispersion relation $\omega = k^2/2m$. Then, the effective action for a ferromagnet describes a single propagating degree of freedom. This can be traced back to the existence of a primary (second class) constraint

$$p^a_\chi - \frac{1}{2}\epsilon^{ab}\chi^b = 0, \tag{6.9}$$

where the p^a_χ's are the momenta conjugate to the χ_a's. The canonical quantization of this constrained theory has been discussed in detail in [222, 42]. One must use care in defining the external states, by proceeding through the Dirac procedure for constrained systems. The Dirac bracket algebra will be satisfied via the field expansions for χ and its conjugate momentum p_χ,

$$\begin{aligned} \chi^a &= \int \frac{d^3k}{(2\pi^3)}(a_k \epsilon^a e^{-ik\cdot x} + a_k^\dagger \epsilon^{a\star} e^{ik\cdot x}) \\ p^a_\chi &= -\frac{1}{2}\int \frac{d^3k}{(2\pi^3)}(a_k \epsilon^a e^{-ik\cdot x} - a_k^\dagger \epsilon^{a\star} e^{ik\cdot x}) \end{aligned} \tag{6.10}$$

where $k \cdot x = -\omega_k t + \vec{k}\cdot\vec{x}$ and $[a_k, a_k^\dagger] = (2\pi)^3\delta^3(\vec{k} - \vec{k}')$, and

$$\epsilon^a = (1, -i)/\sqrt{2}. \tag{6.11}$$

This is equivalent to the statement that the complex field $\Psi = \frac{1}{\sqrt{2}}(\chi_1 + i\chi_2)$ only contains annihilation operators, as is the case for an ordinary non-relativistic field:

$$\Psi = \int \frac{d^3k}{(2\pi^3)}\, a_k e^{-ik\cdot x} \tag{6.12}$$

6.3 Magnon neutron scattering cross-section and EFT matching

To determine the coefficients c_1 reported in Table 4.1, one has to perform a matching calculation between the EFT and a short distance theory. To do this, we compute the one-magnon neutron scattering cross section both within the EFT and within the microscopic theory, which we take to be the Heisenberg model (see for, example, [223] for a pedagogical discussion). This will allow us to extract c_1 in terms of the exchange constants in the Heisenberg model and of the magnon velocities, both of which have been measured in neutron scattering experiments.

We begin with the calculation in the EFT. In a neutron scattering experiment, the interaction between the neutron and the spins of the magnetic material is mediated by an off-shell photon. This is because both the neutron, n, and the spins, $\boldsymbol{\mathcal{S}}_i$, couple to the magnetic field via the Zeeman coupling [39], corresponding to an interaction Lagrangian given by

$$\begin{aligned} \mathcal{L}_{ns} = & -\gamma\mu_n n^\dagger \boldsymbol{\sigma}\, n \cdot \boldsymbol{B} - g\mu_{\rm B} \sum_i \boldsymbol{B}\cdot\boldsymbol{\mathcal{S}}_i \\ \xrightarrow{\rm IR} & -\gamma\mu_n n^\dagger \boldsymbol{\sigma}\, n \cdot \boldsymbol{B} - g\mu_{\rm B} \boldsymbol{B}\cdot\boldsymbol{s}\,, \end{aligned} \tag{6.13}$$

where $\mu_{\rm B} = e/(2m_e)$ is the Bohr magneton, $\mu_n = (m_e/m_n)\mu_{\rm B}$ is the neutron magnetic moment, and the two g-factors are given by $\gamma \simeq 1.9$ and $g \simeq 2$. In going to the second line, we have taken the IR limit where the effective coupling of the magnetic field to the spins is via the spin density. Integrating out the gauge field results in an effective interaction between the neutron and the magnons appearing in the spin density operator. This interaction is given by

$$\mathcal{L}_{ns} = g\mu_B\gamma\mu_n \left(n^\dagger\boldsymbol{\sigma}\, n\right)\cdot\nabla^{-2}\big(\boldsymbol{\nabla}\times(\boldsymbol{\nabla}\times\boldsymbol{s})\big)\,. \tag{6.14}$$

We are interested in the one-magnon cross section due to neutron scattering. The Feynman rule for this interaction can be computed straightforwardly using the expression form the spin-density in Eq. (4.2):

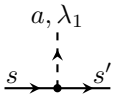

$$= -\gamma\mu_n g\mu_{\rm B}\sqrt{c_1}\omega P_{ia}(\boldsymbol{q})\sigma^i\,,$$

where the solid lines represent the neutron with polarization $s(s')$ and the dashed ones represent the magnon carrying an index a, with momenta $\boldsymbol{q}$ and polarization λ_1. Taking the incoming and outgoing neutron energy-momenta to be $(E,\boldsymbol{k})$ and $(E',\boldsymbol{k}')$

respectively, one can calculate the differential cross section to be

$$\begin{aligned}\frac{d^2\sigma}{d\Omega\, dE'} &= \frac{V}{(2\pi)^2}\frac{m_n k'}{v_n}(\gamma\mu_n g\mu_{\rm B})^2 c_1 \frac{1+\hat{q}_z^2}{4}\omega(q) \\ &\quad\times \delta\big(E'-E-\omega(q)\big) \\ &= V(\gamma r_0)^2\frac{k'}{k}c_1\frac{1+\hat{q}_z^2}{4}\omega(q)\delta\big(E'-E-\omega(q)\big)\end{aligned} \tag{6.15}$$

where we have rewritten the couplings in terms of the classical electron radius, $r_0 \equiv \frac{1}{4\pi}\frac{e^2}{m_e}$. Also, V is the volume of the sample and v_n represents the velocity of the incoming neutron. Since the energy of the outgoing neutron is the one that is measured, the differential rate has been calculated with respect to E'.

Let us now compute this same cross section in the the Heisenberg model which describes the interaction between spins on a lattice, and which is typically employed to report experimental data. We will mostly follow the derivation and notation reported in [180]. The Heisenberg model can be thought of as an effective theory of the Hubbard model which describes the interplay of electrons on a lattice [223]. For an anti-ferromagnet, one can think of the dynamics being described by two sublattices, where the spins belonging to the same sublattice point in the same direction, and the spins belonging to different sublattices point in opposite directions. The Heisenberg Hamiltonian for an anti-ferromagnet can then be written as,

$$\begin{aligned}H = &\sum_{\boldsymbol{x},\boldsymbol{R}} J(R)\,\boldsymbol{\mathcal{S}}_{\boldsymbol{x}}\cdot\boldsymbol{\mathcal{S}}_{\boldsymbol{x}+\boldsymbol{R}} \\ &+\sum_{\boldsymbol{x},\boldsymbol{r}} J'(r)\,\boldsymbol{\mathcal{S}}_{\boldsymbol{x}}\cdot\boldsymbol{\mathcal{S}}_{\boldsymbol{x}+\boldsymbol{r}}\,.\end{aligned} \tag{6.16}$$

Here $\boldsymbol{x}$ is any position on the lattice, $\boldsymbol{R}$ is a vector connecting two sites on opposite sublattices, and $\boldsymbol{r}$ is a vector connecting two sites on the same sublattice. Hence, $J(J')$ describes the exchange interaction between the spins on opposite (same) sublattices. From henceforth, we will work with a cubic lattice, which is sufficient for our discussion and often represents a good approximation of a realistic material. We can define the Fourier space analogs of these couplings as

$$\mathcal{J}(q) \equiv \sum_{\boldsymbol{R}} J(R)e^{-i\boldsymbol{q}\cdot\boldsymbol{R}} \simeq \mathcal{J}_{(0)} - \frac{q^2}{6}\mathcal{J}_{(2)}\,, \tag{6.17a}$$

$$\mathcal{J}'(q) \equiv \sum_{\boldsymbol{r}} J'(r)e^{-i\boldsymbol{q}\cdot\boldsymbol{r}} \simeq \mathcal{J}'_{(0)} - \frac{q^2}{6}\mathcal{J}'_{(2)}\,, \tag{6.17b}$$

where we have expanded in q since we will be interested only in the long wavelength excitations. We also define $\mathcal{J}_{(n)} \equiv \sum_{\boldsymbol{R}} J(R)R^n$ and similarly for $\mathcal{J}'$. Notice that the odd powers vanish due to the symmetry of the cubic lattice, which implies that the sum of every subset of sublattice vectors with fixed magnitude vanishes, $\sum_{R=\text{fix}}\boldsymbol{R} = 0$.

Neglecting lattice vibrations, the differential cross section for inelastic neutron scattering in the Heisenberg model at zero temperature is given by [180]

$$\frac{d^2\sigma}{d\Omega\, dE'} = (\gamma r_0)^2 \frac{k'}{k} |F(\boldsymbol{q})|^2 (\delta_{ij} - \hat{q}_i \hat{q}_j) S^{ij}(\omega, \boldsymbol{q}) \,, \tag{6.18}$$

where $\boldsymbol{q} = \boldsymbol{k}' - \boldsymbol{k}$ and $\omega = E' - E$ are respectively the momentum and energy transfer. Moreover, $F(\boldsymbol{q})$ is the neutron form factor, normalized such that $F(0) = 1$. The van-Hove scattering function, $S^{ij}(\omega, \boldsymbol{q})$, is the Fourier transform of the spin–spin correlator:

$$S^{ij}(\omega, \boldsymbol{q}) = \int \frac{dt}{2\pi} \sum_{\boldsymbol{r}} e^{i\boldsymbol{q}\cdot\boldsymbol{r} - i\omega t} \langle S^i(\boldsymbol{r}, t) S^j(0, 0) \rangle \,. \tag{6.19}$$

For case where the Néel vector of the anti-ferromagnet points in the z-direction, the only relevant spin correlators are the diagonal ones in the transverse directions. For a two-sublattice anti-ferromagnet, one can obtain the scattering function [180] to be

$$S^{ab}(\omega, \boldsymbol{q}) = \frac{\delta^{ab}}{4} \delta\big(\omega - \omega(q)\big) \frac{\mathcal{S}^2 N}{3 v_\theta^2} \big(\mathcal{J}_{(2)} - \mathcal{J}'_{(2)}\big) \omega \,, \tag{6.20}$$

where N is the number of unit cells in the sample and $\mathcal{S}$ is the magnitude of the spins. Now we are in position to compare the cross section computed within the EFT, Eq. (6.15), and within the Heisenberg model, Eq. (6.18), using the above result. Since we are interested in the long-wavelength limit, we can set the neutron form factor to be unity. Matching the two computations, c_1 reads

$$c_1 = \frac{\mathcal{S}^2}{3 V_0 v_\theta^2} \big(\mathcal{J}_{(2)} - \mathcal{J}'_{(2)}\big) \,, \tag{6.21}$$

where $V_0 = V/N$ is the volume of a unit cell. For a cubic lattice $V_0 = a_0^3$, where a_0 is the lattice spacing of the crystal.

We now only need to specify $\mathcal{J}_{(2)}$ and $\mathcal{J}'_{(2)}$ for a given material. We will show how to do that explicitly for NiO. The other anti-ferromagnets considered in this work follow similar procedures, albeit more tedious. The crystal structure of NiO is shown in Figure **??**. The corresponding couplings and crystal parameters have been measured in [193, 224]. From the definitions in Eqs. (6.17), the Fourier space moments are found to be

$$\begin{aligned} \mathcal{J}_{(2)} &= 6R_1^2 J(R_1) + 6R_2^2 J(R_2) + 12R_3^2 J(R_3) + \dots \,, \\ \mathcal{J}'_{(2)} &= 6r_1^2 J'(r_1) + 12r_2^2 J'(r_2) + 12r_3^2 J'(r_3) + \dots \,, \end{aligned}$$

where the numerical factors in front of each term correspond to the number of vectors with the same magnitude, as reported in [224].[1] From Figure **??** we also deduce the

[1] We point out that, in our notation of Eq. (6.16) each coupling $J^{(\prime)}$ is counted twice in the sum, while in the notation of [193, 224] only once. For a proper matching, therefore, one needs to recall that our couplings are half of those measured in [193, 224].

length of the different vectors, i.e.[2]

$$\begin{aligned} R_1 &= \frac{a_0}{\sqrt{2}}\,, \quad R_2 = a_0\,, \quad R_3 = \sqrt{\frac{3}{2}}a_0\,, \\ r_1 &= \frac{a_0}{\sqrt{2}}\,, \quad r_2 = \sqrt{\frac{3}{2}}a_0\,, \quad r_3 = \sqrt{2}a_0\,. \end{aligned} \tag{6.22}$$

For the case of NiO, the next-to-nearest neighbor coupling $J(R_2) \simeq 9.5$ meV is much larger than the other exchange constants [193, 224], and hence dominates the expressions above. We then have,

$$c_1 \simeq \frac{4\mathcal{S}^2}{a_0 v_\theta^2} J(R_2)\,. \tag{6.23}$$

[2]The NiO crystal presents a small anisotropy [224], which makes it deviate from a perfect cubic crystal. This also gives a tiny gap to lowest lying magnon modes. All these effects are negligible for our purposes.

6.4 Non-relativistic limit of the dark matter interactions

To perform the non-relativistic limit at the level of the Lagrangian, one can follow a procedure analogous to what done in Heavy Quark Effective Theory [196], and essentially amounting to integrating out the anti-particles and expanding in small velocities.

Let us consider the electron field as an example; the same procedure applies to any spin-1/2 field. Firstly, one starts from the relativistic 4-component Dirac field and performs the following splitting,

$$e = \mathrm{e}^{-im_e t}\big(e_{\mathrm{L}} + e_{\mathrm{H}}\big)\,, \quad \text{with} \quad \begin{cases} e_{\mathrm{L}} = \mathrm{e}^{im_e t}\frac{\mathbb{1}+\gamma^0}{2}e \\ e_{\mathrm{H}} = \mathrm{e}^{im_e t}\frac{\mathbb{1}-\gamma^0}{2}e \end{cases}, \tag{6.24}$$

where the γ-matrices are written in the Dirac basis. The projectors in the equation above are such that, in the non-relativistic limit, e_{L} only contains the two upper components (associated to the electron), while e_{H} only the two lower ones (associated to the positron). The overall phase ensures that e_{L} has only support on small energies, $\omega \sim k^2/(2m_e) \ll m_e$, while e_{H} contains large energies, $\omega \sim 2m_e$. Indeed, by plugging Eq. (6.24) in the Dirac Lagrangian one gets,

$$\begin{aligned} \mathcal{L}_e \simeq & -\bar{e}_{\mathrm{H}}\,(i\partial_t + 2m_e)\,e_{\mathrm{H}} + \bar{e}_{\mathrm{L}}\,i\partial_t e_{\mathrm{L}} \\ & + \bar{e}_{\mathrm{H}}\,i\boldsymbol{\gamma}\cdot\boldsymbol{\nabla}e_{\mathrm{L}} + \bar{e}_{\mathrm{L}}\,i\boldsymbol{\gamma}\cdot\boldsymbol{\nabla}e_{\mathrm{H}}\,, \end{aligned} \tag{6.25}$$

where we already expanded in the non-relativistic limit.[3] From the Lagrangian above we see that, as anticipated, the particle field e_{L} is massless, while the anti-particle field e_{H} is massive, with mass $2m_e$. As such, it can be integrated out at low-energies. At tree level, the equations of motion give

$$e_{\mathrm{H}} \simeq \frac{i}{2m_e}\boldsymbol{\gamma}\cdot\boldsymbol{\nabla}e_{\mathrm{L}}\,. \tag{6.26}$$

We can now use this to take the non-relativistic limit of the interaction between dark matter and the Standard Model electron. We will work in the simplest case of pseudo-mediated dark matter. The magnetic dipole dark matter follows the same procedure, albeit slightly more tedious. The initial relativistic Lagrangian is the one in Eq. (4.3b). Using the fact that, due to the projectors in Eq. (6.24), $\bar{e}_{\mathrm{H}}e_{\mathrm{L}} = \bar{e}_{\mathrm{H}}\gamma^5 e_{\mathrm{H}} = \bar{e}_{\mathrm{L}}\gamma^5 e_{\mathrm{L}} = 0$, it is simple to show that,

$$\bar{\chi}\chi \simeq \bar{\chi}_{\mathrm{L}}\chi_{\mathrm{L}}\,, \quad \bar{e}\,i\gamma^5 e \simeq \frac{1}{2m_e}\boldsymbol{\nabla}\cdot\big(\bar{e}_{\mathrm{L}}\boldsymbol{\gamma}\gamma^5 e_{\mathrm{L}}\big)\,. \tag{6.27}$$

[3] At lowest order, this corresponds to taking the standard Heavy Quark Effective Theory Lagrangian [196] and set the 4-velocity to $v_\mu = (1, \mathbf{0})$.

Moreover, one also has

$$\boldsymbol{\gamma}\gamma^5\frac{\mathbb{1}+\gamma^0}{2}=\begin{pmatrix}\boldsymbol{\sigma} & 0\\ 0 & 0\end{pmatrix}\equiv\boldsymbol{\Sigma}\,, \tag{6.28}$$

which is precisely the spin operator. It then follow that, including the ultra-light mediator, the non-relativistic Lagrangian reads,

$$\begin{aligned}\mathcal{L}_\chi^{\text{p.m.}} &\simeq \frac{1}{2}\big(\partial\phi\big)^2+g_\chi\phi\,\bar\chi_{\rm L}\chi_{\rm L}+\frac{g_e}{m_e}\phi\,\boldsymbol{\nabla}\cdot\left(\bar e_{\rm L}\frac{\boldsymbol{\Sigma}}{2}e_{\rm L}\right)\\ &\to \frac{g_e g_\chi}{m_e}\bar\chi_{\rm L}\chi_{\rm L}\,\Box^{-1}\boldsymbol{\nabla}\cdot\left(\bar e_{\rm L}\frac{\boldsymbol{\Sigma}}{2}e_{\rm L}\right)\\ &\simeq -\frac{g_e g_\chi}{m_e}\bar\chi_{\rm L}\chi_{\rm L}\,\nabla^{-2}\boldsymbol{\nabla}\cdot\left(\bar e_{\rm L}\frac{\boldsymbol{\Sigma}}{2}e_{\rm L}\right)\\ &= -\frac{g_e g_\chi}{m_e}\chi^\dagger_{\rm rn}\chi_{\rm nr}\nabla^{-2}\boldsymbol{\nabla}\cdot\left(e^\dagger_{\rm nr}\frac{\boldsymbol{\sigma}}{2}e_{\rm nr}\right)\,,\end{aligned} \tag{6.29}$$

where we first integrated out the mediator and then performed the non-relativistic limit again. In the last line we switched to the two-component fields, related to the light field by $e_{\rm L}=(e_{\rm nr}\;0)^{\rm t}$.

6.5 Computation of dark matter event rates

To compute the event rates, one calculates the convolution of the dark matter velocity distribution function and the decay rates as in Eq. (4.5). The velocity distribution function boosted to the Earth's rest frame is given by

$$f(\boldsymbol{v}_\chi + \boldsymbol{v}_\mathrm{e}) = \frac{1}{N_0} \mathrm{e}^{-\frac{(\boldsymbol{v}_\chi + \boldsymbol{v}_\mathrm{e})^2}{v_0^2}} \Theta(v_\mathrm{esc} - |\boldsymbol{v}_\chi + \boldsymbol{v}_\mathrm{e}|)\,, \tag{6.30}$$

where $N_0 = \pi v_0^2[\sqrt{\pi} v_0 \mathrm{erf}(v_\mathrm{esc}/v_0) - 2 v_\mathrm{esc} \exp(-v_\mathrm{esc}^2/v_0^2)]$. Shifting the velocity to $\boldsymbol{v}_\chi \to \boldsymbol{v}_\chi - \boldsymbol{v}_\mathrm{e}$, one finds the total event rate,

$$R = \frac{\rho_\chi}{\rho_\mathrm{T} m_\chi N_0} \int_{v_\chi \leq v_\mathrm{esc}} d^3 v_\chi \mathrm{e}^{-v_\chi^2/v_0^2} \Gamma(|\boldsymbol{v}_\chi - \boldsymbol{v}_\mathrm{e}|, \theta')\,, \tag{6.31}$$

where θ' is the relative angle between the direction of the incoming dark matter, $\hat{\boldsymbol{v}}_\chi$, and the magnetization $\boldsymbol{\mathcal{N}}$. This is related to the angle between the momentum transfer and the magnetization, η, appearing in Eq. (4.6) by [152],

$$\cos\eta = \cos\theta \cos\theta' + \sin\theta \sin\theta' \sin(\phi - \phi')\,, \tag{6.32}$$

with (θ', ϕ') denoting the angle between the incoming dark matter and the magnetization vector and (θ, ϕ) denoting the angle between the momentum transfer and the incoming dark matter. From momentum conservation, one obtains $\cos\theta = q/(2 m_\chi v_\chi) + \omega/(v_\chi q)$. When considered for single magnon emission (i.e., $\omega = v_\theta q$) this returns the usual Cherenkov condition.

After integrating over the direction of $\boldsymbol{v}_\chi$ in Eq. (6.31), the final event rate depends only on the relative angle between the Earth's velocity and the magnetization. Our results of Figure 4.1 are computed in the simplified case where $\hat{\boldsymbol{v}}_\mathrm{e} \cdot \hat{\boldsymbol{\mathcal{N}}} = 1$. The integral in Eq. (6.31) is evaluated numerically.

Bibliography

[1] Anubhav Jain, Shyue Ping Ong, Geoffroy Hautier, Wei Chen, William Davidson Richards, Stephen Dacek, Shreyas Cholia, Dan Gunter, David Skinner, Gerbrand Ceder, and Kristin A. Persson. Commentary: The materials project: A materials genome approach to accelerating materials innovation. *APL Materials*, 1(1):011002, 2013.

[2] Alexander L Gaunt, Tobias F Schmidutz, Igor Gotlibovych, Robert P Smith, and Zoran Hadzibabic. Bose-einstein condensation of atoms in a uniform potential. *Physical review letters*, 110(20):200406, 2013.

[3] G. Benfatto and G. Gallavotti. Renormalization-group approach to the theory of the Fermi surface. *Phys. Rev. B*, 42:9967–9972, 1990.

[4] Ira Z. Rothstein and Prashant Shrivastava. Symmetry Obstruction to Fermi Liquid Behavior in the Unitary Limit. *Phys. Rev. B*, 99(3):035101, 2019.

[5] Ira Z. Rothstein and Prashant Shrivastava. Symmetry Realization via a Dynamical Inverse Higgs Mechanism. *JHEP*, 05:014, 2018.

[6] E. A. Ivanov and V. I. Ogievetsky. The Inverse Higgs Phenomenon in Nonlinear Realizations. *Teor. Mat. Fiz.*, 25:164–177, 1975.

[7] Dmitri V. Volkov. Phenomenological Lagrangians. *Fiz. Elem. Chast. Atom. Yadra*, 4:3–41, 1973.

[8] Lasma Alberte and Alberto Nicolis. Spontaneously broken boosts and the Goldstone continuum. *JHEP*, 07:076, 2020.

[9] Alberto Nicolis, Riccardo Penco, Federico Piazza, and Riccardo Rattazzi. Zoology of condensed matter: Framids, ordinary stuff, extra-ordinary stuff. *JHEP*, 06:155, 2015.

[10] H-W Hammer and RJ Furnstahl. Effective field theory for dilute fermi systems. *Nuclear Physics A*, 678(3):277–294, 2000.

[11] Haruki Watanae and Ashvin Vishwanath. Criterion for stability of Goldstone Modes and Fermi Liquid behavior in a metal with broken symmetry. *Proc. Nat. Acad. Sci.*, 111:16314, 2014.

[12] Eric Braaten and H-W Hammer. Universality in few-body systems with large scattering length. *Physics Reports*, 428(5-6):259–390, 2006.

[13] Shina Tan. Energetics of a strongly correlated fermi gas. *Annals of Physics*, 323(12):2952–2970, 2008.

[14] JT Stewart, JP Gaebler, TE Drake, and DS Jin. Verification of universal relations in a strongly interacting fermi gas. *Physical Review Letters*, 104(23):235301, 2010.

[15] Andrey V. Chubukov and Dmitrii L. Maslov. First-matsubara-frequency rule in a fermi liquid. i. fermionic self-energy. *Phys. Rev. B*, 86:155136, Oct 2012.

[16] R. Haussmann, M. Punk, and W. Zwerger. Spectral functions and rf response of ultracold fermionic atoms. *Phys. Rev. A*, 80:063612, Dec 2009.

[17] C. A. R. Sá de Melo, Mohit Randeria, and Jan R. Engelbrecht. Crossover from bcs to bose superconductivity: Transition temperature and time-dependent ginzburg-landau theory. *Phys. Rev. Lett.*, 71:3202–3205, Nov 1993.

[18] Xufei Wu, Zeyu Liu, and Tengfei Luo. Magnon and phonon dispersion, lifetime, and thermal conductivity of iron from spin-lattice dynamics simulations. *Journal of Applied Physics*, 123(8):085109, 2018. _eprint: https://doi.org/10.1063/1.5020611.

[19] Tai-Min Cheng and Lin Li. Magnon–phonon coupling in two-dimensional heisenberg ferromagnetic system. *Journal of Magnetism and Magnetic Materials*, 320(1):1–7, 2008.

[20] Jung Hoon Kim and Jung Hoon Han. Coupling of phonons and spin waves in a triangular antiferromagnet. *Phys. Rev. B*, 76:054431, Aug 2007.

[21] R. F. Sabiryanov and S. S. Jaswal. Magnons and magnon-phonon interactions in iron. *Phys. Rev. Lett.*, 83:2062–2064, Sep 1999.

[22] RICHARD SILBERGLITT. Effect of spin waves on the phonon energy spectrum of a heisenberg ferromagnet. *Phys. Rev.*, 188:786–792, Dec 1969.

[23] AE Lord. Sound wave velocity change due to the magnon-phonon interaction. *Phys. Status Solidi*, B26(2):717–724, 1968.

[24] P. Erdős. Low-temperature thermal conductivity of ferromagnetic insulators containing impurities. *Phys. Rev.*, 139:A1249–A1262, Aug 1965.

[25] A I Akhiezer, V G Bar'yakhtar, and Moisei I Kaganov. SPIN WAVES IN FERROMAGNETS AND ANTIFERROMAGNETS. i. *Soviet Physics Uspekhi*, 3(4):567–592, apr 1961.

[26] C. Kittel. Interaction of spin waves and ultrasonic waves in ferromagnetic crystals. *Phys. Rev.*, 110:836–841, May 1958.

[27] Joosung Oh, Manh Duc Le, Ho-Hyun Nahm, Hasung Sim, Jaehong Jeong, T. G. Perring, Hyungje Woo, Kenji Nakajima, Seiko Ohira-Kawamura, Zahra Yamani, Y. Yoshida, H. Eisaki, S. W. Cheong, A. L. Chernyshev, and Je-Geun Park. Spontaneous decays of magneto-elastic excitations in non-collinear antiferromagnet (Y,Lu)MnO3. *Nature Communications*, 7(1):13146, October 2016.

[28] Andreas Rückriegel, Peter Kopietz, Dmytro A. Bozhko, Alexander A. Serga, and Burkard Hillebrands. Magnetoelastic modes and lifetime of magnons in thin yttrium iron garnet films. *Phys. Rev. B*, 89:184413, May 2014.

[29] M. Agrawal, V. I. Vasyuchka, A. A. Serga, A. D. Karenowska, G. A. Melkov, and B. Hillebrands. Direct measurement of magnon temperature: New insight into magnon-phonon coupling in magnetic insulators. *Phys. Rev. Lett.*, 111:107204, Sep 2013.

[30] Sidney R. Coleman, J. Wess, and Bruno Zumino. Structure of phenomenological Lagrangians. 1. *Phys.Rev.*, 177:2239–2247, 1969.

[31] Jr. Callan, C. G., S. R. Coleman, J. Wess, and B. Zumino. Structure of phenomenological Lagrangians. 2. *Phys.Rev.*, 177:2247–2250, 1969.

[32] Dmitri V. Volkov. Phenomenological Lagrangians. *Fiz. Elem. Chast. Atom. Yadra*, 4:3–41, 1973.

[33] V. I. Ogievetsky. Nonlinear realizations of internal and space-time symmetries. In *X-th winter school of theoretical physics in Karpacz, Poland*, 1974.

[34] Shashin Pavaskar, Riccardo Penco, and Ira Z. Rothstein. *to appear.*

[35] D. E. Soper. *Classical Field Theory.* 1976.

[36] S. Dubovsky, T. Gregoire, A. Nicolis, and R. Rattazzi. Null energy condition and superluminal propagation. *JHEP*, 03:025, 2006.

[37] A. Nicolis, R. Penco, and R. A. Rosen. Relativistic Fluids, Superfluids, Solids and Supersolids from a Coset Construction. *Phys.Rev.*, D89(4):045002, 2014.

[38] Jonghee Kang and Alberto Nicolis. Platonic solids back in the sky: Icosahedral inflation. *JCAP*, 03:050, 2016.

[39] C. P. Burgess. Goldstone and pseudoGoldstone bosons in nuclear,particle and condensed matter physics. *Phys. Rept.*, 330:193–261, 2000.

[40] Ian Low and Aneesh V. Manohar. Spontaneously broken space-time symmetries and Goldstone's theorem. *Phys. Rev. Lett.*, 88:101602, 2002.

[41] Riccardo Penco. An Introduction to Effective Field Theories. 6 2020.

[42] Shinya Gongyo, Yuta Kikuchi, Tetsuo Hyodo, and Teiji Kunihiro. Effective field theory and the scattering process for magnons in ferromagnets, antiferromagnets, and ferrimagnets. *Progr. Theor. Exp. Phys.*, 2016(8), 2016. 083B01.

[43] H. Leutwyler. Nonrelativistic effective Lagrangians. *Phys.Rev.*, D49:3033–3043, 1994.

[44] JOSÉ MARÍA ROMÁN and JOAN SOTO. EFFECTIVE FIELD THEORY APPROACH TO FERROMAGNETS AND ANTIFERROMAGNETS IN CRYSTALLINE SOLIDS. *International Journal of Modern Physics B*, 13(07):755–789, March 1999. Publisher: World Scientific Publishing Co.

[45] Christoph P. Hofmann. Spin wave scattering in the effective Lagrangian perspective. *Phys. Rev. B*, 60:388, 1999.

[46] Slobodan M. Radošević. Magnon–magnon interactions in o(3) ferromagnets and equations of motion for spin operators. *Annals of Physics*, 362:336–362, 2015.

[47] E.A. Ivanov and V.I. Ogievetsky. The Inverse Higgs Phenomenon in Nonlinear Realizations. *Teor.Mat.Fiz.*, 25(2):1050–1059, 1975.

[48] Garrett Goon, Kurt Hinterbichler, Austin Joyce, and Mark Trodden. Galileons as Wess-Zumino Terms. *JHEP*, 1206:004, 2012.

[49] Eric D'Hoker and Steven Weinberg. General effective actions. *Phys.Rev.*, D50(10):R6050–R6053, 1994.

[50] Luca V. Delacrétaz, Alberto Nicolis, Riccardo Penco, and Rachel A. Rosen. Wess-Zumino Terms for Relativistic Fluids, Superfluids, Solids, and Supersolids. *Phys. Rev. Lett.*, 114(9):091601, 2015.

[51] Stanley Deser. Selfinteraction and gauge invariance. *Gen. Rel. Grav.*, 1:9–18, 1970.

[52] Angelo Esposito, Rafael Krichevsky, and Alberto Nicolis. Solidity without inhomogeneity: Perfectly homogeneous, weakly coupled, UV-complete solids. *JHEP*, 11:021, 2020.

[53] LALE Landau and Es Lifshitz. On the theory of the dispersion of magnetic permeability in ferromagnetic bodies. *Phys. Z. Sowjetunion*, 8(153):101–114, 1935.

[54] Chad R. Galley. Classical Mechanics of Nonconservative Systems. *Phys. Rev. Lett.*, 110(17):174301, 2013.

[55] Alberto Nicolis, Riccardo Penco, Federico Piazza, and Rachel A. Rosen. More on gapped Goldstones at finite density: More gapped Goldstones. *JHEP*, 11:055, 2013.

[56] Haruki Watanabe, Tomáš Brauner, and Hitoshi Murayama. Massive Nambu-Goldstone Bosons. *Phys. Rev. Lett.*, 111(2):021601, 2013.

[57] Gabriel Cuomo, Angelo Esposito, Emanuele Gendy, Andrei Khmelnitsky, Alexander Monin, and Riccardo Rattazzi. Gapped Goldstones at the cut-off scale: a non-relativistic EFT. *JHEP*, 21:068, 2020.

[58] Ira Z. Rothstein. TASI lectures on effective field theories. 8 2003.

[59] Benjamin Grinstein and Ira Z. Rothstein. Effective field theory and matching in nonrelativistic gauge theories. *Phys. Rev. D*, 57:78–82, 1998.

[60] Elihu Abrahams and C. Kittel. Spin-lattice relaxation in ferromagnets. *Phys. Rev.*, 88:1200–1200, Dec 1952.

[61] C. Kittel and Elihu Abrahams. Relaxation process in ferromagnetism. *Rev. Mod. Phys.*, 25:233–238, Jan 1953.

[62] MI Kaganov and VM Tsukernik. Phenomenological theory of kinetic processes in ferromagnetic dielectrics. ii. interaction of spin waves with phonons. *Sov. Phys. JETP*, 36:151–156, 1959.

[63] Simon Streib, Nicolas Vidal-Silva, Ka Shen, and Gerrit E. W. Bauer. Magnon-phonon interactions in magnetic insulators. *Phys. Rev. B*, 99:184442, May 2019.

[64] Sebastian F. Maehrlein, Ilie Radu, Pablo Maldonado, Alexander Paarmann, Michael Gensch, Alexandra M. Kalashnikova, Roman V. Pisarev, Martin Wolf, Peter M. Oppeneer, Joseph Barker, and Tobias Kampfrath. Dissecting spin-phonon equilibration in ferrimagnetic insulators by ultrafast lattice excitation. *Science Advances*, 4(7):eaar5164, 2018.

[65] Shu Zhang, Gyungchoon Go, Kyung-Jin Lee, and Se Kwon Kim. Su(3) topology of magnon-phonon hybridization in 2d antiferromagnets. *Phys. Rev. Lett.*, 124:147204, Apr 2020.

[66] Thuc T. Mai, Kevin F. Garrity, Amber McCreary, Joshua Argo, Jeffrey R. Simpson, Vicky Doan-Nguyen, Rolando Valdés Aguilar, and Angela R. Hight Walker. Magnon-phonon hybridization in 2d antiferromagnet mnpse¡sub¿3¡/sub¿. *Science Advances*, 7(44):eabj3106, 2021.

[67] Hiroto Adachi, Ken-ichi Uchida, Eiji Saitoh, Jun-ichiro Ohe, Saburo Takahashi, and Sadamichi Maekawa. Gigantic enhancement of spin seebeck effect by phonon drag. *Applied Physics Letters*, 97(25):252506, 2010.

[68] K. Uchida, T. Ota, H. Adachi, J. Xiao, T. Nonaka, Y. Kajiwara, G. E. W. Bauer, S. Maekawa, and E. Saitoh. Thermal spin pumping and magnon-phonon-mediated spin-seebeck effect. *Journal of Applied Physics*, 111(10):103903, 2012.

[69] Takashi Kikkawa, Ka Shen, Benedetta Flebus, Rembert A. Duine, Ken-ichi Uchida, Zhiyong Qiu, Gerrit E. W. Bauer, and Eiji Saitoh. Magnon polarons in the spin seebeck effect. *Phys. Rev. Lett.*, 117:207203, Nov 2016.

[70] Alexander G Gurevich and Gennadii A Melkov. *Magnetization oscillations and waves*. CRC press, 2020.

[71] Chad M. Landis. A continuum thermodynamics formulation for micro-magneto-mechanics with applications to ferromagnetic shape memory alloys. *Journal of the Mechanics and Physics of Solids*, 56(10):3059–3076, 2008.

[72] Reem Jaafar, E. M. Chudnovsky, and D. A. Garanin. Dynamics of the einstein–de haas effect: Application to a magnetic cantilever. *Phys. Rev. B*, 79:104410, Mar 2009.

[73] J. B. Alblas. The cosserat continuum with electronic spin. In Ekkehart Kröner, editor, *Mechanics of Generalized Continua*, pages 350–354, Berlin, Heidelberg, 1968. Springer Berlin Heidelberg.

[74] M. Beneke and Vladimir A. Smirnov. Asymptotic expansion of Feynman integrals near threshold. *Nucl. Phys. B*, 522:321–344, 1998.

[75] Sayak Dasgupta and Ji Zou. Zeeman term for the néel vector in a two sublattice antiferromagnet. *Phys. Rev. B*, 104:064415, Aug 2021.

[76] Andreas Rückriegel, Simon Streib, Gerrit E. W. Bauer, and Rembert A. Duine. Angular momentum conservation and phonon spin in magnetic insulators. *Phys. Rev. B*, 101:104402, Mar 2020.

[77] H. A. Brown. Biquadratic exchange and first-order ferromagnetic phase transitions. *Phys. Rev. B*, 11:4725–4727, Jun 1975.

[78] H. Georgi. *Weak Interactions and Modern Particle Theory*. 1984.

[79] Steven Weinberg. *The quantum theory of fields. Vol. 2: Modern applications.* Cambridge University Press, 1996.

[80] I. Dzyaloshinsky. A thermodynamic theory of "weak" ferromagnetism of antiferromagnetics. *Journal of Physics and Chemistry of Solids*, 4(4):241–255, 1958.

[81] Tôru Moriya. Anisotropic superexchange interaction and weak ferromagnetism. *Phys. Rev.*, 120:91–98, Oct 1960.

[82] Kei Yosida. *Theory of magnetism.* Springer series in solid-state sciences; 122. Springer, Berlin, 1996.

[83] P Bak and M H Jensen. Theory of helical magnetic structures and phase transitions in MnSi and FeGe. *Journal of Physics C: Solid State Physics*, 13(31):L881–L885, nov 1980.

[84] A.R. Fert. Magnetic and transport properties of metallic multilayers. In *Metallic Multilayers*, volume 59 of *Materials Science Forum*, pages 439–480. Trans Tech Publications Ltd, 1 1991.

[85] U. K. Rößler, A. N. Bogdanov, and C. Pfleiderer. Spontaneous skyrmion ground states in magnetic metals. *Nature*, 442(7104):797–801, August 2006.

[86] S. Seki, J.-H. Kim, D. S. Inosov, R. Georgii, B. Keimer, S. Ishiwata, and Y. Tokura. Formation and rotation of skyrmion crystal in the chiral-lattice insulator cu_2oseo_3. *Phys. Rev. B*, 85:220406, Jun 2012.

[87] T. Adams, A. Chacon, M. Wagner, A. Bauer, G. Brandl, B. Pedersen, H. Berger, P. Lemmens, and C. Pfleiderer. Long-wavelength helimagnetic order and skyrmion lattice phase in cu_2oseo_3. *Phys. Rev. Lett.*, 108:237204, Jun 2012.

[88] S. Seki, X. Z. Yu, S. Ishiwata, and Y. Tokura. Observation of skyrmions in a multiferroic material. *Science*, 336(6078):198–201, 2012.

[89] X. Z. Yu, N. Kanazawa, Y. Onose, K. Kimoto, W. Z. Zhang, S. Ishiwata, Y. Matsui, and Y. Tokura. Near room-temperature formation of a skyrmion crystal in thin-films of the helimagnet FeGe. *Nature Materials*, 10(2):106–109, February 2011.

[90] W. Münzer, A. Neubauer, T. Adams, S. Mühlbauer, C. Franz, F. Jonietz, R. Georgii, P. Böni, B. Pedersen, M. Schmidt, A. Rosch, and C. Pfleiderer. Skyrmion lattice in the doped semiconductor $fe_{1-x}co_xSi$. *Phys. Rev. B*, 81:041203, Jan 2010.

[91] C Pfleiderer, T Adams, A Bauer, W Biberacher, B Binz, F Birkelbach, P Böni, C Franz, R Georgii, M Janoschek, F Jonietz, T Keller, R Ritz, S Mühlbauer, W Münzer, A Neubauer, B Pedersen, and A Rosch. Skyrmion lattices in metallic and semiconducting b20 transition metal compounds. *Journal of Physics: Condensed Matter*, 22(16):164207, mar 2010.

[92] A. Bogdanov and A. Hubert. Thermodynamically stable magnetic vortex states in magnetic crystals. *Journal of Magnetism and Magnetic Materials*, 138(3):255–269, 1994.

[93] AN Bogdanov and DA Yablonskii. Thermodynamically stable" vortices" in magnetically ordered crystals. the mixed state of magnets. *Zh. Eksp. Teor. Fiz*, 95:182, 1989.

[94] X. Z. Yu, Y. Onose, N. Kanazawa, J. H. Park, J. H. Han, Y. Matsui, N. Nagaosa, and Y. Tokura. Real-space observation of a two-dimensional skyrmion crystal. *Nature*, 465(7300):901–904, June 2010.

[95] Naoto Nagaosa and Yoshinori Tokura. Topological properties and dynamics of magnetic skyrmions. *Nature Nanotechnology*, 8(12):899–911, December 2013.

[96] S. Mühlbauer, B. Binz, F. Jonietz, C. Pfleiderer, A. Rosch, A. Neubauer, R. Georgii, and P. Böni. Skyrmion lattice in a chiral magnet. *Science*, 323(5916):915–919, 2009.

[97] Albert Fert, Nicolas Reyren, and Vincent Cros. Magnetic skyrmions: advances in physics and potential applications. *Nature Reviews Materials*, 2(7):17031, June 2017.

[98] Stefan Heinze, Kirsten von Bergmann, Matthias Menzel, Jens Brede, André Kubetzka, Roland Wiesendanger, Gustav Bihlmayer, and Stefan Blügel. Spontaneous atomic-scale magnetic skyrmion lattice in two dimensions. *Nature Physics*, 7(9):713–718, September 2011.

[99] Benedetta Flebus, Ka Shen, Takashi Kikkawa, Ken-ichi Uchida, Zhiyong Qiu, Eiji Saitoh, Rembert A. Duine, and Gerrit E. W. Bauer. Magnon-polaron transport in magnetic insulators. *Phys. Rev. B*, 95:144420, Apr 2017.

[100] Sergio C. Guerreiro and Sergio M. Rezende. Magnon-phonon interconversion in a dynamically reconfigurable magnetic material. *Phys. Rev. B*, 92:214437, Dec 2015.

[101] Akashdeep Kamra, Hedyeh Keshtgar, Peng Yan, and Gerrit E. W. Bauer. Coherent elastic excitation of spin waves. *Phys. Rev. B*, 91:104409, Mar 2015.

[102] Ka Shen and Gerrit E. W. Bauer. Laser-induced spatiotemporal dynamics of magnetic films. *Phys. Rev. Lett.*, 115:197201, Nov 2015.

[103] R. Agnese et al. New Results from the Search for Low-Mass Weakly Interacting Massive Particles with the CDMS Low Ionization Threshold Experiment. *Phys. Rev. Lett.*, 116(7):071301, 2016.

[104] D. S. Akerib et al. Results from a search for dark matter in the complete LUX exposure. *Phys. Rev. Lett.*, 118(2):021303, 2017.

[105] R. Agnese et al. First Dark Matter Constraints from a SuperCDMS Single-Charge Sensitive Detector. *Phys. Rev. Lett.*, 121(5):051301, 2018. [Erratum: Phys.Rev.Lett. 122, 069901 (2019)].

[106] E. Aprile et al. Light Dark Matter Search with Ionization Signals in XENON1T. *Phys. Rev. Lett.*, 123(25):251801, 2019.

[107] A. H. Abdelhameed et al. First results from the CRESST-III low-mass dark matter program. *Phys. Rev. D*, 100(10):102002, 2019.

[108] Qiuhong Wang et al. Results of dark matter search using the full PandaX-II exposure. *Chin. Phys. C*, 44(12):125001, 2020.

[109] C. Boehm, Pierre Fayet, and J. Silk. Light and heavy dark matter particles. *Phys. Rev. D*, 69:101302, 2004.

[110] C. Boehm and Pierre Fayet. Scalar dark matter candidates. *Nucl. Phys. B*, 683:219–263, 2004.

[111] Matthew J. Strassler and Kathryn M. Zurek. Echoes of a hidden valley at hadron colliders. *Phys. Lett. B*, 651:374–379, 2007.

[112] Dan Hooper and Kathryn M. Zurek. A Natural Supersymmetric Model with MeV Dark Matter. *Phys. Rev. D*, 77:087302, 2008.

[113] Jonathan L. Feng and Jason Kumar. The WIMPless Miracle: Dark-Matter Particles without Weak-Scale Masses or Weak Interactions. *Phys. Rev. Lett.*, 101:231301, 2008.

[114] Adam Falkowski, Joshua T. Ruderman, and Tomer Volansky. Asymmetric Dark Matter from Leptogenesis. *JHEP*, 05:106, 2011.

[115] Tongyan Lin, Hai-Bo Yu, and Kathryn M. Zurek. On Symmetric and Asymmetric Light Dark Matter. *Phys. Rev. D*, 85:063503, 2012.

[116] Yonit Hochberg, Eric Kuflik, Tomer Volansky, and Jay G. Wacker. Mechanism for Thermal Relic Dark Matter of Strongly Interacting Massive Particles. *Phys. Rev. Lett.*, 113:171301, 2014.

[117] Raffaele Tito D'Agnolo and Joshua T. Ruderman. Light Dark Matter from Forbidden Channels. *Phys. Rev. Lett.*, 115(6):061301, 2015.

[118] Eric Kuflik, Maxim Perelstein, Nicolas Rey-Le Lorier, and Yu-Dai Tsai. Elastically Decoupling Dark Matter. *Phys. Rev. Lett.*, 116(22):221302, 2016.

[119] Daniel Green and Surjeet Rajendran. The Cosmology of Sub-MeV Dark Matter. *JHEP*, 10:013, 2017.

[120] Raffaele Tito D'Agnolo, Cristina Mondino, Joshua T. Ruderman, and Po-Jen Wang. Exponentially Light Dark Matter from Coannihilation. *JHEP*, 08:079, 2018.

[121] Rouven Essig, Jeremy Mardon, and Tomer Volansky. Direct Detection of Sub-GeV Dark Matter. *Phys. Rev. D*, 85:076007, 2012.

[122] Peter W. Graham, David E. Kaplan, Surjeet Rajendran, and Matthew T. Walters. Semiconductor Probes of Light Dark Matter. *Phys. Dark Univ.*, 1:32–49, 2012.

[123] Rouven Essig, Marivi Fernandez-Serra, Jeremy Mardon, Adrian Soto, Tomer Volansky, and Tien-Tien Yu. Direct Detection of sub-GeV Dark Matter with Semiconductor Targets. *JHEP*, 05:046, 2016.

[124] Yonit Hochberg, Tongyan Lin, and Kathryn M. Zurek. Absorption of light dark matter in semiconductors. *Phys. Rev. D*, 95(2):023013, 2017.

[125] Itay M. Bloch, Rouven Essig, Kohsaku Tobioka, Tomer Volansky, and Tien-Tien Yu. Searching for Dark Absorption with Direct Detection Experiments. *JHEP*, 06:087, 2017.

[126] Simon Knapen, Jonathan Kozaczuk, and Tongyan Lin. Migdal Effect in Semiconductors. *Phys. Rev. Lett.*, 127(8):081805, 2021.

[127] Zheng-Liang Liang, Chongjie Mo, Fawei Zheng, and Ping Zhang. Phonon-mediated Migdal effect in semiconductor detectors. *Phys. Rev. D*, 106(4):043004, 2022.

[128] Kim V. Berghaus, Angelo Esposito, Rouven Essig, and Mukul Sholapurkar. The Migdal Effect in Semiconductors for Dark Matter with Masses below ~ 100 MeV. 10 2022.

[129] Yonit Hochberg, Yue Zhao, and Kathryn M. Zurek. Superconducting Detectors for Superlight Dark Matter. *Phys. Rev. Lett.*, 116(1):011301, 2016.

[130] Yonit Hochberg, Tongyan Lin, and Kathryn M. Zurek. Detecting Ultralight Bosonic Dark Matter via Absorption in Superconductors. *Phys. Rev. D*, 94(1):015019, 2016.

[131] Yonit Hochberg, Ilya Charaev, Sae-Woo Nam, Varun Verma, Marco Colangelo, and Karl K. Berggren. Detecting Sub-GeV Dark Matter with Superconducting Nanowires. *Phys. Rev. Lett.*, 123(15):151802, 2019.

[132] Sinéad M. Griffin, Yonit Hochberg, Katherine Inzani, Noah Kurinsky, Tongyan Lin, and To Chin. Silicon carbide detectors for sub-GeV dark matter. *Phys. Rev. D*, 103(7):075002, 2021.

[133] Yonit Hochberg, Benjamin V. Lehmann, Ilya Charaev, Jeff Chiles, Marco Colangelo, Sae Woo Nam, and Karl K. Berggren. New Constraints on Dark Matter from Superconducting Nanowires. 10 2021.

[134] Yonit Hochberg, Yonatan Kahn, Mariangela Lisanti, Kathryn M. Zurek, Adolfo G. Grushin, Roni Ilan, Sinéad M. Griffin, Zhen-Fei Liu, Sophie F. Weber, and Jeffrey B. Neaton. Detection of sub-MeV Dark Matter with Three-Dimensional Dirac Materials. *Phys. Rev. D*, 97(1):015004, 2018.

[135] Ahmet Coskuner, Andrea Mitridate, Andres Olivares, and Kathryn M. Zurek. Directional Dark Matter Detection in Anisotropic Dirac Materials. *Phys. Rev. D*, 103(1):016006, 2021.

[136] R. Matthias Geilhufe, Felix Kahlhoefer, and Martin Wolfgang Winkler. Dirac Materials for Sub-MeV Dark Matter Detection: New Targets and Improved Formalism. *Phys. Rev. D*, 101(5):055005, 2020.

[137] L. M. Capparelli, G. Cavoto, D. Mazzilli, and A. D. Polosa. Directional Dark Matter Searches with Carbon Nanotubes. *Phys. Dark Univ.*, 9-10:24–30, 2015. [Erratum: Phys.Dark Univ. 11, 79–80 (2016)].

[138] Yonit Hochberg, Yonatan Kahn, Mariangela Lisanti, Christopher G. Tully, and Kathryn M. Zurek. Directional detection of dark matter with two-dimensional targets. *Phys. Lett. B*, 772:239–246, 2017.

[139] G. Cavoto, E. N. M. Cirillo, F. Cocina, J. Ferretti, and A. D. Polosa. WIMP detection and slow ion dynamics in carbon nanotube arrays. *Eur. Phys. J. C*, 76(6):349, 2016.

[140] G. Cavoto, F. Luchetta, and A. D. Polosa. Sub-GeV Dark Matter Detection with Electron Recoils in Carbon Nanotubes. *Phys. Lett. B*, 776:338–344, 2018.

[141] Asimina Arvanitaki, Savas Dimopoulos, and Ken Van Tilburg. Resonant absorption of bosonic dark matter in molecules. *Phys. Rev. X*, 8(4):041001, 2018.

[142] Philip C. Bunting, Giorgio Gratta, Tom Melia, and Surjeet Rajendran. Magnetic Bubble Chambers and Sub-GeV Dark Matter Direct Detection. *Phys. Rev. D*, 95(9):095001, 2017.

[143] Hao Chen, Rupak Mahapatra, Glenn Agnolet, Michael Nippe, Minjie Lu, Philip C. Bunting, Tom Melia, Surjeet Rajendran, Giorgio Gratta, and Jeffrey Long. Quantum Detection using Magnetic Avalanches in Single-Molecule Magnets. 2 2020.

[144] Wei Guo and Daniel N. McKinsey. Concept for a dark matter detector using liquid helium-4. *Phys. Rev. D*, 87(11):115001, 2013.

[145] Katelin Schutz and Kathryn M. Zurek. Detectability of Light Dark Matter with Superfluid Helium. *Phys. Rev. Lett.*, 117(12):121302, 2016.

[146] Simon Knapen, Tongyan Lin, and Kathryn M. Zurek. Light Dark Matter in Superfluid Helium: Detection with Multi-excitation Production. *Phys. Rev. D*, 95(5):056019, 2017.

[147] S. A. Hertel, A. Biekert, J. Lin, V. Velan, and D. N. McKinsey. Direct detection of sub-GeV dark matter using a superfluid ^{4}He target. *Phys. Rev. D*, 100(9):092007, 2019.

[148] Francesca Acanfora, Angelo Esposito, and Antonio D. Polosa. Sub-GeV Dark Matter in Superfluid He-4: an Effective Theory Approach. *Eur. Phys. J. C*, 79(7):549, 2019.

[149] Andrea Caputo, Angelo Esposito, and Antonio D. Polosa. Sub-MeV Dark Matter and the Goldstone Modes of Superfluid Helium. *Phys. Rev. D*, 100(11):116007, 2019.

[150] Andrea Caputo, Angelo Esposito, Emma Geoffray, Antonio D. Polosa, and Sichun Sun. Dark Matter, Dark Photon and Superfluid He-4 from Effective Field Theory. *Phys. Lett. B*, 802:135258, 2020.

[151] Gordon Baym, D. H. Beck, Jeffrey P. Filippini, C. J. Pethick, and Jessie Shelton. Searching for low mass dark matter via phonon creation in superfluid ^{4}He. *Phys. Rev. D*, 102(3):035014, 2020. [Erratum: Phys.Rev.D 104, 019901 (2021)].

[152] Andrea Caputo, Angelo Esposito, Fulvio Piccinini, Antonio D. Polosa, and Giuseppe Rossi. Directional detection of light dark matter from three-phonon events in superfluid ^{4}He. *Phys. Rev. D*, 103(5):055017, 2021.

[153] Konstantin T. Matchev, Jordan Smolinsky, Wei Xue, and Yining You. Superfluid effective field theory for dark matter direct detection. *JHEP*, 05:034, 2022.

[154] Yining You, Jordan Smolinsky, Wei Xue, Konstantin T. Matchev, Keegan Gunther, Yoonseok Lee, and Tarek Saab. Signatures and Detection Prospects for sub-GeV Dark Matter with Superfluid Helium. 8 2022.

[155] Belina von Krosigk et al. DELight: a Direct search Experiment for Light dark matter with superfluid helium. In *14th International Workshop on the Identification of Dark Matter 2022*, 9 2022.

[156] George M. Seidel and Christian Enss. Use of Superfluid Helium to Observe Directionality of Galactic Dark Matter. 10 2022.

[157] Simon Knapen, Tongyan Lin, Matt Pyle, and Kathryn M. Zurek. Detection of Light Dark Matter With Optical Phonons in Polar Materials. *Phys. Lett. B*, 785:386–390, 2018.

[158] Sinead Griffin, Simon Knapen, Tongyan Lin, and Kathryn M. Zurek. Directional Detection of Light Dark Matter with Polar Materials. *Phys. Rev. D*, 98(11):115034, 2018.

[159] Brian Campbell-Deem, Peter Cox, Simon Knapen, Tongyan Lin, and Tom Melia. Multiphonon excitations from dark matter scattering in crystals. *Phys. Rev. D*, 101(3):036006, 2020. [Erratum: Phys.Rev.D 102, 019904 (2020)].

[160] Peter Cox, Tom Melia, and Surjeet Rajendran. Dark matter phonon coupling. *Phys. Rev. D*, 100(5):055011, 2019.

[161] Brian Campbell-Deem, Simon Knapen, Tongyan Lin, and Ethan Villarama. Dark matter direct detection from the single phonon to the nuclear recoil regime. *Phys. Rev. D*, 106(3):036019, 2022.

[162] Sinéad M. Griffin, Katherine Inzani, Tanner Trickle, Zhengkang Zhang, and Kathryn M. Zurek. Multichannel direct detection of light dark matter: Target comparison. *Phys. Rev. D*, 101(5):055004, 2020.

[163] Tanner Trickle, Zhengkang Zhang, Kathryn M. Zurek, Katherine Inzani, and Sinéad M. Griffin. Multi-Channel Direct Detection of Light Dark Matter: Theoretical Framework. *JHEP*, 03:036, 2020.

[164] Yonatan Kahn and Tongyan Lin. Searches for light dark matter using condensed matter systems. *Rept. Prog. Phys.*, 85(6):066901, 2022.

[165] Humphrey J. Maris, George M. Seidel, and Derek Stein. Dark Matter Detection Using Helium Evaporation and Field Ionization. *Phys. Rev. Lett.*, 119(18):181303, 2017.

[166] D. Osterman, H. Maris, G. Seidel, and D. Stein. Development of a Dark Matter Detector that Uses Liquid He and Field Ionization. *J. Phys. Conf. Ser.*, 1468(1):012071, 2020.

[167] S. A. Lyon, Kyle Castoria, Ethan Kleinbaum, Zhihao Qin, Arun Persaud, Thomas Schenkel, and Kathryn Zurek. Single Phonon Detection for Dark Matter via Quantum Evaporation and Sensing of ^{3}Helium. 1 2022.

[168] Anirban Das, Noah Kurinsky, and Rebecca K. Leane. Dark Matter Induced Power in Quantum Devices. 10 2022.

[169] Tanner Trickle, Zhengkang Zhang, and Kathryn M. Zurek. Detecting Light Dark Matter with Magnons. *Phys. Rev. Lett.*, 124(20):201801, 2020.

[170] Andrea Mitridate, Tanner Trickle, Zhengkang Zhang, and Kathryn M. Zurek. Detectability of Axion Dark Matter with Phonon Polaritons and Magnons. *Phys. Rev. D*, 102(9):095005, 2020.

[171] So Chigusa, Takeo Moroi, and Kazunori Nakayama. Detecting light boson dark matter through conversion into a magnon. *Phys. Rev. D*, 101(9):096013, 2020.

[172] Shashin Pavaskar, Riccardo Penco, and Ira Z. Rothstein. An effective field theory of magneto-elasticity. *SciPost Phys.*, 12(5):155, 2022.

[173] Dany Lachance-Quirion, Samuel Piotr Wolski, Yutaka Tabuchi, Shingo Kono, Koji Usami, and Yasunobu Nakamura. Entanglement-based single-shot detection of a single magnon with a superconducting qubit. *Science*, 367(6476):425–428, 2020.

[174] Dany Lachance-Quirion, Yutaka Tabuchi, Arnaud Gloppe, Koji Usami, and Yasunobu Nakamura. Hybrid quantum systems based on magnonics. *Applied Physics Express*, 12(7):070101, 2019.

[175] Dany Lachance-Quirion, Yutaka Tabuchi, Seiichiro Ishino, Atsushi Noguchi, Toyofumi Ishikawa, Rekishu Yamazaki, and Yasunobu Nakamura. Resolving quanta of collective spin excitations in a millimeter-sized ferromagnet. *Science Advances*, 3(7):e1603150, 2017.

[176] CM Srivastava and R Aiyar. Spin wave stiffness constants in some ferrimagnetics. *Journal of Physics C: Solid State Physics*, 20(8):1119, 1987.

[177] M. Pajda, J. Kudrnovský, I. Turek, V. Drchal, and P. Bruno. Ab initio calculations of exchange interactions, spin-wave stiffness constants, and curie temperatures of fe, co, and ni. *Phys. Rev. B*, 64:174402, Oct 2001.

[178] Jan Schütte-Engel, David J. E. Marsh, Alexander J. Millar, Akihiko Sekine, Francesca Chadha-Day, Sebastian Hoof, Mazhar N. Ali, Kin-Chung Fong, Edward Hardy, and Libor Šmejkal. Axion quasiparticles for axion dark matter detection. *JCAP*, 08:066, 2021.

[179] Gordon Leslie Squires. *Introduction to the theory of thermal neutron scattering*. Courier Corporation, 1996.

[180] S.W. Lovesey. *Theory of Neutron Scattering from Condensed Matter: Nuclear scattering*. International series of monographs on physics. Clarendon Press, 1984.

[181] Freeman J Dyson. General theory of spin-wave interactions. *Physical review*, 102(5):1217, 1956.

[182] N.W. Ashcroft and N.D. Mermin. *Solid State Physics*. Cengage Learning, 2011.

[183] Tanner Trickle, Zhengkang Zhang, and Kathryn M. Zurek. Effective field theory of dark matter direct detection with collective excitations. *Phys. Rev. D*, 105(1):015001, 2022.

[184] Kris Sigurdson, Michael Doran, Andriy Kurylov, Robert R. Caldwell, and Marc Kamionkowski. Dark-matter electric and magnetic dipole moments. *Phys. Rev. D*, 70:083501, 2004. [Erratum: Phys.Rev.D 73, 089903 (2006)].

[185] Eduard Masso, Subhendra Mohanty, and Soumya Rao. Dipolar Dark Matter. *Phys. Rev. D*, 80:036009, 2009.

[186] Spencer Chang, Neal Weiner, and Itay Yavin. Magnetic Inelastic Dark Matter. *Phys. Rev. D*, 82:125011, 2010.

[187] Vernon Barger, Wai-Yee Keung, and Danny Marfatia. Electromagnetic properties of dark matter: Dipole moments and charge form factor. *Phys. Lett. B*, 696:74–78, 2011.

[188] A. Liam Fitzpatrick, Wick Haxton, Emanuel Katz, Nicholas Lubbers, and Yiming Xu. The Effective Field Theory of Dark Matter Direct Detection. *JCAP*, 02:004, 2013.

[189] Moira I. Gresham and Kathryn M. Zurek. Effect of nuclear response functions in dark matter direct detection. *Phys. Rev. D*, 89(12):123521, 2014.

[190] Eugenio Del Nobile, Graciela B. Gelmini, Paolo Gondolo, and Ji-Haeng Huh. Direct detection of Light Anapole and Magnetic Dipole DM. *JCAP*, 06:002, 2014.

[191] Bradley J. Kavanagh, Paolo Panci, and Robert Ziegler. Faint Light from Dark Matter: Classifying and Constraining Dark Matter-Photon Effective Operators. *JHEP*, 04:089, 2019.

[192] Xiaoyong Chu, Josef Pradler, and Lukas Semmelrock. Light dark states with electromagnetic form factors. *Phys. Rev. D*, 99(1):015040, 2019.

[193] M. T. Hutchings and E. J. Samuelsen. Inelastic neutron scattering measurement of spin waves and magnetic interactions in NiO. *Solid State Communications*, 9(13):1011–1014, 1971.

[194] G. Pepy. Spin waves in mno; from 4°k to temperatures close to tn. *Journal of Physics and Chemistry of Solids*, 35(3):433–444, 1974.

[195] E.J. Samuelsen, M.T. Hutchings, and G. Shirane. Inelastic neutron scattering investigation of spin waves and magnetic interactions in cr2o3. *Solid State Communications*, 7(15):1043–1045, 1969.

[196] Aneesh V. Manohar and Mark B. Wise. *Heavy quark physics*, volume 10. 2000.

[197] Til Piffl et al. The RAVE survey: the Galactic escape speed and the mass of the Milky Way. *Astron. Astrophys.*, 562:A91, 2014.

[198] G. Monari, B. Famaey, I. Carrillo, T. Piffl, M. Steinmetz, R. F. G. Wyse, F. Anders, C. Chiappini, and K. Janßen. The escape speed curve of the Galaxy obtained from Gaia DR2 implies a heavy Milky Way. *Astron. Astrophys.*, 616:L9, 2018.

[199] Yonit Hochberg, Matt Pyle, Yue Zhao, and Kathryn M. Zurek. Detecting superlight dark matter with fermi-degenerate materials. *Journal of High Energy Physics*, 2016(8), aug 2016.

[200] A. I. Kakhidze and I. V. Kolokolov. Antiferromagnetic axions detector. *Sov. Phys. JETP*, 72:598–600, 1991.

[201] David J. E. Marsh, Kin-Chung Fong, Erik W. Lentz, Liboř Smejkal, and Mazhar N. Ali. Proposal to Detect Dark Matter using Axionic Topological Antiferromagnets. *Phys. Rev. Lett.*, 123(12):121601, 2019.

[202] R. Barbieri, C. Braggio, G. Carugno, C. S. Gallo, A. Lombardi, A. Ortolan, R. Pengo, G. Ruoso, and C. C. Speake. Searching for galactic axions through magnetized media: the QUAX proposal. *Phys. Dark Univ.*, 15:135–141, 2017.

[203] N. Crescini et al. Operation of a ferromagnetic axion haloscope at $m_a = 58\,\mu$eV. *Eur. Phys. J. C*, 78(9):703, 2018. [Erratum: Eur.Phys.J.C 78, 813 (2018)].

[204] N. Crescini et al. Axion search with a quantum-limited ferromagnetic haloscope. *Phys. Rev. Lett.*, 124(17):171801, 2020.

[205] J. P. Hirth and J. Lothe. Theory of dislocations. 1982.

[206] M. Li et. al. Theory of electron–phonon–dislon interacting system—toward a quantized theory of dislocations. *New Journal of Physics*, 20, 2018.

[207] Holger Bech Nielsen and S. Chadha. On How to Count Goldstone Bosons. *Nucl.Phys.*, B105:445, 1976.

[208] Thomas Schäfer, D. T. Son, Misha A. Stephanov, D. Toublan, and J. J. M. Verbaarschot. Kaon condensation and Goldstone's theorem. *Phys. Lett. B*, 522:67–75, 2001.

[209] Haruki Watanabe and Hitoshi Murayama. Unified Description of Nambu-Goldstone Bosons without Lorentz Invariance. *Phys. Rev. Lett.*, 108:251602, 2012.

[210] Haruki Watanabe and Tomas Brauner. Spontaneous breaking of continuous translational invariance. *Phys. Rev. D*, 85:085010, 2012.

[211] Alberto Nicolis and Ira Z. Rothstein. Apparent fine tunings for field theories with broken space-time symmetries. 2022.

[212] Hagen Kleinert. *Multivalued fields. In condensed matter, electromagnetism, and gravitation*. 2008.

[213] D. Z. Freedman and P. K. Townsend. Antisymmetric Tensor Gauge Theories and Nonlinear Sigma Models. *Nucl. Phys. B*, 177:282–296, 1981.

[214] Aron J. Beekman, Jaakko Nissinen, Kai Wu, and Jan Zaanen. Dual gauge field theory of quantum liquid crystals in three dimensions. *Phys. Rev. B*, 96:165115, Oct 2017.

[215] Bart Horn, Alberto Nicolis, and Riccardo Penco. Effective string theory for vortex lines in fluids and superfluids. *JHEP*, 10:153, 2015.

[216] Alberto Nicolis, Riccardo Penco, Federico Piazza, and Riccardo Rattazzi. Zoology of condensed matter: Framids, ordinary stuff, extra-ordinary stuff. *JHEP*, 06:155, 2015.

[217] Sergei Dubovsky, Thomas Grégoire, Alberto Nicolis, and Riccardo Rattazzi. Null energy condition and superluminal propagation. *Journal of High Energy Physics*, 2006(03):025–025, mar 2006.

[218] D. E. Soper. *Classical Field Theory*. 1976.

[219] Jonghee Kang and Alberto Nicolis. Anisotropic tensor modes from icosahedral inflation. 7 2018.

[220] P. Chaikin and T. Lubensky. Principles of condensed matter physics. In *Principles of Condensed Matter Physics*. Cambridge University Press, 2000.

[221] Aron J. Beekman, Jaakko Nissinen, Kai Wu, Ke Liu, Robert-Jan Slager, Zohar Nussinov, Vladimir Cvetkovic, and Jan Zaanen. Dual gauge field theory of quantum liquid crystals in two dimensions. *Physics Reports*, 683:1–110, apr 2017.

[222] Shinya Gongyo and Shintaro Karasawa. Nambu-Goldstone bosons and the Higgs mechanism without Lorentz invariance: Analysis based on constrained-system theory. *Phys. Rev. D*, 90(8):085014, 2014.

[223] Alexander Altland and Ben D. Simons. *Condensed Matter Field Theory*. Cambridge University Press, 2 edition, 2010.

[224] Mo T Hutchings and EJ Samuelsen. Measurement of spin-wave dispersion in nio by inelastic neutron scattering and its relation to magnetic properties. *Physical Review B*, 6(9):3447, 1972.